UNIVERSITY OF OKLAHOMA

GRADUATE COLLEGE

QUANTUM REACTIVE SCATTERING: COLLISION INDUCED DISSOCIATION

A DISSERTATION

SUBMITTED TO THE GRADUATE FACULTY

in partial fulfillment of the requirements for the

Degree of

DOCTOR OF PHILOSOPHY

BY

Daniel Alan Brue
Norman, Oklahoma
2010

QUANTUM REACTIVE SCATTERING: COLLISION INDUCED DISSOCIATION

A DISSERTATION APPROVED FOR THE
HOMER L. DODGE DEPARTMENT OF PHYSICS AND ASTRONOMY

BY

Dr. Gregory A. Parker, Chair

Dr. Eric R. I. Abraham

Dr. Deborah K. Watson

Dr. Neil Shafer-Ray

Dr. Roger Frech

Acknowledgments

The road to finishing a Ph.D. project in physics is sometimes hard, and sometimes it is very hard. This is a good thing. Finishing *should* be hard. It *should* take a lot of effort. If it wasn't hard, the degree wouldn't be worth much. Still, it seems a common affliction for graduate students to experience days, weeks, or even months when progress is slow, the end is far, and quitting would be a relief. Sometimes one can make it through these periods with shear determination, and other times with an excess of pride. But sometimes, making it through is only possible with the help of those wonderful, caring people who give support when it is needed. These people, who have always been there for me, I cannot thank enough.

Since Dr. Gregory Parker first accepted me as a graduate student, there hasn't been a single instance when he didn't do everything he could to help prepare me to be a professional scientist. He has been unfailingly generous with his time, patience, and teaching. Dr. Parker would drop anything he was working on to answer a question, discuss theory, or help look for problems. None of this work would have been possible without him. I have been exceptionally privileged with the opportunity to work with him and learn from him, and I will always been grateful for his training and friendship.

I would like to thank my advisory committee members: Dr. Neil Shafer-Ray, Dr. Eric Abraham, Dr. Deborah Watson, and Dr. Roger Frech. I am grateful for their their advice, which has always been significantly helpful, and also for their time, flexibility, and patience in working with me.

I would also like to especially thank Dr. Michael Morrison. For years he has graciously answered questions when I have appeared in his doorway, or engaged in hours long email conversations through the middle of the night. I have always enjoyed talking with him, and his insights have always been enlightening. I am

very grateful for all of the time he has spent talking with me and helping me to see new perspectives.

I have been immensely fortunate to get to work with some really excellent people in my years with Dr. Parker's research group. The hours or days long discussions on science between Xuan Li, Jeff Crawford, and myself are the most fun experiences I've had as a physicist to date. It has been a privilege to work with Xuan and Jeff, and I deeply value their friendship. I am also grateful to Dr. Andrew Feldt for helping me over the years to keep our computer systems running, without which, any attempt at computational physics would have been much, much more challenging.

I would like to thank the University of Oklahoma for the priceless gift of education. From the very beginning of my college career, OU has provided countless opportunities for me to learn and improve myself.

I am grateful to my family and friends for giving me a life that contained more than school alone.

And ultimately, I am eternally thankful to my wife, Mollie. She never failed to give love and encouragement when I needed it, or to leave me alone to work when I needed it. She always found the perfect balance of being reassuringly patient or motivatingly impatient. But most of all, Mollie took my goals and dreams and made them hers, also. Nothing greater could be expected or wished for, and so to her I dedicate this work.

Contents

Chapter 1

Introduction

A tremendous amount of what we know about the physical world, we have learned from scattering processes. From simply looking at something with our eyes to see what color it is or throwing rocks at windows to see if they break, to complex processes like x-ray crystallography or scanning electron microscopes, we have been learning by bouncing things off of each other since the beginning of history. Young children might perform several scattering experiments every day.

We use scattering to probe that which we don't know, and we do this usually by taking that which we don't know and making it interact with something we do know. We can tell the color of some object easily if we know that we are looking at it in the presence of a faithfully white light source. We know the light is white, so the color we see must be the object's true color. In exactly the same way, we use electron microscopes to explore very small things by taking a beam of electrons, the known part, and looking at how they interact with the object under observation, the unknown part.

In fact, the more we know about the "known" part before the scattering, the more we can learn from the "unknown" part afterward. This is why the invention of lasers was so profound. Never before did we have anything that we knew so much

about as these coherent beams of light, and suddenly new worlds of measurement and research opened.

Suffice to say, aiming to understand scattering is a worthwhile goal. And, as new areas of science become interesting, new types of scattering processes will be developed in order to learn about them.

So, let us define a scattering process to be any one in which two or more bodies are brought into close proximity of each other such that their behavior is affected, then the aim of any scattering calculation is to determine the effects of this interaction. In literal collisions, this interaction is the physical contact of the bodies in question, such as the scattering of billiard balls. In a quantum mechanical treatment, this interaction is just that the bodies come close enough to exert significant[1] force on each other, usually through electromagnetic fields, that the presence of each influences the behavior of the others. There might be no direct contact in quantum scattering, but the process is still called a collision.

This work aims to study the collision of three atoms by theoretical calculations, and then use the understanding gained from this to either explain or predict experimental results. In this way, like nearly every other scientific endeavor, scattering theory works in tandem with experiment. However, this work is novel in that it expands on existing work in this field by employing new methodologies to treat the situation where all three atoms are separated. That is, the system may be three separated atoms in its initial state or its final state or both. The scenario where the three atoms begin separated but collide to form a atom and diatomic

[1]It is worth noting that the meaning of "significant" in this context is dependent entirely on the magnitude of these forces and the degree of accuracy desired from the calculation.

molecule (diatom) pair is called three-body recombination (3BR). The time reversal of three-body recombination is where an atom and diatomic molecule collide to form three free atoms, and is called collision-induced dissociation (CID).

Three-body recombination and collision-induced dissociation are physical processes that occur in a large number of chemical reactions, and these reactions themselves occur in a wide variety of regimes in natural science. Such processes happen in upper atmosphere ozone production and are responsible for a vast number of the chemical processes that occur in combustion, and also are of vital importance to thorough understanding of cold and ultra-cold chemical dynamics; a field that has been of great interest in recent decades and has produced multiple Nobel laureates. It this field of cold and ultra-cold chemical processes where we focus our interests.

Certainly for as long as this area of physics has been interesting, it has also been difficult. Theoretical predictions of these processes can be very complicated, having to account for numerous possible outcomes. The limiting factor is computational power, both in time and memory, since many of these calculations could easily grow to be impossibly large for today's computers, or take a prohibitively long time to conduct. An atom-diatom interaction has the possibility of scattering elastically, inelastically, or reactively, and the atoms could all break apart entirely in collision-induced dissociation. Accurately representing all of these possibilities in a scattering calculation is an arduous task, one that requires basis functions that accurately describe all of these possible outcomes. This is exceptionally difficult for states were all atoms break apart and are free (CID), since the basis functions corresponding to such outcome states must span enormous regions of space. In many calculations over the years, this task has been simplified by restricting the collision energy to sufficiently low values that CID processes are not possible.

The goal of this work is to remove this restriction by developing a methodology of constructing a set of basis functions that are highly efficient and accurate. These basis functions are *physically motivated*, which in the simplest sense means that the form of the basis functions is influenced by the physical potential of the system as well as the boundary conditions. Other methods such as a discrete variable representation (DVR)[1, 2], finite element methods (FEM)[3], or distributed approximating functionals (DAF)[4], rely on a basis set that does obey the boundary conditions, but otherwise attempts to solve for physical states by employing a large basis set.

In brief overview, this method constructs basis functions for the three-body system by first calculating the two-body wave functions for each possible pair of atoms. Between two atoms, there will be a finite number of bound and quasibound wavefunctions, and and infinite number of continuum states, i.e. those for which the two atoms break apart. All of the bound and quasibound wavefunctions are calculated as functions of the internuclear distance between the two atoms. These two-body wavefunctions are then projected onto a set of hyperspherical coordinates for the three-body system. The continuum state basis functions are constructed from a direct product of the zero-potential solutions to the hyperspherical coordinate Hamiltonian, and the linear combination of the zero-energy solutions to each set of two-atom Hamiltonians. The resultant functions have appropriate behavior in the regions where all three atoms are widely separated, as well as in regions where the two-atom potentials are not negligible. If possible, any available symmetry afforded by the system is used to simplify the projected wavefunctions and reduce computation. For systems of three like atoms, this savings can be significant.

As the three atoms separate after collision, either each individually or as an atom-diatom product, this basis set becomes more accurate as the three-body effects of the potential diminish. At short ranges, when the three atoms are near each other and the three-body interaction effects are large, this basis method is less effective because it does not account for these effects. However, at short distances, the space spanned by the wavefunctions is much smaller than at large distances, and the basis functions require much less storage and computation. Therefore, when the three atoms are close, the basis set can be augmented easily and inexpensively to compensate for any shortcomings in the basis without adding any significant costs in time or memory. Thus, this basis can be used quickly and effectively throughout the entire scattering process.

The layout of this document is organized to first provide a theoretical background of the quantum treatment of scattering for a three-body system, and then to introduce the new basis method as applied to the HNe_2 model problem. This application to the HNe_2 model problem demonstrates the effectiveness, efficiency, and accuracy of the new basis method against existing solutions of a CID/3BR problem. Next, the development of the basis method is given for a realistic, three-body homonuclear system, along with an explanation of how group theory can be applied to take advantage of the system's symmetries in order to reduce the computational overhead. The results of these calculations is then presented.

Chapter 2

Three-Body Scattering

This work concerns three-body scattering of atoms A, B, and C, such that the possible processes of the collision are

$$\left.\begin{array}{r} A+BC \\ B+AC \\ C+AB \\ A+B+C \end{array}\right\} \longleftrightarrow \left\{\begin{array}{l} A+BC \\ B+AC \\ C+AB \\ A+B+C \end{array}\right.$$

where any of these may be an elastic or inelastic process, which is to say that the collision of an atom A with diatom BC may result in $A+BC \rightarrow A+BC$ or $A+BC \rightarrow A+BC^*$, where BC^* is a different internal state of the BC diatom. This work treats the three-body scattering problem in a time-independent quantum formalism[5, 6] in which we solve for wavefunctions at a single constant energy. At that constant energy we can find the probabilities of transition between all of these processes simultaneously, whereas in a time-dependent calculation, one would solve for a range of energies, but only get the transition probabilities of one initial state per calculation. In terms of reactive scattering, where we are just looking at $A+BC \leftrightarrow B+AC \leftrightarrow C+AB$, each of the different diatomic outcomes

is generally called an *arrangement channel*. This, however, can often be confused with the general term of *channel*, which often refers to a of specific quantum state being considered in the calculation. Using *channel* to refer to a specific quantum state is very common in the literature[1] and does not generally refer to a specific atom-diatom permutation and can refer to a three-body breakup state.

Ultimately, the goal is to solve for the total wavefunction of the system, Π, which is a solution of the equation

$$H\Pi_i^p = E\Pi_i^p \tag{2.1}$$

where E is the total scattering energy and H is the time-independent Hamiltonian. The subscript i represents a composite quantum number that specifies a specific state and/or arrangement channel. The subscript f will also be used in this capacity, and thus i and f loosely refer to initial and final states, respectively. While *initial* and *final* are not meaningful terms in a time-independent formalism, in discussing scattering generally, they are useful in labeling the *from* and *to* states.

We say that when the scattering bodies are removed to the point that they are no longer reacting, that the potential between them is negligible, then the system is *asymptotic*. We assume that the initial state of the system is asymptotic and that the final state is asymptotic. The range of asymptotic depends highly on the type of particles being scattered and the extent of the long-range potential energy factors [7]. If we describe such asymptotic states by $A_i(\mathbf{x})$, where $\mathbf{x}$ here refers

[1] see referenced works by M. H. Alexander, G. C. Schatz, W. Miller, B. R. Johnson, W. A. Lester, Jr., J. C. Light, K. D. McLenithan, G. A. Parker, R. T Pack, D. Secrest, R. B. Walker, A. Kuppermann, B. K. Kendrick, and others

to the nine coordinates describing the positions of the three atoms, then in the asymptotic limit we have

$$\Pi_i \rightarrow A_i(\mathbf{x}) + \sum_f F\left(f \leftarrow i|\mathbf{k}_i, \mathbf{k}_f\right) A_f(\mathbf{x}) \tag{2.2}$$

The vector $\mathbf{k}_f$ is the wave number vector with a magnitude given by

$$k_i = \left[\frac{2\mu}{\hbar^2}(E - \epsilon_f)\right]^{1/2} \tag{2.3}$$

where E is the total energy, ϵ_f is the energy of the f state, and μ is the system reduced mass. The direction of the $\mathbf{k}_f$ vector is that of the vector separating the products of the reaction, and the angles used to describe this direction depend on the chosen coordinate system chosen. The quantity $F\left(f \leftarrow i|\mathbf{k}_i, \mathbf{k}_f\right)$ is the scattering amplitude[5, 6, 8], which contains all information that we can possibly know about the collision interaction and is a function of the initial and finial internal energies.

The next step is to expand Π_i as a series of partial waves labeled by an angular momentum[9], J, and by M which is the projection of J on a space-fixed axis.

$$\Pi_i = \frac{2\pi}{k_i^{1/2}} \sum_{JM\ell_i} i^{l_i+1} C(j_i \ell_i J; m_i, M - m_i, M) Y_{l_i, M-m_i}(\hat{k}_i) \Psi^{JMi} \tag{2.4}$$

where ℓ_i is the orbital angular momentum of state i about the system center of mass, and j_i is the internal angular momentum of the collision products, and C is a Clebsch-Gordan coefficient. The problem now becomes one of solving for Ψ^{JMi}, which is an eigenfunction of an angular momentum operator with eigenvalue J and

an eigenfunction of the operator of the projection of J on an axis with eigenvalue M.

There are two main reasons for expressing Π as the expansion of equation 2.4. First, solving for Ψ functions is theoretically and computationally simpler since only one total angular momentum J must be considered at a time. Second, and the more significant reason, is that expressing Π in this fashion illuminates physical reasons for limiting the number of initial and final states that need to be considered. At small collision energies, only a very limited number of Ψ^{JM} wavefunctions, specifically those with small or zero values of J, are involved in the collision process, and the rest are unaffected. As the energy increases, Ψ^{JM} wavefunctions with higher values of J must be solved for in order to get accurate scattering cross sections, but it is always a finite number. This means that only a limited number of Ψ^{JM} states need to be considered for a given collision process, and only the initial and final states related to J by the Clebsch-Gordan coefficient need to be considered in the scattering calculation.

The formulation of three-body scattering has been, so far, as generic as possible. To describe this process in more detail requires a choice of coordinates in which to define $\mathbf{k}_{i,f}$, $\mathbf{x}$, and definitions of the asymptotic states $A_{i,f}(\mathbf{x})$. We will now look at some of the ways to do this that are relevant to the present work.

Formally, a quantum description of the three-body scattering process requires nine dimensions. Usually three of these coordinates can be ignored by factoring out the center of mass motion of the system, which has no influence on the interaction of the particles, and then attempt to solve the equation in the remaining six coordinates. While there are means to solve such a differential equation with direct numerical solvers, such a computation is prohibitively extremely expensive

and time consuming. Instead, the problem is broken into smaller, more manageable pieces by solving only portions of the full Hamiltonian at a time and then expanding the full wavefunction in a basis of partial solutions.

In the rest of this chapter, we describe the Hamiltonians and Ψ wavefunctions in the coordinates that are relevant to this present work on collision-induced dissociation. Later, we draw parallels to these formulations to show how the basis set used for CID is developed.

2.1 Jacobi Hamiltonian and Wavefunctions

A review of Jacobi coordinates[10, 11] is given in appendix B.1, but in brief, there are three sets of Jacobi coordinates for a three atom system. These sets are labeled by τ, where $\tau = A, B, C$. The coordinates, minus center of mass, are given by r_τ, which is the vector between the $\tau+1$ and $\tau+2$ atoms, and R_τ, which is the vector between the center of mass of the diatom and the τ atom.

It is more convenient, however, to work in *mass-scaled* Jacobi coordinates that are defined as

$$\mathbf{S}_\tau = \mathbf{R}_\tau d_\tau \tag{2.5}$$

$$\mathbf{s}_\tau = \mathbf{r}_\tau / d_\tau \tag{2.6}$$

where d_τ is a mass-scaling factor defined as

$$d_\tau = \left[\frac{m_\tau}{\mu} \left(1 - \frac{m_\tau}{M} \right) \right]^{1/2} \tag{2.7}$$

where M is the total mass, $M = m_A + m_B + m_C$ and μ is the three-body reduced mass given as

$$\mu = \sqrt{\frac{m_A m_B m_C}{M}} \tag{2.8}$$

The effects of this mass-scaling on $\mathbf{R}_\tau$ and $\mathbf{r}_\tau$ can be seen in figure B.2, but it should be noted that d_τ is not far from one for systems of atoms with similar masses, and d_τ only effects an order of magnitude difference on R_τ and r_τ if the atomic masses differ by three or four orders of magnitude. If the masses are all identical, then $d_\tau = 1.07457$ for all τ.

There are two distinct advantages to using mass-scaled Jacobi coordinates over the standard definition. First, the kinetic energy operators $\nabla^2_{s_\tau}$ and $\nabla^2_{S_\tau}$ both have the same reduced mass, μ as defined above. The kinetic terms in r_τ and R_τ have different reduced mass factors. This change merely allows the kinetic energy operator to be written more simply. The second benefit is more substantial. By using mass-scaled coordinates, the transformation from one set of mass-scaled Jacobi coordinates to another, say from those oriented for channel τ to those oriented for channel τ+1, is simply a kinematic rotation on a six-dimensional vector comprised of the components of $\mathbf{S}_\tau$ and $\mathbf{s}_\tau$. Furthermore, this transformation is a continuous and unitary transformation that is a function of only a single angle (see appendix B.1 or reference [8]). Thus this mass-scaling affords an easy way to change from one set of Jacobi coordinates to another, and so the S_τ and s_τ coordinates are used throughout this work.

$$H = \frac{-\hbar^2}{2\mu}\left[\frac{1}{S_\tau}\frac{\partial^2}{\partial S_\tau^2}S_\tau + \frac{1}{s_\tau}\frac{\partial^2}{\partial s_\tau^2}s_\tau\right] + \frac{\mathcal{L}_\tau^2}{2\mu S_\tau^2} + \frac{\mathcal{J}_\tau^2}{2\mu s_\tau^2} + V(\mathbf{s}_\tau, \mathbf{S}_\tau) \tag{2.9}$$

where $\mathcal{J}$ is the rotational angular momentum operator of the diatomic molecule, $\mathcal{L}$ is the orbital angular momentum operator of the third atom about the diatom center of mass. The total angular momentum operator J is defined as

$$J = \mathcal{J}_\tau + \mathcal{L}_\tau \tag{2.10}$$

and μ is the three-body reduced mass,

$$\mu = \left[\frac{m_A m_B m_C}{m_A + m_B + m_C}\right]^{1/2} \tag{2.11}$$

First, for mass-scaled Jacobi coordinates, Ψ is expanded in functions of $\mathbf{s}_\tau, \mathbf{S}_\tau$, and the angles that define $\hat{s}_\tau$ and $\hat{S}_\tau$, totaling six coordinates, such that we have for a given J total angular momentum with space-fixed (SF) projection M,

$$\Psi^{JM\tau_i\nu_i j_i \ell_i} = \sum_{\tau_f \nu_f j_f \ell_f} \frac{1}{s_{\tau_f} S_{\tau_f}} G^{J\tau_i\nu_i j_i \ell_i}_{\tau_f \nu_f j_f \ell_f}(S_{\tau_f}) \zeta_{\nu_f j_f}(s_{\tau_f}) \mathscr{Y}^{JM}_{j_f \ell_f}(\hat{s}_{\tau_f} \hat{S}_{\tau_f}) \tag{2.12}$$

where i and f are initial and final state labels, τ labels the arrangement channel, ν and j define the vibrational and rotational quantum numbers of the diatom, and ℓ is the angular momentum of the atom and diatom about the system center of mass. For simplicity, here on i and f may be used to represent any or all of the channel dependent labels.

The $\mathscr{Y}(\hat{s_\tau}, \hat{S}_\tau)$, are defined as

$$\mathscr{Y}^{JM}_{j\ell}(\hat{S}_\tau, \hat{s}_\tau) = \sum_m C(j, \ell, J; m, M-m, M) Y_{jm}(\hat{s}_\tau) Y_{\ell, M-m}(\hat{S}_\tau) \tag{2.13}$$

where C is the appropriate Clebsch-Gordan coefficient. The $\mathscr{Y}$ are eigenfunctions of the $J^2, J_z, \mathcal{J}^2, \mathcal{L}^2$ operators with eigenvalues of $J(J+1)\hbar^2, M\hbar, j(j+1)\hbar^2, \ell(\ell+1)\hbar^2$

respectively. The basis functions, $\zeta_{\nu j}$ are defined as solutions to the vibrational diatomic equation,

$$\left[\frac{-\hbar^2}{2\mu}\frac{\partial^2}{\partial s_\tau^2} + \frac{j(j+1)\hbar^2}{2\mu s_\tau^2} + V_2(s_\tau)\right]\zeta_{\nu j}(s_\tau) = \mathcal{E}_{\nu j}\zeta_{\nu j}(s_\tau) \tag{2.14}$$

where $V_2(s_\tau)$ is the diatomic potential between the $\tau+1$ and $\tau+2$ atoms.

The Ψ wavefunction is expanded in these sets of ζ and $\mathscr{Y}$ functions, and a set of coupled channel matrix equations are formed by expanding the wavefunction and Hamiltonian in the $\zeta\mathscr{Y}$ basis to form matrices with elements labeled by the basis quantum numbers $\nu j\ell$,

$$\left\langle \zeta_{\nu' j'\ell'}\mathscr{Y}^{JM}_{j'\ell'}\middle| H+V\middle|\Psi\right\rangle = \mathbf{H}G(S_\tau) + \mathbf{V}G(S_\tau) = \mathbf{E}G(S_\tau) \tag{2.15}$$

where $\mathbf{H}$ and $\mathbf{V}$ are matrices in the $\zeta\mathscr{Y}$ basis. The solutions of these coupled equations is a set of $G(S_\tau)$. These G functions are usually found numerically by applying any one of several methods to solve these coupled differential equations.

The states that are considered *bound* are those basis functions $\zeta\mathscr{Y}$ that correspond to diatomic energies that are less than zero. These correspond to distinct rovibrational states labeled by $\nu j\ell$, for when the third atom is far away and the potential reduces to the diatomic potential, the Jacobi Hamiltonian reduces to a two body Hamiltonian, as will be shown explicitly in section.

Likewise, the *continuum* states are those for which the two-body energy is greater than zero asymptotically. Since the third atom is already assumed to be infinitely far away, a continuum diatomic state means that the energy is sufficient that all three atoms can separate infinitely. These wavefunctions oscillate indefinitely to $s_\tau \to \infty$.

2.2 Delves Hamiltonian and Wavefunctions

The relationship between Delves[12] and Jacobi coordinates is as simple as that of polar to Cartesian coordinates,

$$s_\tau = \rho \sin(\vartheta_\tau) \tag{2.16}$$

$$S_\tau = \rho \cos(\vartheta_\tau) \tag{2.17}$$

and so the formulation of the Hamiltonian and wavefunctions is quite similar. In Delves hyperspherical coordinates, the wavefunction Ψ is expanded as

$$\Psi^{JMi} = 2 \sum_f \frac{1}{\rho^{5/2}} \Gamma^J_{fi}(\rho) \frac{\Upsilon_f(\vartheta_{\tau f}; \rho_\xi)}{\sin(2\vartheta_{\tau f})} \mathscr{Y}^{JM}_f(\hat{s}_f, \hat{S}_f) \tag{2.18}$$

which is a solution to

$$\begin{aligned} H = & \frac{-\hbar^2}{2\mu} \left[\frac{1}{\rho^5} \frac{\partial}{\partial \rho} \rho^5 \frac{\partial}{\partial \rho} + \frac{2}{\rho \sin(2\vartheta_\tau)} \left(\frac{\partial^2}{\partial \vartheta_\tau^2} \right) \frac{\sin(2\vartheta_\tau)}{2} + \frac{4}{\rho^2} \right] \\ & + \frac{\mathcal{J}^2}{\rho^2 \sin^2(\vartheta_\tau)} + \frac{\mathcal{L}^2}{\rho^2 \cos^2(\vartheta_\tau)} + V(\vec{\rho}) \end{aligned} \tag{2.19}$$

The $\mathscr{Y}$ functions used here are identical to those of equation 2.13 used in the Jacobi formulation, and the Υ functions are the solutions to the "vibrational" equation of

$$\begin{aligned} & \left[\frac{-\hbar^2}{2\mu\rho_\xi^2} \left(\frac{\partial^2}{\partial \vartheta_\tau^2} - \frac{j(j+1)}{\sin^2(\vartheta_\tau)} - \frac{\ell(\ell+1)}{\cos^2(\vartheta_\tau)} \right) + V^{BC}(\rho_\xi \sin \vartheta_\tau) \right] \Upsilon_{\nu j \ell}(\rho_\xi; \vartheta_\tau) \\ & = H_{vib} \Upsilon_{\nu j \ell}(\rho_\xi; \vartheta_\tau) = \mathcal{E}_{\nu j \ell}(\rho_\xi) \Upsilon_{\nu j \ell}(\rho_\xi; \vartheta_\tau) \end{aligned} \tag{2.20}$$

where ρ_ξ is some fixed value of ρ and is a parameter of this equation. The potential V^{BC} is the two-body potential energy curve between atoms B and C. The Υ functions represent vibrations of the triatomic system, since $\vartheta_\tau$depends only on the magnitudes of s_τ and S_τ. At a large ρ_ξ, the $\Upsilon(\vartheta_\tau)$ functions for bound states closely resemble the $\zeta(s_\tau)$ functions, since the range for which the bound states have appreciable amplitude is limited to a finite range of s_τ. In this case, a small-angle approximation can be used, $s_\tau = \rho \sin\vartheta_\tau \approx \rho\vartheta_\tau$ and $S_\tau = \rho\cos\vartheta_\tau \approx \rho$, and so the Υ functions can be thought of as though representing the vibrational motion of the diatom. At short or moderate ρ_ξ values this is not necessarily a good analogy; the bound wavefunctions have amplitude across the entire [0,π/2] domain of ϑ_τ, and so while not a vibration of the diatom, it is still a vibrational motion and ν is a vibrational quantum number.

The Delves Hamiltonian is expanded in this basis of $\Upsilon(\vartheta_\tau)\mathscr{Y}(\hat{s},\hat{S})$, and the set of coupled equations is solved for solutions $\Gamma(\rho)$. The combination

$$\frac{\Upsilon_{\nu j\ell}(\vartheta_\tau)\mathscr{Y}^{JM}_{j\ell}(\hat{s},\hat{S})}{\rho^{(5/2)}\sin(2\vartheta_\tau)} \tag{2.21}$$

is called a *surface function*, as it is a function that spans the surface of the hyper-sphere at a particular value of ρ.

It should be noted that this formulation of the surface functions is intended to produce an expansion basis that is close to physical. Any set of functions could be used provided that they are complete and obey the boundary conditions. By using differential equations that are subsets of the terms of the full Hamiltonian, it is hoped that these basis functions will be more efficient, that is, we will need fewer of them to obtain an accurate Ψ, than what a generic, non-physically motivated basis could provide.

If we multiply from the left by a $\mathscr{Y}^{JM}$ function and integrate over the angles of the **s** and **S** vectors, we get matrix elements in the basis of the coupled-angular functions. The $\mathscr{Y}$ functions are orthogonal with respect to J and M, so the matrices produced by the kinetic energy terms are diagonal – ρ and ϑ_τ depend only on the magnitudes of **s** and **S**, and derivatives with respect to these variables have no effect on $\mathscr{Y}$. The potential matrix elements, however, are not generally diagonal. For a single matrix element where a specific value of ℓ and j have been selected, the Hamiltonian becomes

$$\langle \mathscr{Y}_{j\ell}|H|\Psi\rangle = \left\{ \frac{-\hbar^2}{2\mu}\frac{2}{\rho^{5/2}\sin(2\vartheta_\tau)}\left[\frac{\partial^2}{\partial\rho^2}+\frac{1}{4\rho^2}\right]\frac{\rho^{5/2}\sin(2\vartheta_\tau)}{2} + \sum_{j'\ell'} V^{ABC}_{jj'\ell\ell'}(\rho,\vartheta_\tau) \right.$$
$$\left. -\frac{\hbar^2}{2\mu\rho^2}\frac{2}{\rho^{5/2}\sin(2\vartheta_\tau)}\left[\frac{\partial^2}{\partial\vartheta_\tau^2}-\frac{\ell(\ell+1)}{\cos^2\vartheta_\tau}-\frac{j(j+1)}{\sin^2\vartheta_\tau}\right]\frac{\rho^{5/2}\sin(2\vartheta_\tau)}{2} \right\} \langle \mathscr{Y}_{j\ell}|\Psi\rangle \tag{2.22}$$

Now we both subtract and add the diatomic potential, V^{BC}, so that the full Delves Hamiltonian can be written with terms that exactly match equation 2.20,

$$V^{ABC}_{jj'\ell\ell'}(\vec{\rho}) = V^{ABC}_{jj'\ell\ell'}(\vec{\rho}) + V^{BC}(\rho\sin\vartheta_\tau) - V^{BC}(\rho\sin\vartheta_\tau) \tag{2.23}$$

Note that $V^{BC}(s)$ does not depend on the angles defining $\hat{s}_\tau$ or $\hat{S}_\tau$, and thus matrix elements of this potential are diagonal with regard to the angular momentum basis

functions; $\left\langle \mathscr{Y}_{j\ell}|V^{BC}|\mathscr{Y}_{j'\ell'}\right\rangle = \delta_{jj'}\delta_{\ell\ell'}$. After making this change and rearranging we have

$$\begin{aligned}\langle \mathscr{Y}_{j\ell}|H|\Psi\rangle = \Bigg\{ &\frac{-\hbar^2}{2\mu}\frac{2}{\rho^{5/2}\sin(2\vartheta_\tau)}\left[\frac{\partial^2}{\partial\rho^2}+\frac{1}{4\rho^2}\right]\frac{\rho^{5/2}\sin(2\vartheta_\tau)}{2} \\ &+\sum_{j'\ell'} V^{ABC}_{jj'\ell\ell'}(\vec{\rho}) - V^{BC}(\rho\sin\vartheta_\tau) \\ &-\frac{\hbar^2}{2\mu\rho^2}\left[\frac{\partial^2}{\partial\vartheta_\tau^2}-\frac{\ell(\ell+1)}{\cos^2\vartheta_\tau}-\frac{j(j+1)}{\sin^2\vartheta_\tau}+V^{BC}(\rho\sin\vartheta_\tau)\right]\Bigg\}\langle \mathscr{Y}_{j\ell}|\Psi\rangle\end{aligned} \tag{2.24}$$

It is important to make the distinction that integrating over the angles of s_τ and S_τ changes H; the angular momentum operators are replaced by their eigenvalues. Making use of the identity operator $\mathrm{I} = \sum_n |\mathscr{Y}_n\rangle\langle\mathscr{Y}_n|$ with n as a composite index representing j and ℓ, we have

$$\sum_n \langle \mathscr{Y}_m|H|\mathscr{Y}_n\rangle\langle \mathscr{Y}_n|\Psi\rangle = H'\delta_{mn}\langle \mathscr{Y}_n|\Psi\rangle \tag{2.25}$$

Furthermore, we can see from equation 2.18 that

$$\left\langle \mathscr{Y}_n(\hat{s},\hat{S})\middle|\Psi(\vec{\rho})\right\rangle = \frac{2}{\rho^{5/2}\sin(2\vartheta_\tau)}\Upsilon_n(\rho;\vartheta_\tau)\Gamma_n(\rho) \tag{2.26}$$

so making this substitution and then multiplying from the left by $\rho^{5/2}\sin\vartheta_\tau/2$ gives

$$\begin{aligned}H'\Upsilon(\rho;\vartheta_\tau)\Gamma(\rho) = \Bigg\{ &\frac{-\hbar^2}{2\mu}\left[\frac{\partial^2}{\partial\rho^2}+\frac{1}{4\rho^2}\right]+\sum_{j'\ell'} V^{ABC}_{jj'\ell\ell'}(\vec{\rho}) - V^{BC}(\rho\sin\vartheta_\tau) \\ &-\frac{\hbar^2}{2\mu\rho^2}\left[\frac{\partial^2}{\partial\vartheta_\tau^2}-\frac{\ell(\ell+1)}{\cos^2\vartheta_\tau}-\frac{j(j+1)}{\sin^2\vartheta_\tau}+V^{BC}(\rho\sin\vartheta_\tau)\right]\Bigg\}\Upsilon(\rho;\vartheta_\tau)\Gamma(\rho)\end{aligned} \tag{2.27}$$

where again $s_\tau = \rho \sin \vartheta_\tau$. For a given value of ρ, the terms in square brackets in the second line of equation 2.27 above are identical to those of vibrational Hamiltonian in equation 2.20. By multiplying from the left with an Υ function and integrating over ϑ_τ, we now create matrix elements that are labeled by j, ℓ, and ν. Because Υ depends on ρ only parametrically, the kinetic energy matrix is still diagonal, but it is important to note that the set of Υ functions change continuously as ρ is varied – each new value of ρ requires a new basis set, but this is a difficulty handled by the propagator algorithm. Because of this parametrization, the terms in square brackets mentioned earlier can be replaced by the eigenvalue, $\mathcal{E}$, of equation 2.20,

$$H'' \left\langle \Upsilon_{\nu j \ell} \mathscr{Y}_{j\ell} | \Psi \right\rangle = \left\{ \frac{-\hbar^2}{2\mu} \left[\frac{\partial^2}{\partial \rho^2} + \frac{1}{4\rho^2} \right] + \sum_{j'\ell'\nu'} V^{ABC}_{jj'\ell\ell'\nu\nu'} i(\rho) - \sum_{\nu'} V^{BC}_{\nu\nu'}(\rho) - [\mathcal{E}_{\nu j \ell}(\rho)] \right\} \left\langle \Upsilon_{\nu j \ell} \mathscr{Y}_{j\ell} | \Psi \right\rangle \quad (2.28)$$

where in similar fashion to equation 2.25, we have

$$\sum_n \left\langle \Upsilon_m | H' | \Upsilon_n \right\rangle \left\langle \Upsilon_n | \Psi \right\rangle = H'' \delta_{mn} \left\langle \Upsilon_n | \Psi \right\rangle \quad (2.29)$$

As matrices, the above equation 2.28 can be more simply expressed using the notation

$$[\mathbf{T}_\rho]_{mn} = \left\langle \Upsilon_m \mathscr{Y}_m \left| \frac{-\hbar^2}{2\mu} \frac{\partial^2}{\partial \rho^2} \right| \Upsilon_n \mathscr{Y}_n \right\rangle \qquad Diagonal \quad (2.30)$$

$$\left[\mathbf{V^{ABC}}\right]_{mn} = \left\langle \Upsilon_m \mathscr{Y}_m \left| \frac{-\hbar^2}{2\mu} V^{ABC} \right| \Upsilon_n \mathscr{Y}_n \right\rangle \qquad Non-Diagonal \quad (2.31)$$

$$\left[\mathbf{V^{BC}}\right]_{mn} = \left\langle \Upsilon_m \mathscr{Y}_m \left| \frac{-\hbar^2}{2\mu} V^{BC} \right| \Upsilon_n \mathscr{Y}_n \right\rangle \qquad Diagonal \quad (2.32)$$

$$[\mathbf{E}]_{mn} = \left\langle \Upsilon_m \mathscr{Y}_m \left| \mathcal{E} - \frac{\hbar^2}{8\mu\rho^2} \right| \Upsilon_n \mathscr{Y}_n \right\rangle \qquad Diagonal \quad (2.33)$$

where m and n have been used as composite indices to represent one or all ν,j, and ℓ, as appropriate. With these, equation 2.28 can be rewritten as

$$[\mathbf{H}] = [\mathbf{T}] + \left[\mathbf{V^{ABC}}\right] - \left[\mathbf{V^{BC}}\right] - [\mathbf{E}] \tag{2.34}$$

Like the Jacobi $\zeta(s_\tau)$ functions, the states considered "bound" are those that correspond to a atom+diatom result, and for these the $\Upsilon(\vartheta_\tau)$ functions have a negative energy relative to the three-body break-up limit. Also, the continuum states here have positive energies that approach zero. Different from the continuum $\zeta(s_\tau)$ functions, though, the continuum $\Upsilon(\vartheta_\tau)$ states are bounded by the finite domain of ϑ_τ, which is $[0, \pi/2]$. Therefore, they have a discrete energy spectrum and a finite range of amplitude in hyperspherical coordinates, and integrals over these states are manageable.

2.3 APH Hamiltonian and Wavefunctions

The APH coordinates of Pack and Parker[8] have a much more complicated transformation from Delves or Jacobi coordinates than what what Delves and Jacobi coordinates share between them, and visualizing the motion of the atoms in relation to changes in the coordinates is more difficult. An explanation of these coordinates is given in appendix B.3. The APH Hamiltonian is

$$\begin{aligned} H = &- \frac{\hbar^2}{2\mu\rho^5}\frac{\partial}{\partial\rho}\rho^5\frac{\partial}{\partial\rho} - \frac{\hbar^2}{2\mu\rho^2}\left[\frac{4}{\sin 2\theta}\frac{\partial}{\partial\theta}\sin 2\theta\frac{\partial}{\partial\theta} + \frac{1}{\sin^2\theta}\frac{\partial^2}{\partial\chi^2}\right] \\ &+ \frac{J_x^2}{\mu\rho^2(1+\sin\theta)} + \frac{J_y^2}{2\mu\rho^2\sin^2\theta} + \frac{J_z^2}{\mu\rho^2(1-\sin\theta)} - \frac{i\hbar\cos\theta}{\mu\rho^2\sin^2\theta}J_y\frac{\partial}{\partial\chi} + V(\vec{\rho} \end{aligned} \tag{2.35}$$

As before, the intention is to propagate in ρ, and so we expand Ψ in a set of functions in the coordinates θ and χ, with a set of coefficients $\psi(\rho)$,

$$\Psi^{JMpn} = 4\sum_{t,\Lambda} \frac{1}{\rho^{5/2}} \psi_{t\Lambda}^{Jpn}(\rho) \Phi^{Jp} t\Lambda(\theta, \chi; \rho_\xi) \hat{D}^{Jp}_{\Lambda M}(\alpha, \beta, \gamma) \tag{2.36}$$

where here Λ is the body-fixed (BF) projection of J. The $\hat{D}$ functions are the Wigner rotation functions of the Euler angles, $\alpha\beta\gamma$, that rotate from a space-fixed coordinate system to a body-fixed one. The $\Phi(\theta, \chi; \rho_\xi)$ function is called a *surface function*, as it is the solution to the Hamiltonian of the APH surface at a constant ρ_ξ.

It should be noted that the Hamiltonians of equations 2.9, 2.19, and 2.35 are all the same Schrödinger equation, just expressed in different coordinate systems. Furthermore, while labeled differently depending on the definition of an initial and final channel, the full wavefunctions, Ψ, defined in equations 2.12, 2.18, and 2.36 are all equivalent.

The motions of the three atoms described by changing either θ or χ alone is not easily describable as a rotational or vibrational motion, and the APH Hamiltonian of equation 2.35 is not separable into equations that could define functions of θ alone or χ alone, as was done in the Jacobi system with $s_\tau, S_\tau, \Theta_\tau$, or in the Delves system with $\rho, \vartheta_\tau, \Theta_\tau$. The Φ surface functions are solutions to the differential equation (equation 164 in reference [8]),

$$H^{J\Lambda}_{surf} \Phi^J_{t\Lambda}(\theta, \chi; \rho_\xi) = \mathcal{E}^J_{t\Lambda}(\rho_\xi) \Phi^J_{t\Lambda}(\theta, \chi; \rho_\xi) \tag{2.37}$$

where H_{surf} is the APH surface Hamiltonian defined at a constant value of $\rho = \rho_\xi$, which is given as,

$$H_{surf} = \frac{-\hbar^2}{2\mu\rho_\xi^2}\left[\frac{4}{\sin(2\theta)}\frac{\partial}{\partial\theta}\sin(2\theta)\frac{\partial}{\partial\theta} + \frac{1}{\sin^2(\theta)}\frac{\partial^2}{\partial\chi^2}\right] + \frac{A+B}{2}\hbar^2 J(J+1) + \frac{15\hbar^2}{8\mu\rho_\xi^2} + \left[C - \frac{A+B}{2}\right]\hbar^2\Lambda^2 + V(\rho_\xi, \theta, \chi) \quad (2.38)$$

where A, B, and C are defined as

$$A = \frac{1}{\mu\rho_\xi^2(1+\sin\theta)} \quad (2.39\text{-a})$$

$$B = \frac{1}{2\mu\rho_\xi^2\sin^2\theta} \quad (2.39\text{-b})$$

$$C = \frac{1}{\mu\rho_\xi^2(1-\sin\theta)} \quad (2.39\text{-c})$$

It is possible to solve for $\Phi(\theta, \chi; \rho_\xi)$ numerically by several methods. In Pack and Parker's original paper on the APH coordinate system[8], surface functions were generated for the H_3 system using a finite element method (FEM). It is also possible to use analytic functions, such as hyperspherical harmonics or set of orthogonal polynomials, but such bases usually do not represent the physical system well, and many basis functions are required.

A notable difference to the Delves and Jacobi formulation is that this equation has body-fixed labels rather than space-fixed. Either a space-fixed or body-fixed system can be used, they are equivalent up to a unitary transformation by Wigner rotation functions. In the space-fixed frame, a set of coordinate axes is chooses such that the projection of the total angular momentum along the z axis is given by M. In a body-fixed frame, a set of coordinates is chosen relative to the position

of the atoms, and the total angular momentum projection on the body-fixed z axis is given by Λ. The choice to use a body-fixed coordinate system here will be explained in section 4.3.

With the definition of H_{surf} in equation 2.38, the APH Hamiltonian of 2.35 can be written as

$$H = H_{surf} + T_\rho + T_c + T_a \tag{2.40}$$

where T_ρ are the kinetic terms associated with ρ, and T_c and T_a are the Coriolis and Asymmetric-Top terms that arise from the angular momentum operators. The Coriolis and asymmetric-top terms will be discussed in more detail in chapter 4, but for now it should be noted that these two terms couple the $\Phi^J_{t\Lambda}$ functions of different Λ values; the Coriolis terms couple states of Λ with $\Lambda \pm 1$, and the asymmetric-top operator couples states of Λ with $\Lambda \pm 2$.

Chapter 3

Collision Induced Dissociation of the Helium-Neon$_2$ System

The method of constructing physically-motivated basis functions from asymptotic states was first tested on the HNe_2 system that was studied by Parker et al.[13] and Colavecchia et al.[14] as a system to exemplify collision-induced dissociation (CID) in a single channel.

In the above-noted work on HNe_2, the masses of the atoms were reduced from their physical values to 0.7 amu for Hydrogen and to 16.025757 amu for Neon. The purpose behind this alteration was that, with these masses, there existed n HNe diatomic bound states. As a result, there was no possibility of a reactive scattering process (i.e. no H + NeNe $\rightarrow$ Ne+HNe reaction), and the problem can be handled effectively with a single channel set of Delves or Jacobi coordinates.

In this chapter we look at the methods used by Parker et al.[13] and Colavecchia et al.[14] to solve the problem and compare these methods to one where we replace the basis set with the asymptotic bound, quasibound, and continuum solutions. The results of these calculations are then presented in section 3.6.

3.1 Replacement Functions

In the work done on the HNe_2 system[13, 14], the $\Upsilon(\vartheta_\tau)$ vibrational basis functions were determined by calculating numerical solutions of the equation 2.20, rewritten here,

$$\left[\frac{-\hbar^2}{2\mu\rho_\xi^2}\left(\frac{\partial^2}{\partial\vartheta_\tau^2} - \frac{j(j+1)}{\sin^2(\vartheta_\tau)} - \frac{\ell(\ell+1)}{\cos^2(\vartheta_\tau)}\right) + V^{BC}(\rho_\xi \sin\vartheta_\tau)\right]\Upsilon_{\nu j\ell}(\rho_\xi;\vartheta_\tau)$$
$$= H_{vib}\Upsilon_{\nu j\ell}(\rho_\xi;\vartheta_\tau) = \mathcal{E}_{\nu j\ell}(\rho_\xi)\Upsilon_{\nu j\ell}(\rho_\xi;\vartheta_\tau)$$

where again, V^{BC} is the two body potential of diatom BC. This set of functions, in conjunction with the coupled spherical harmonic functions $\mathscr{Y}_{j\ell}^{JM}(\hat{s_\tau},\hat{S_\tau})$, form the "propagation" or "adiabatic" basis set. This basis is ideal in that it it automatically forms a set of orthonormalized, physically motivated basis functions, and as ρ increases and the three-body contributions to the potential energy surface diminish, this basis approaches exact solutions for the Delves surface functions.

The downside to this basis is the need to recalculate it at every propagation step. For a small basis, this is not infeasible, but it does become unwieldy or impossible for a large basis set. The HNe_2 problem also has a distinct advantage in calculating basis functions in this way because only one channel needs to be accounted for; there is no HNe diatom. Furthermore, the Delves surface functions are separable in terms of ϑ_τ and Θ_τ. The coupled spherical harmonic functions, $\mathscr{Y}(\Theta_\tau)$, are analytically known, and only the vibrational Υ functions need to be calculated.

The intention is to replace these Υ functions with bound and quasibound state functions that are based on the diatomic Hamiltonian for the Ne_2 diatom, and continuum functions that are related to the zero energy solutions of equation 2.20.

The diatomic Hamiltonian in mass-scaled Jacobi coordinates is

$$H^{BC}\zeta_\nu(s) = \epsilon_\nu\zeta_\nu(s) = \left[\frac{-\hbar^2}{2\mu}\frac{\partial^2}{\partial s^2} + \frac{\hbar^2}{2\mu}\frac{j(j+1)}{s^2} + V^{BC}(s)\right]\zeta_\nu(s) \tag{3.1}$$

where by virtue of using the three-body reduced mass, μ, the two-body Hamiltonian can be written in terms of s, a three-body coordinate, that still describes the internuclear distance between atoms B and C.

To understand how making basis functions from a diatomic Hamiltonian for use in a triatomic scattering problem, it is important to show the connection between the Υ and ζ functions, and the Hamiltonian equations that define them (equations 2.20 and 3.1).

As the system approaches the A+BC asymptotic configuration, the value of ρ becomes very large while the value of $s_\tau = \rho\sin(\vartheta_\tau)$ remains relatively small. Thus, using the large ρ limit and the small ϑ_τ approximation of $\vartheta_\tau \approx \sin\vartheta_\tau$, we have

$$\frac{\partial^2}{\partial s_\tau^2} = \frac{\partial^2}{\partial(\rho^2\sin^2\vartheta_\tau)^2} = \frac{1}{\rho^2}\frac{\partial^2}{\partial\vartheta_\tau^2} \tag{3.2}$$

It can also be shown that there is a direct relationship between derivatives with respect to the mass-scaled Jacobi coordinate s_τ, and the non-mass-scaled Jacobi coordinate r_τ such that

$$\frac{\partial^2}{\partial s_\tau^2} = d_\tau^2\frac{\partial^2}{\partial r_\tau^2} \tag{3.3}$$

where d_τ is the mass-scaling factor and is dependent on the arrangement channel, τ, which in this example is arrangement A. It can be further shown, with a bit of

algebra, that there is a relationship between the three-body reduced mass, μ, the two-body reduced mass for the diatom BC, μ_2, and the mass-scaling factor d_A,

$$\mu = \mu_2 / d_\tau^2 \tag{3.4}$$

which allows for the relation (in the limit of $S_\tau \to \infty$),

$$\frac{1}{2\mu}\frac{1}{\rho^2}\frac{\partial^2}{\partial\vartheta_\tau^2} \to \frac{1}{2\mu}\frac{\partial^2}{\partial(\rho\sin\vartheta_\tau)^2} = \frac{1}{2\mu}\frac{\partial^2}{\partial s_\tau^2} = \frac{d_\tau^2}{2\mu}\frac{\partial^2}{\partial r_\tau^2} = \frac{1}{2\mu_2}\frac{\partial^2}{\partial r_\tau^2} \tag{3.5}$$

Here we can see that in the asymptotic limit of $S_\tau \to \infty$, the derivative term with respect to ϑ_τ in equation 2.20 directly relates to the derivative term with respect to r_τ, the BC diatomic internuclear distance, that is in equation 3.1.

Now we look at the other terms of equation 2.20 in the limit of $\rho \to \infty$ and $\vartheta_\tau \approx \sin\vartheta_\tau$ (or $S_\tau \to \infty$, s_τ finite):

$$\frac{\hbar^2}{2\mu\rho^2}\frac{\ell(\ell+1)}{\cos^2\vartheta_\tau} \to \frac{\hbar^2}{2\mu}\frac{\ell(\ell+1)}{S_\tau^2} = 0 \tag{3.6}$$

$$\frac{\hbar^2}{2\mu\rho^2}\frac{j(j+1)}{\sin^2\vartheta_\tau} \to \frac{\hbar^2}{2\mu}\frac{j(j+1)}{s_\tau^2} = \frac{\hbar^2}{2\mu_2}\frac{j(j+1)}{r_\tau^2} \tag{3.7}$$

$$V^{ABC}(\vec{\rho}) \to V^{BC}(r) \tag{3.8}$$

where equation 3.8 is necessarily true as atom A is being removed infinitely far away as $S \to \infty$.

Observing the terms of equation 2.20, which I will reprint here for convenience,

$$\begin{aligned} H_{vib}\Upsilon_{j\ell\nu}(\rho_\xi;\vartheta_\tau) &= \left[\frac{-\hbar^2}{2\mu\rho_\xi^2}\left[\frac{\partial^2}{\partial\vartheta_\tau^2} - \frac{j(j+1)}{\sin^2(\vartheta_\tau)} - \frac{\ell(\ell+1)}{\cos^2(\vartheta_\tau)}\right] + V^{BC}(\rho_\xi\sin\vartheta_\tau)\right]\Upsilon_{j\ell\nu}(\rho_\xi;\vartheta_\tau) \\ &= \mathcal{E}_{j\ell\nu}(\rho_\xi)\Upsilon_{j\ell\nu}(\rho_\xi;\vartheta_\tau) \end{aligned}$$

and the terms of equation 3.1,

$$H^{BC}\zeta_\nu(s_\tau) = \epsilon_\nu\zeta_\nu(s_\tau) = \left[\frac{-\hbar^2}{2\mu}\frac{\partial^2}{\partial s_\tau^2} + \frac{\hbar^2}{2\mu_2}\frac{j(j+1)}{s_\tau^2} + V^{BC}(s)\right]\zeta_\nu(s_\tau)$$

it is apparent that in the limit of $S_\tau \to \infty$ or $\rho \to \infty$ and $\vartheta_\tau \approx \sin\vartheta_\tau$, these two equations are identical; $H_{vib} \to H^{BC}$. Therefore, it can be concluded that

$$\Upsilon(\rho, \vartheta_\tau) \to \zeta(r_\tau) \tag{3.9}$$

For clarity, it must be noted that this is true only for the bound states – that is, those states corresponding to a low enough energy that it is not possible for atoms B and C to separate and the small angle approximation can be used for ϑ_τ. It is only with this condition that these limits may be taken. Otherwise, it would be possible for s_τ to approach infinity as well, but as it stands, s_τ is finite and only the limit of $S_\tau \to \infty$ need be considered.

3.2 Bound, Quasibound State Replacement

The bound and quasibound $\Upsilon(\vartheta_\tau)$ functions are replaced with projections of the bound and quasibound $\zeta(\rho\sin\vartheta_\tau)$ functions at some intermediate value of ρ. As discussed in reference [13], asymptotically the bound state basis functions approach a constant, negative energy, while the quasibound states approach a constant, positive energy.

This is accomplished by identifying the Υ functions with quantum labels $\nu j\ell$that correspond to the known bound and quasibound "asymptotic" states, which are the known diatomic solutions $\zeta(s_\tau)$ and substituting ζ functions that correspond

to the same values of ϑ_τ as the original Υ functions did. The ζ are functions of s_τ, not ϑ_τ, what we are really doing is projecting the function $\zeta(s)$ onto the constant ρ_ξ surface by use of the relation $s_\tau = \rho_\xi \sin(\vartheta_\tau)$.

In section 2.2, we showed how the full Hamiltonian of the problem could be simplified by expanding the solution, Ψ, in a basis set where the basis functions were defined by some of the operators in the Hamiltonian, thereby allowing us to substitute operators with eigenvalues.

We have shown that the solutions to equation 2.20, Υ, are equivalent to the solutions to equation 3.1,ζ, in the asymptotic case. For $S < \infty$, this equivalence is not true. This is of critical importance, because using the solutions to the vibrational, three-body Hamiltonian in equation 2.20 as a basis set is only sensible while the functions are orthogonal to each other, are representative of the physical system, and as a basis are compete enough to accurately describe Ψ. The substituted ζ functions, while they do represent an asymptotic case of the $A + BC$ system, are not orthogonal to the continuum state solutions of the vibrational surface function equation, 2.20.

The new basis most easily represented as

$$\{\bar{\Upsilon}\} = \{\Upsilon\} - \{\Upsilon_{bound}\} + \{\zeta_{bound}\} \tag{3.10}$$

In order to recreate an orthonormal basis set to represent the vibrational motion of the BC diatom, we must orthonormalize the set of functions. There are multiple ways in which we can do this, and the option of which method to use is left open.

Once the set of functions $\{\bar{\Upsilon}\}$ have been orthonormalized, the matrix elements of equation 2.28 must be recalculated. The $\{\bar{\Upsilon}\}$ basis functions are *not* eigenfunctions of the Hamiltonian operator in equation 2.20, and therefore the operator

terms in the Full Hamiltonian that are used in the vibrational Hamiltonian, equation 2.20, to define the Υ functions cannot be replaced with the eigenvalues $\mathcal{E}$, as was done with the $\{\Upsilon\}$ basis. This means that the matrix, whose elements are defined by equation 2.33, is no longer diagonal, and a new equation for propagation must be employed after this replacement is made.

Similar to equations 2.30-2.33, we now have

$$[\mathbf{T}_\rho]_{mn} = \left\langle \bar{\Upsilon}_m \mathscr{Y}_m \middle| \frac{-\hbar^2}{2\mu} \frac{\partial^2}{\partial \rho^2} \middle| \bar{\Upsilon}_n \mathscr{Y}_n \right\rangle \qquad Diagonal \qquad (3.11)$$

$$\left[\bar{\mathbf{V}}^{\mathbf{ABC}}\right]_{mn} = \left\langle \bar{\Upsilon}_m \mathscr{Y}_m \middle| \frac{-\hbar^2}{2\mu} V^{ABC} \middle| \bar{\Upsilon}_n \mathscr{Y}_n \right\rangle \qquad Non-Diagonal \qquad (3.12)$$

$$\left[\mathbf{V}^{\mathbf{BC}}\right]_{mn} = \left\langle \bar{\Upsilon}_m \mathscr{Y}_m \middle| \frac{-\hbar^2}{2\mu} V^{BC} \middle| \bar{\Upsilon}_n \mathscr{Y}_n \right\rangle \qquad Diagonal \qquad (3.13)$$

$$\left[\bar{\mathbf{E}}\right]_{mn} = \left\langle \bar{\Upsilon}_m \mathscr{Y}_m \middle| H_{vib} - \frac{\hbar^2}{8\mu\rho^2} \middle| \bar{\Upsilon}_n \mathscr{Y}_n \right\rangle \qquad Non-Diagonal \qquad (3.14)$$

Note that the full potential term is different than in equation 2.31 due to integration over a different basis set, as is the $\mathbf{E}$ term different. The most notable change is in equation 3.14, in which the eigenvalue $\mathcal{E}$ has been replaced with the vibrational Hamiltonian since $\bar{\Upsilon}$ is no longer an eigenfunction of this operator. This also means that $\mathbf{E}$ is not diagonal. The $\mathscr{Y}$ functions are not altered; $\mathbf{E}$ is still block-diagonal with respect to given values of j and ℓ. The only matrix elements of $\mathbf{E}$ that need to be calculated directly are those with the same values of j and ℓ.

3.3 Continuum State Replacement

The continuum state functions are physically motivated by the structure of the zero-potential continuum solutions of the Delves internal Hamiltonian, equation 2.20, rewritten here for convenience,

$$H_{vib}\Upsilon_{j\ell\nu}(\rho_\xi;\vartheta_\tau) = \left[\frac{-\hbar^2}{2\mu\rho_\xi^2}\left[\frac{\partial^2}{\partial\vartheta_\tau^2} - \frac{j(j+1)}{\sin^2(\vartheta_\tau)} - \frac{\ell(\ell+1)}{\cos^2(\vartheta_\tau)}\right] + V^{BC}(\rho_\xi \sin\vartheta_\tau)\right]\Upsilon_{j\ell\nu}(\rho_\xi;\vartheta_\tau)$$
$$= \mathcal{E}_{j\ell\nu}(\rho_\xi)\Upsilon_{j\ell\nu}(\rho_\xi;\vartheta_\tau) \tag{3.15}$$

The solutions to this differential equation for a zero potential are Jacobi polynomials, $\mathscr{P}_{\nu j\ell}(\vartheta_\tau)$, multiplied by sine and cosine terms that depend on the values of j and ℓ. They have the form of

$$\varphi^C_{j\ell n}(\vartheta_\tau) = \sin^{j+1}(\vartheta_\tau)\cos^{\ell+1}(\vartheta_\tau)\mathscr{P}_{j\ell n}(2\vartheta_\tau) \tag{3.16}$$

where the superscript C denotes the continuum function. The Jacobi polynomials are analytically known, and the function $\phi^C(\vartheta_\tau)$ is the exact solution of the internal Delves Hamiltonian with a zero potential. These functions are also labeled by j, ℓ, and n, which serve as the quantum number labels for these "vibrational" continuum functions.

An important note to make regarding the "vibrational" quantum number ν and its relation to the label n in the above functions is that, though they represent the same *quality* of the function, they are not the same number. The basis functions label $\nu = 0$ as the lowest state, which in this case and most others, is the lowest bound state. A value of $n = 0$ in equation 3.16 gives the Jacobi polynomial with zero nodes, which is the lowest continuum state. Therefore, n relates to ν as

$\nu = n + n_{bqb}$, where n_{bqb} is the number of bound and quasibound states. Some care must be taken in keeping these number straight in practice to ensure the continuum states are faithfully represented, for neglecting this difference produces continuum states with too many nodes.

As $\rho \to \infty$, the range for the diatom well region diminishes to zero, and the continuum eigenstates approach the functions of equation 3.16. The effect of the two-body potential is that more nodes are added in the well region, and the wavefunction is shifted in accordance with the two-body scattering length.

These effects can be included in the constructed continuum states by first calculating the two-body, zero energy wavefunction in s, converting this to be a function of ϑ_τ, and using this data in place of the $\sin^{j+1}$ term. Thus, we seek the solution to

$$\frac{-\hbar^2}{2\mu}\left(\frac{\partial^2}{\partial s_\tau^2} + \frac{j(j+1)}{s_\tau^2}\right)\phi_j^{C0}(s_\tau) + V(s_\tau)\varphi_j^{C0}(s_\tau) = 0 \tag{3.17}$$

This appropriately adds the extra nodes to the continuum functions, as well as shifting the wavefunction closer or farther from the diatom coalition point. Since this zero-energy, non-zero potential diatom solution is constant (as a function of s_τ) throughout the propagation, it needs to be calculated only once for each value of j.

Thus, the constructed continuum function in entirety for the ϑ_τ coordinate is

$$\varphi_{j\ell\nu}^{C}(\vartheta_\tau) = \varphi_j^{C0}(\vartheta_\tau)\cos^{\ell+1}(\vartheta_\tau)\mathscr{P}_{j,\ell,\nu-nbqb}(\vartheta_\tau) \tag{3.18}$$

and, like for the bound states, the surface function is φ^C multiplied by the coupled spherical harmonic function, $\mathscr{Y}_{j\ell}^{JM}(\hat{s_\tau}, \hat{S_\tau})$

3.4 Orthonormalization and Eigenvalues

The ϕ functions so far constructed for the bound, quasibound, and continuum states are not orthonormal, though they do represent the physical features of the exact eigenfunctions of the internal Hamiltonian. For the propagation stage, it is necessary to get the eigenvalues of the internal Hamiltonian in this basis, and for matching it is important that these basis functions, which are serving as the primitive basis, be orthonormal.

Orthonormalization can be accomplished by a Graham-Schmidt procedure, or through an overlap matrix. Computationally, constructing an overlap matrix is no more expensive than the Graham-Schmidt procedure, and has the benefit that can be incorporated directly with diagonalizing the Hamiltonian. This is done by solving the eigenvalue equation

$$H_{int}X = OXE \tag{3.19}$$

Where H is the Hamiltonian matrix in the ϕ basis, and O is the overlap matrix, and X are the non-orthonormal eigenvectors. By multiplying on the left by $O^{-1/2}$ and using an identity between H and X, we can rewrite this equation as

$$O^{-1/2}HO^{-1/2}O^{1/2}X = O^{1/2}XE \tag{3.20}$$

Solving this equation for $O^{1/2}X$ does give orthonormal eigenvectors, and the correct eigenvalues of the internal Hamiltonian as solved by the orthonormalized set of the ϕ functions. Multiplying H_{int} on both sides with $O^{-1/2}$ has the effect of orthonormalizing the basis H_{int} is represented in, which is in this case the constructed basis.

However, to calculate the $O^{1/2}$ matrices requires another diagonalization step. The O matrix is constructed and diagonalized. The eigenvectors of this diagonalization step are stored. Then, the square root of each eigenvalue is taken, and the matrix transformed back by reapplying the transformation matrix of eigenvectors, requiring two matrix multiplications and one matrix solve. This is in addition to diagonalizing the H_{int} matrix. For a large basis set, this can greatly increase the time required in the calculation.

After diagonalization of the Hamiltonian, by which ever orthonormalization procedure, the eigenvectors produced are, as normal, coefficients of the given basis that produce orthonormalized eigenvectors associated with the Hamiltonian's eigenvalues.

There are a few more points in this process that one must be very careful about. Diagonalization routines generally order the eigenvalues of the matrix in some fashion. The LAPACK eigenvalue routines order the eigenvalues in ascending order. If one is trying to maintain labels on the basis functions, an unnecessary but often useful practice, then the diagonalization procedure can reorder the states, and thus confuse the state labels. This is especially true when the spectrum of eigenenergies spans many rovibrational states. In practice if the states are sorted by rotational quantum numbers, this ordering will be destroyed if the states are reordered by energy. Therefore it is useful to construct and diagonalize the internal Hamiltonian in blocks of like angular momentum quantum numbers. In Delves coordinates, this is particularly useful since the angular momentum functions associated with the basis are coupled spherical harmonics indexed by the j and ℓ quantum numbers.

Basis states of different j and ℓ values are orthogonal by definition of the spherical harmonics, and there is no coupling between angular momentum blocks in the internal Hamiltonian matrix or the overlap matrix.

Within a specific angular momentum block, energy sorting can still mis-align the states with their labels. This can occur if there are quasibound states among the basis functions. Asymptotically, continuum states approach zero energy, while quasibound states approach a positive constant. Continuum states that are at one value of ρ higher in energy than the quasibound states will eventually drop below the quasibound state in energy ordering. If only a set number of the lowest energy states are kept in the basis, then the basis function representing the quasibound states eventually drops from the basis as more continuum states are included. However, if in the formulation process of the basis the quasibound state is faithfully represented, then there is no concern of whether it stays in the basis. If the labels can be disregarded, then there is no concern of this reordering.

3.5 HNe_2 Symmetry Analysis

The potential energy surface for the HNe_2 system belongs to the totally symmetric A_1 irreducible representation of the C_{2v} point group. In this point group, there are two reflection planes, and a single C_2 rotation, which can be seen in Figure 3.1. The dashed line in the figure is a reflection plane, as is the horizontal solid line (all of the solid lines represent reaction channels). A positive reflection in the plane of the dashed line corresponds to an even parity, as does a positive C_2 rotation. The reflection plane containing the horizontal solid line along the NeNe channel can also be positive or negative. It is positive for all states of the Ne_2 diatom that

have an even j rotation quantum number, and the reflection is likewise negative for all rotations for which j is odd for the diatom.

The Ne_2 diatomic arrangement channel is the horizontal solid line in Figure 3.1. This channel is aligned with a reflection plane element of the C_{2v} group. If this reflection is even, then it means that the rotational quantum number of the Ne_2 diatom cannot be odd, for if j were odd, then the wavefunction value would be a different sign above this line then it would be below, constituting an odd reflection. Therefore, when calculating this scattering interaction for a single irreducible representation, only even or odd values of j can be included for this channel.

This is not to say that even and odd values of j cannot be coupled, ever. It does mean that they cannot be coupled when it violates the symmetry of the wavefunction, and this is simply because states belonging to different irreducible

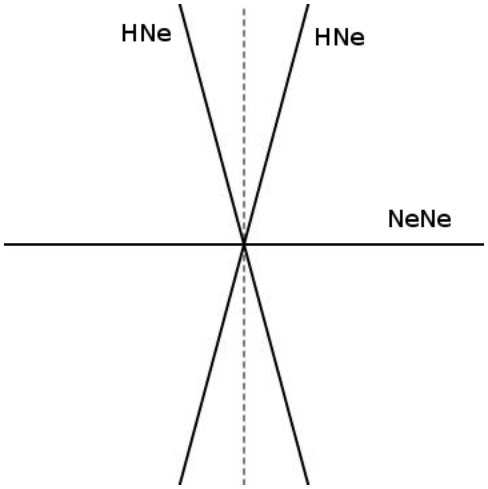

Figure 3.1: Potential surface symmetry for the HNe_2 system in APH coordinates, belonging to the C_{2v} point group in APH coordinates. The solid lines show where two atoms coalesce in a given arrangement channel. The vertical dashed line and the horizontal solid line represent the two reflection planes of C_{2v}.

representations cannot couple. Therefore, all wavefunctions in irreducible representation A_1 will have even values of j, all wavefunctions in irreducible representation A_2 will have odd j values, and so on for B_1 and B_2.

This separation of even and odd j values is not true for the other two channels. In the calculated and published results for HNe2 [13, 14], the masses of the nuclei were scaled to disallow any HNe channels. Still, for this an any AAB type system where the irreducible representation is C_{2v} the heteronuclear diatomic channels are not aligned with any reflection symmetry elements, and therefore the irreducible representation of the system does not affect the rotational levels

3.6 Results of HNe_2 Calculations

The goal of this calculation was to test whether using an asymptotic basis set for the formulation of adiabatic bases was effective. To this end, it is worth noting that there were no changes in the transition probabilities of the bound state interactions. This is not true of the continuum functions due to the quasibound state.

Figure 3.2 shows an energy correlation diagram for a 25 channel problem. All states up to $\lambda = 16$, where λ is defined as $2\nu + j + \ell$, were included in the propagation. Notable is the mostly flat line at positive energies that corresponds to the $j = 4$ quasibound state. In the original formulation of the problem, the lowest 25 energy states were included in the propagation basis, according to their allowable values of $\nu j \ell$, and we see that at around 235 Bohr, this state looses quasibound character. Were more basis functions included, we would see avoided crossing instead. As it is, by this point, the quasibound state is no longer represented in the basis functions.

In the new method, the eigenfunctions of the Delves' vibrational equation (eqn. 2.20) for bound and quasibound states are explicitly included in the basis as projections of the asymptotic states. As a result, the quasibound state never leaves the basis, as is shown in figure 3.3.

The transition probabilities for energies less than three-body breakup were not affected significantly by this change, as can be seen in comparing the ground state to ground state $\nu = 0, j = 0$ to $\nu = 0, j = 0$ transition probabilities in figures 3.4, transition probabilities without bound and quasibound state replacement, and 3.5, with the bound and quasibound state replacement.

It is very difficult to see the difference between the numbers in comparing the data in figures 3.4 and 3.5. The numbers actually differ by about 0.001% between the cases of using the replacement basis functions and the original basis functions at the lowest propagation energy. At higher energies, the transition probabilities differ by as much as 5%, but in either case of using the original basis functions or the replacement functions, the transition probabilities still oscillate at 300 Bohr with an amplitude of 10-15%, which indicates they are not converged results. The basis is simply too small at this energy, but the two methods to agree to within the margins of error. This indicates that the constructed basis set works nearly as well as using numerically exact solutions to the Delves' vibrational equations.

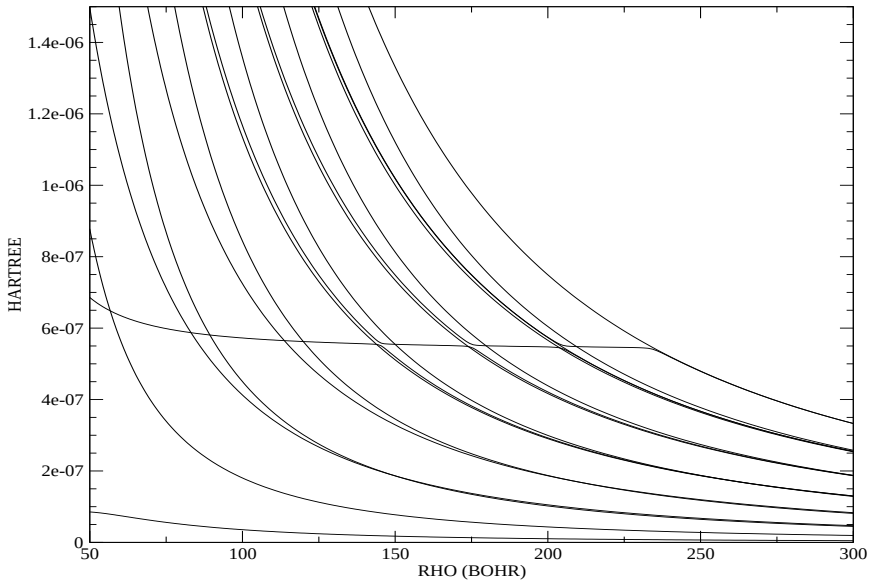

Figure 3.2: HNe_2 energy correlation diagram for 25 channels with the standard $\Upsilon(\vartheta_\tau)$ basis functions. No replacement functions used. Note that the quasibound state, appearing here as a line approaching a positive constant energy, eventually drops out of the basis.

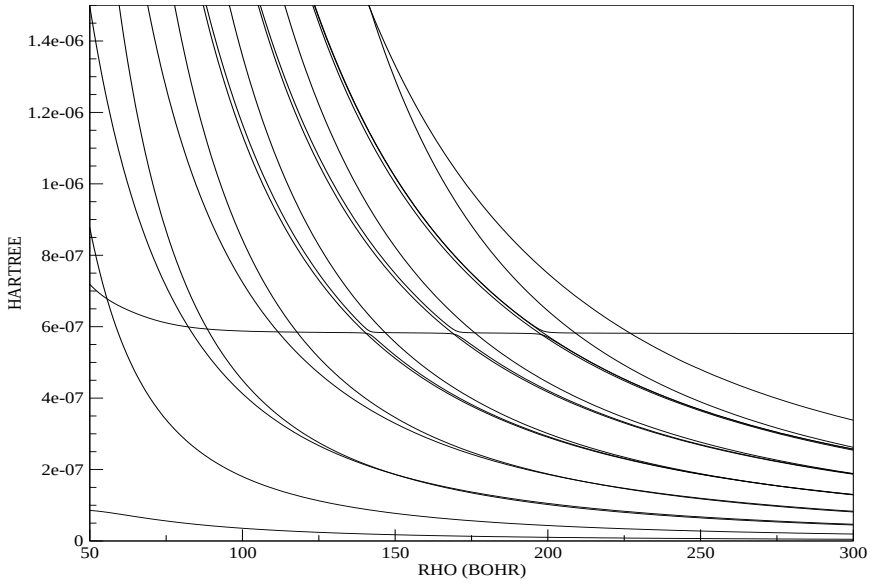

Figure 3.3: HNe_2 energy correlation with bound and quasibound states replace with asymptotic $\zeta(s_\tau)$ functions. Note that in comparison to figure 3.2, the quasibound state is kept in the basis.

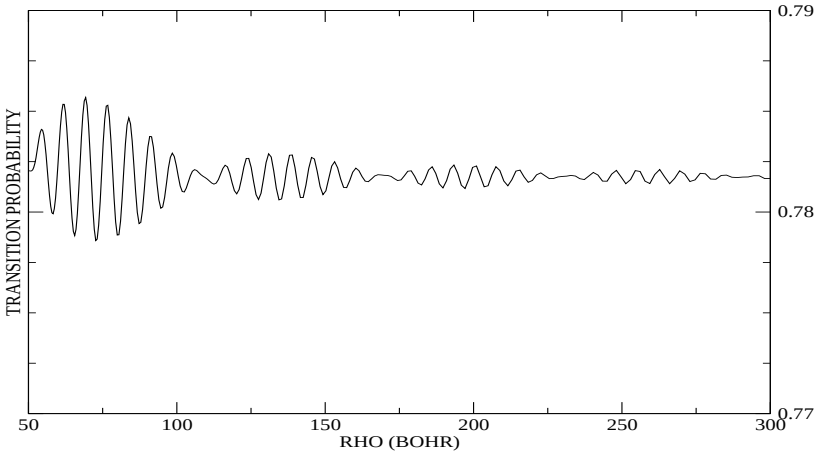

Figure 3.4: HNe_2 transition probabilities for $\nu j = 00$ to $\nu j = 00$, 25 channels, at $-47.5e-6$ Hartree without replacing bound or quasibound basis functions

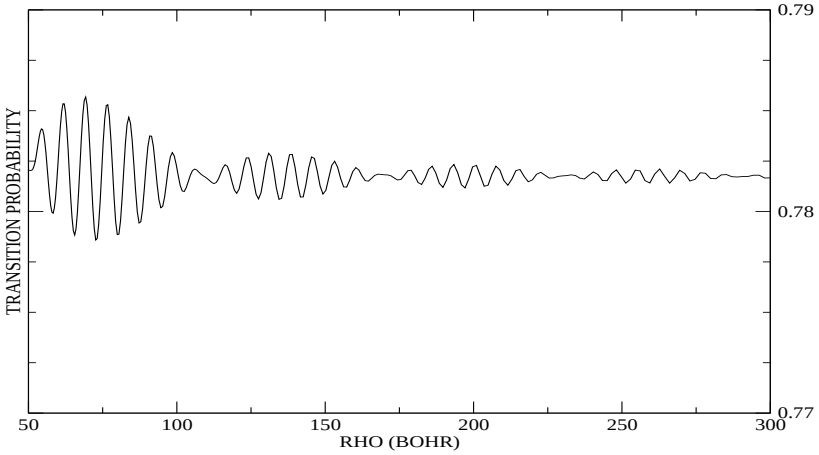

Figure 3.5: HNe_2 transition probabilities for $\nu j = 00$ to $\nu j = 00$, 25 channels, at $-47.5e-6$ Hartree with replacing bound and quasibound basis states with asymptotic diatom states.

Chapter 4

Three Atom Reactive Scattering with Collision Induced Dissociation

4.1 Introduction

Finding solutions to the Schrödinger equation in which the possible products of the scattering process are

$$\begin{aligned} &A + BC \\ &B + AC \\ &C + AB \\ &A + B + C \end{aligned} \tag{4.1}$$

is best handled in a coordinate system that can universally treat all channels without giving preference to any specific channel. For this we employ the Adiabatically Adjusting Principle-Axis Hyperspherical coordinate system of Pack and Parker[8]. A brief description of these coordinates is given in appendix B.3. This is an *internal* coordinate system, in that it describes the three coordinates that show the

relative positions of the atoms to each other, with the other six dimensions of the wavefunction described by the three Euler angles, $\alpha\beta\gamma$, and the three coordinates of the system's center of mass.

This problem differs from the discussion of the HNe_2 system in that all reactive scattering is possible, such that the system may undergo the exchange reactions of

$$A + BC \rightleftharpoons B + AC \rightleftharpoons C + AB \tag{4.2}$$

in addition to the possibility of $A + B + C$. The full Hamiltonian in this system is given by

$$H = T + V(\rho, \theta, \chi) \tag{4.3}$$

where

$$\begin{aligned} T = &- \frac{\hbar^2}{2\mu\rho^5}\frac{\partial}{\partial\rho}\rho^5\frac{\partial}{\partial\rho} - \frac{\hbar^2}{2\mu\rho^2}\left[\frac{4}{\sin 2\theta}\frac{\partial}{\partial\theta}\sin 2\theta\frac{\partial}{\partial\theta} + \frac{1}{\sin^2\theta}\frac{\partial^2}{\partial\chi^2}\right] \\ &+ \frac{J_x^2}{\mu\rho^2(1+\sin\theta)} + \frac{J_y^2}{2\mu\rho^2\sin^2\theta} + \frac{J_z^2}{\mu\rho^2(1-\sin\theta)} - \frac{i\hbar\cos\theta}{\mu\rho^2\sin^2\theta}J_y\frac{\partial}{\partial\chi} \end{aligned} \tag{4.4}$$

and $V(\rho, \theta, \chi)$ is the full three-body potential, which for our purposes here we assume to be defined at all points of ρ, θ, χ and to approach zero where all three atoms are infinitely separated.

We wish to find solutions to this equation, Ψ, that are wavefunctions with good quantum numbers of the total angular momentum J, the projection M of J on a fixed axis, and parity, p, such that we have

$$H\Psi^{JMpn}(\rho, \theta, \chi) = E_n\Psi^{JMpn}(\rho, \theta, \chi) \tag{4.5}$$

where n refers to the n^{th} solution of the Hamiltonian.

In six coordinates, including the rotations of the system described by the Euler angles, we define the n^{th} solution Ψ as in equation 2.36, repeated here

$$\Psi^{JMpn} = 4 \sum_{t,\Lambda} \rho^{-5/2} \psi_{t\Lambda}^{Jpn}(\rho) \Phi_{t\Lambda}^{Jp}(\theta, \chi; \rho_\xi) \hat{D}_{\Lambda M}^{Jp}(\alpha_Q, \beta_Q, \gamma_Q) \tag{4.6}$$

where t is simply a counting number, Λ is the body-fixed projection of the total angular momentum J, $\hat{D}$ are normalized Wigner rotation functions, and the Q labels on the Euler angles define a set of body fixed axes.

It should be noted that this is exactly the same wavefunction as that expressed in Delves hyperspherical coordinates in equation 2.18; the expansions are different, but the full wavefunction must be identical.

The challenge is to construct basis functions Φ that can be used for this expansion without solving for them by expensive direct numerical processes. As noted in section 2.3, the Φ functions should be solutions to the surface Hamiltonian of equation 2.38, reprinted here,

$$\begin{aligned} H_{surf} = & \frac{-\hbar^2}{2\mu\rho_\xi^2} \left[\frac{4}{\sin(2\theta)} \frac{\partial}{\partial\theta} \sin(2\theta) \frac{\partial}{\partial\theta} + \frac{1}{\sin^2(\theta)} \frac{\partial^2}{\partial\chi^2} \right] \\ & + \frac{A+B}{2} \hbar^2 J(J+1) + \frac{15\hbar^2}{8\mu\rho_\xi^2} + \left[C - \frac{A+B}{2} \right] \hbar^2 \Lambda^2 + V(\rho_\xi, \theta, \chi) \end{aligned}$$

We do this by projecting asymptotic states onto the APH hypersphere of a constant ρ_ξ, just as was done with the HNe_2 formulation in chapter 3.

It is useful to understand the symmetry properties of the APH Hamiltonian before discussing how the basis states are constructed. The kinetic terms of the surface Hamiltonian are unchanged by symmetry operations; the symmetry of the potential $V(\theta, \chi; \rho_\xi)$ is the term that dictates the appropriate symmetry group. For an AAA system, i.e. all atoms are identical, this symmetry is C_{6v} in APH

coordinates. In the next section, we discuss how this symmetry influences the construction of the basis states and how it can be used to simplify the general problem.

4.2 Symmetry Analysis for AAA (C_{6v}) Systems

We use asymptotic states associated with each arrangement channel to construct symmetrized basis functions according to the irreducible representation of the symmetry group that is defined by the potential. In the HNe_2 problem described earlier, the Born-Oppenheimer potential energy surface as represented in APH coordinates belonged to the C_{2v} symmetry point group, and the nuclear wavefunction solutions belonged to the irreducible representation of that group. Whether this solution was even or odd with respect to the reflection plane containing the Ne_2 diatomic arrangement channel determined what values of j were allowed in that channel for that irreducible representation.

For an AAA system, the symmetry and irreducible representations play a greater role. With all three atoms being identical, then there now do exist reflection plans for each of the different arrangement channels (see Figure 4.1), and the system now belongs to the C_{6v} symmetry point group. A similar situation exists to that with the Ne_2 channel being aligned with a reflection plane, but here *all* of the channels now contain a reflection plane. Therefore, a nuclear wavefunction of A_1 symmetry in the C_{6v} point group must have even rotational j values for all three of the arrangement channels. Likewise, an A_2 solution must have odd values of j for each of them. These restrictions do not apply to solutions of E_1 or E_2 irreducible representation .

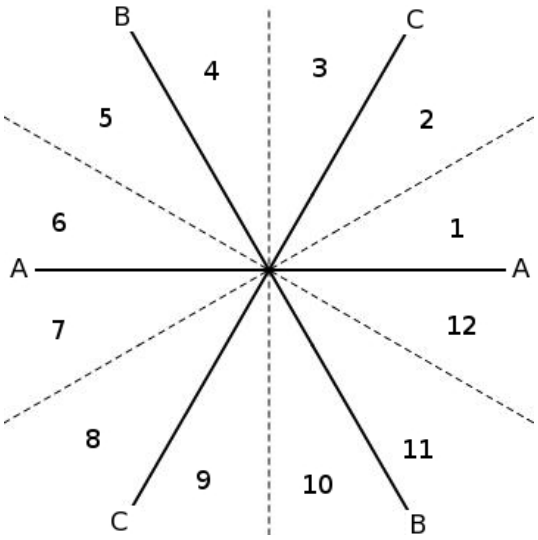

Figure 4.1: This image depicts the C_{6v} symmetry of an AAA system in APH coordinates. The solid lines represent the arrangement channels, and both the solid and dashed lines represent reflection planes. The label "A" denotes the A+BC arrangement channel, and so on. The numbers 1-12 denote different regions of the plot, and likewise different functions.

C_{6v}	E	$2C_6$	$2C_3$	C_2	$3\sigma_v$	$3\sigma_d$
A_1	1	1	1	1	1	1
A_2	1	1	1	1	-1	-1
B_1	1	-1	1	-1	1	-1
B_2	1	-1	1	-1	-1	1
E_1	2	1	-1	-2	0	0
E_2	2	-1	-1	2	0	0

Table 4.1: C_{6v} point group character table.

Construction of the basis states according to the irreducible representation is done by applying the symmetry elements of the point group to a single function using the character table to provide coefficients for the linear combinations. The character table for C_{6v} is shown in table 4.1

Symmetrized surface functions are constructed by defining a function in the regions defined by the C_{6v} symmetry, as shown in Figure 4.1. Each of the twelve

numbered sections describe a basis function, but to avoid overuse of the term "basis", we will call them the "numbered" functions. Alone, these functions need not posses any symmetry of their own, but they *are* are related to each other by the symmetry operations of the C_{6v} point group. A single C_6 rotation moves function $|1\rangle$ to $|3\rangle$, and a single C_3 rotation moves function $|1\rangle$ to $|5\rangle$. The σ_d reflections applied to function $|1\rangle$ produce functions $|2\rangle$, $|6\rangle$, and $|10\rangle$. The symmetry of the system dictates that these functions are identical except for position or reflection.

It is important to note that these functions need not be localized to the regions where their labels are. Each function can, and generally will, span the full surface space. Furthermore, for this reason, there is no claim that these functions are orthogonal. What these functions do accomplish is that the form a reducible representation of the C_{6v} point group. This reducible representation has a definite character set, and can be decomposed into the irreducible representations. It is useful to look at this decomposition explicitly. To form the character table for this 12-function representation, we apply the symmetry operations to the numbers in Figure 4.1 and with each operation, we note how many of the functions changed their positions, and the resulting characters are how many have not changed position. This is related to the characters of the matrices that represent the symmetry operations (see appendix C).

The E operation changes none of the functions, and so with 12 functions remaining unchanged, the E character is 12. Every other operation moves each function to some other location, and so each other character is 0. This representation has a character table of

	E	$2C_6$	$2C_3$	C_2	$3\sigma_v$	$3\sigma_d$
Γ	12	0	0	0	0	0

Following standard methods [15], to decompose Γ we project onto each of the irreducible representations and count their multiplicity. First, we multiply the characters of each irreducible representation with the character of the Γ representation, and again multiply by how many operations are in each symmetry class (e.g. three for σ_v, two for C_6, etc.), and then divide by the order of the group, which in the case of C_{6v} is 12 (there are 12 symmetry operations). Since the characters of Γ are zero for every symmetry element but the identity operation, E, we have

$$N(A_1) = \frac{1}{12}\left(1 * 12 * 1 + 0 + \ldots\right) = 1 \tag{4.7-a}$$

$$N(A_2) = \frac{1}{12}\left(1 * 12 * 1 + 0 + \ldots\right) = 1 \tag{4.7-b}$$

$$N(B_1) = \frac{1}{12}\left(1 * 12 * 1 + 0 + \ldots\right) = 1 \tag{4.7-c}$$

$$N(B_2) = \frac{1}{12}\left(1 * 12 * 1 + 0 + \ldots\right) = 1 \tag{4.7-d}$$

$$N(E_1) = \frac{1}{12}\left(2 * 12 * 1 + 0 + \ldots\right) = 2 \tag{4.7-e}$$

$$N(E_2) = \frac{1}{12}\left(2 * 12 * 1 + 0 + \ldots\right) = 2 \tag{4.7-f}$$

From this we see that Γ contains one instance of each of A_1, A_2, B_1, B_2, and two instances of both E_1 and E_2. We should then be able to construct functions that represent each of these irreducible representations from the 12 numbered functions. Note that because the E_1 and E_2 irreducible representations are two dimensional, each of them contains two symmetry functions. This count shows that with the 12 numbered, we can create 12 symmetrized functions, as should be expected.

To produce the A_1 symmetry surface state, we use the character table of Table 4.1 for the A_1 symmetry. This is the totally symmetric state, so the linear combination of the basis functions are totally symmetric. Explicitly, we have (using the notation of $\zeta^X_{A_1}$ representing the character for the A_1 irreducible representation for symmetry element X),

$$\begin{aligned}
|A_1\rangle &= \zeta^E_{A_1} E\,|1\rangle + \zeta^{C_6}_{A_1} C_6\,|1\rangle + \zeta^{C_3}_{A_1} C_3\,|1\rangle + \zeta^{C_2}_{A_1} C_2\,|1\rangle + \zeta^{C_3^2}_{A_1} C_3^2\,|1\rangle + \zeta^{C_6^5}_{A_1} C_6^5\,|1\rangle \\
&\quad + \zeta^{\sigma_{v1}}_{A_1}\sigma_{v1}\,|1\rangle + \zeta^{\sigma_{v2}}_{A_1}\sigma_{v2}\,|1\rangle + \zeta^{\sigma_{v3}}_{A_1}\sigma_{v3}\,|1\rangle + \zeta^{\sigma_{d1}}_{A_1}\sigma_{d1}\,|1\rangle + \zeta^{\sigma_{d2}}_{A_1}\sigma_{d2}\,|1\rangle + \zeta^{\sigma_{d3}}_{A_1}\sigma_{d3}\,|1\rangle \\
&= |1\rangle + |3\rangle + |5\rangle + |7\rangle + |9\rangle + |11\rangle \\
&\quad + |4\rangle + |8\rangle + |12\rangle + |2\rangle + |6\rangle + |10\rangle
\end{aligned} \tag{4.8}$$

Likewise for the A_2 symmetry, we have

$$\begin{aligned}
|A_2\rangle &= \zeta^E_{A_2} E\,|1\rangle + \zeta^{C_6}_{A_2} C_6\,|1\rangle + \zeta^{C_3}_{A_2} C_3\,|1\rangle + \zeta^{C_2}_{A_2} C_2\,|1\rangle + \zeta^{C_3^2}_{A_2} C_3^2\,|1\rangle + \zeta^{C_6^5}_{A_2} C_6^5\,|1\rangle \\
&\quad + \zeta^{\sigma_{v1}}_{A_2}\sigma_{v1}\,|1\rangle + \zeta^{\sigma_{v2}}_{A_2}\sigma_{v2}\,|1\rangle + \zeta^{\sigma_{v3}}_{A_2}\sigma_{v3}\,|1\rangle + \zeta^{\sigma_{d1}}_{A_2}\sigma_{d1}\,|1\rangle + \zeta^{\sigma_{d2}}_{A_2}\sigma_{d2}\,|1\rangle + \zeta^{\sigma_{d3}}_{A_2}\sigma_{d3}\,|1\rangle \\
&= |1\rangle + |3\rangle + |5\rangle + |7\rangle + |9\rangle + |11\rangle \\
&\quad - |4\rangle - |8\rangle - |12\rangle - |2\rangle - |6\rangle - |10\rangle
\end{aligned} \tag{4.9}$$

Examples of these functions, as well as those for the B_1 and B_2 irreducible representations can be seen in Figure 4.2.

From these figures one can note the effect of the σ_v reflection planes. The A_2 and B_2 states are odd with respect to this reflection, indicating that the A_2 and B_2 surface functions have a node in these planes. Since we are attempting to describe wavefunctions, which must be continuous, the surface function should be smoothly varying across these planes. Diatomic wavefunctions with odd values of

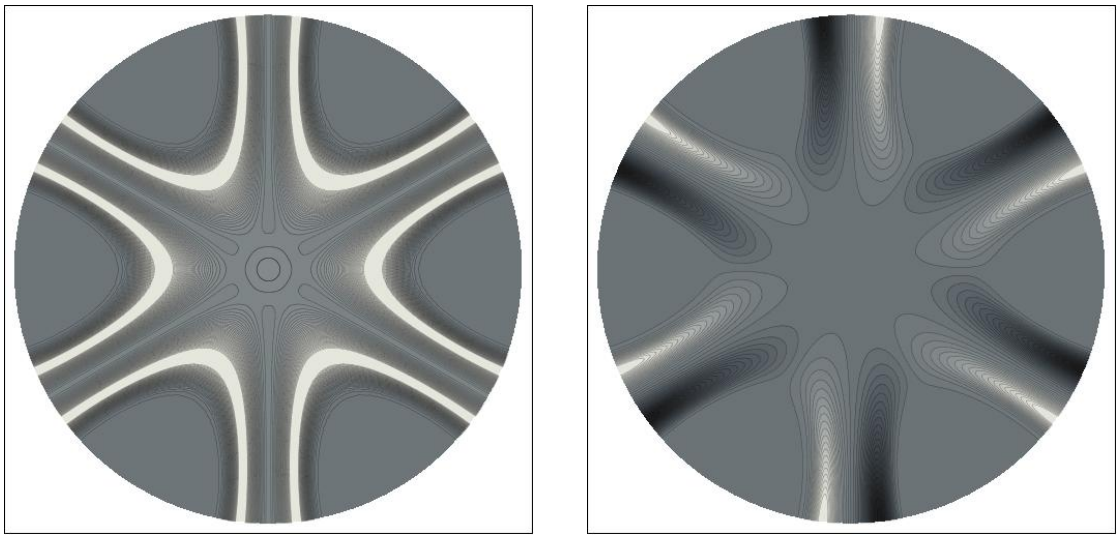

(A1) (A2)

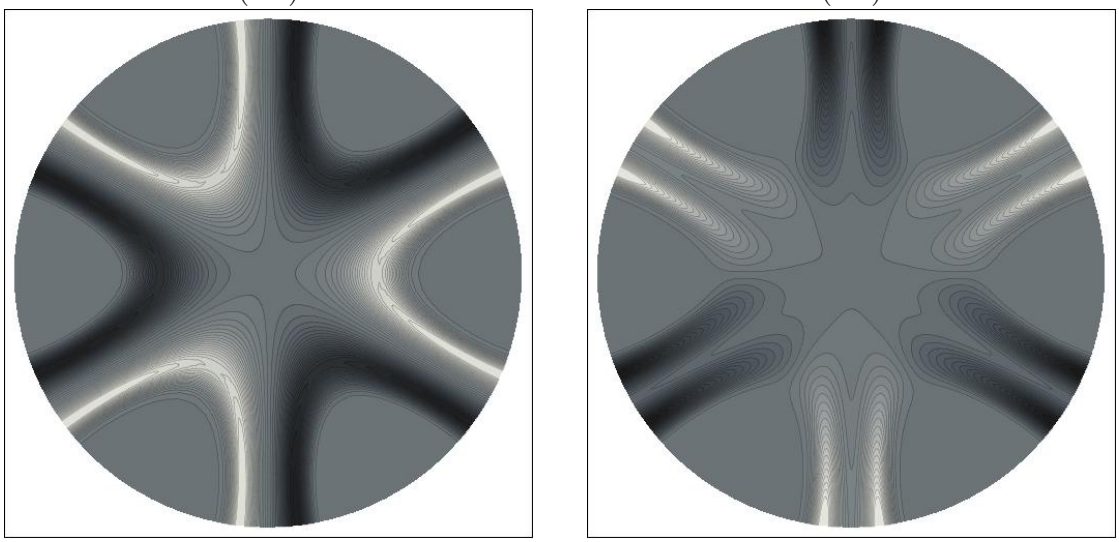

(B1) (B2)

Figure 4.2: Stereographic plots of example functions of the one-dimensional C_{6v} irreducible representations . See appendix B.3 for more explanation of APH surface plots.

the rotational j quantum number satisfy this requirement. Furthermore, the C_2 rotation corresponds to parity in APH coordinates, and so we see that the A_1 and A_2 functions are even with respect to parity, while the B_1 and B_2 functions are odd.

The E_1 and E_2 states, being two dimensional in their representation of the C_{6v} point group, do not contain definite characters with respect to the reflection planes, and so are not directly associated with even or odd values of j. Thus, j can be even or odd in the E_x symmetries (where E_x means either E_1 or E_2), and this explains why the Γ representation of the 12 numbered functions contained two instances of each of E_1 and E_2, one of each for the even j states and one of each for the odd.

The E_1 and E_2 states do have definite characters with respect to the C_2 rotation symmetry element, and so do represent states of definite parity. Inclusion of these states, however, is necessary in order to ensure the set of states is complete. Individual incoming and outgoing wavefunctions in a specific channel cannot be represented without the E irreducible representations included in the basis set. Examples of the symmetries of these functions can be seen in figures 4.3 and 4.4.

The E_x irreducible representations are constructed in the same way as the one-dimensional representations: by applying the symmetry operators and characters of the representation to the numbered functions. However, this method only produces one of the two E_x basis functions. To find the other, we must find the symmetrized function that also exhibits the character of the E_x irreducible representation but is orthogonal to the one produced by the character table.

First, let us determine the first symmetrized function for the j-even E_1 symmetry, and we'll call this function $E_1^{(1)}$. Just as in equation 4.8 Since there is

no explicit definition for the reflection operations, it is useful to define new numbered functions that are linear combinations of the existing functions, minus the reflection symmetry:

$$\begin{aligned}
|i\rangle &= (|1\rangle \pm |12\rangle)/N \\
|ii\rangle &= (|2\rangle \pm |3\rangle)/N \\
|iii\rangle &= (|4\rangle \pm |5\rangle)/N \\
|iv\rangle &= (|6\rangle \pm |7\rangle)/N \\
|v\rangle &= (|8\rangle \pm |9\rangle)/N \\
|vi\rangle &= (|10\rangle \pm |11\rangle)/N
\end{aligned} \tag{4.10}$$

where N is an unknown normalization factor.

While the E_x states do not dictate a symmetry between the even and odd numbered states, the physical rotational symmetry of the diatomic channels does, and therefore whether the linear combinations of Equation 4.10 are positive or negative depends on whether we are interested in states of even or odd j, respectively. Using the Roman numeral states simplifies the symmetrized state construction, and the results apply equally to even or odd j values.

For $E_1^{(1)}$, we have

$$\left|E_1^{(1)}\right\rangle = 2\,|i\rangle + |ii\rangle - |iii\rangle - 2\,|iv\rangle - |v\rangle + |vi\rangle \tag{4.11}$$

and for the first state of the E_2 representation, we have

$$\left|E_2^{(1)}\right\rangle = 2\,|i\rangle - |ii\rangle - |iii\rangle + 2\,|iv\rangle - |v\rangle - |vi\rangle \tag{4.12}$$

To find the $E_x^{(2)}$ states that are orthogonal to the $E_x^{(1)}$ states, we can apply a symmetry operation. This will give us a new state, let's call it Q_x, that is *not* orthogonal to the $E_x^{(1)}$ states, but the Hilbert space spanned by the E_1 states (or the E_2) is only two dimensional, and thus the new function Q_x acquired by the symmetry operation must contain, in some part, the other orthogonal state. Using the C_6 rotation, the Q_x functions are,

$$Q_1 = C_6 E_1^{(1)} = 2\,|ii\rangle + |iii\rangle - |iv\rangle - 2\,|v\rangle - |vi\rangle + |i\rangle \tag{4.13}$$

$$Q_2 = C_6 E_2^{(2)} = 2\,|ii\rangle - |iii\rangle - |iv\rangle + 2\,|v\rangle - |vi\rangle - |i\rangle \tag{4.14}$$

and now, we look for the solutions of

$$\left|E_x^{(2)}\right\rangle = Q_x - \frac{\left\langle E_x^{(1)}\middle|Q_x\right\rangle}{\left\langle E_x^{(1)}\middle|E_x^{(1)}\right\rangle}\left|E_x^{(1)}\right\rangle \tag{4.15}$$

A very important point must be made at this stage. So far, we have allowed for the Arabic-numbered functions ($|1\rangle$, etc.) to span the whole space of the surface. We have not performed any integrals over the functions, and we have left the normalization factor N in equations 4.10 undefined. Were the Arabic-numbered functions orthonormal, this normalization would be trivial, but this is generally not the case, and likewise, integrals between two different Roman-numbered functions is generally not zero. For the one dimensional irreducible representations , this did not cause any problem in their construction (though as defined so far, they too are not normalized). Now, though, we apparently need both the overlap between the Q_x functions with $E_x^{(1)}$, as well as $\left\langle E_x^{(1)}\middle|E_x^{(1)}\right\rangle$ in order to construct $E_x^{(2)}$. It turns

out, though, that we do not need to calculate these values explicitly in order to construct the second E_x state, and again it is for reasons of symmetry.

We know that $|ii\rangle = C_6\,|i\rangle$, and for this reason $\langle i|i\rangle = \langle ii|ii\rangle$. By the rotational symmetries, we also know that $\langle i|ii\rangle = \langle ii|iii\rangle$. What this means is that all integrals between any two adjacent Roman-numbered functions are equal, and furthermore all integrals between two functions that differ by a C_3 rotation are equal and all integrals between two functions that differ by a C_2 rotation. Let us define m_0 to be the value of an integral between a function an itself, m_1 to be the value of an integral between a function and one differing by a C_6 rotation, m_2 the integral between functions differing by a C_3 rotation, and m_3 those differing by a C_2 rotation. More than this is not necessary, since these describe all possible combinations of the six Roman-numbered functions.

Looking at the integral of $E_1^{(1)}$ with itself, we have (noting $\langle i|j\rangle = \langle j|i\rangle$),

$$\begin{aligned}\left\langle E_1^{(1)}\middle|E_1^{(1)}\right\rangle &= 4\langle i|i\rangle + \langle ii|ii\rangle + \langle iii|iii\rangle + 4\langle iv|iv\rangle + \langle v|v\rangle + \langle vi|vi\rangle \\ &\quad + 4\langle i|ii\rangle - 2\langle ii|iii\rangle + 4\langle iii|iv\rangle + 4\langle iv|v\rangle - 2\langle v|vi\rangle + 4\langle vi|i\rangle \\ &\quad - 4\langle i|iii\rangle - 4\langle ii|iv\rangle + 2\langle iii|v\rangle - 4\langle iv|vi\rangle + 2\langle ii|vi\rangle - 4\langle i|v\rangle \\ &\quad - 8\langle i|iv\rangle - 2\langle ii|v\rangle - 2\langle iii|vi\rangle \qquad (4.16) \\ &= 12m_0 + 12m_1 - 12m_2 - 12m_3 \qquad (4.17)\end{aligned}$$

Likewise, calculating $\left\langle Q_1\middle|E_1^{(1)}\right\rangle$ gives,

$$\begin{aligned}\left\langle Q_1 \middle| E_1^{(1)} \right\rangle &= 2\langle i|i\rangle + 2\langle ii|ii\rangle - \langle iii|iii\rangle + 2\langle iv|iv\rangle + 2\langle v|v\rangle - \langle vi|vi\rangle \\ &\quad + 5\langle i|ii\rangle - \langle ii|iii\rangle - \langle iii|iv\rangle + 5\langle iv|v\rangle - \langle v|vi\rangle - \langle vi|i\rangle \\ &\quad + \langle i|iii\rangle - 5\langle ii|iv\rangle + \langle iii|v\rangle + \langle iv|vi\rangle - 5\langle v|i\rangle + \langle ii|vi\rangle \\ &\quad - 4\langle i|iv\rangle - 4\langle ii|v\rangle + 2\langle iii|vi\rangle \qquad (4.18) \\ &= 6m_0 + 6m_1 - 6m_2 - 6m_3 \qquad (4.19)\end{aligned}$$

From this we can get the following,

$$\frac{\langle Q_1|E_1(1)\rangle}{\left\langle E_1^{(1)} \middle| E_1^{(1)} \right\rangle} = \frac{6(m_0 + m_1 - m_2 - m_3)}{12(m_0 + m_1 - m_2 - m_3)} = \frac{1}{2} \qquad (4.20)$$

The same formulation applied to the E_2 symmetry gives a factor of $-1/2$. Therefore, without having to know any of the integrals, we can still construct the orthogonal state because the explicit integral values cancel. This directly results from the integrals between the numbered functions being equivalent for all functions related by the same symmetry operation.

Also, if we were to choose to normalize the $E_x^{(1)}$ functions before this process, the overall normalization would also drop out of this relation, as the factor that normalizes $E_x^{(1)}$ would also normalize Q_x, and thus divides out directly.

From this result we can now solve equation 4.15 to get

$$\left| E_1^{(2)} \right\rangle = \frac{3}{2}\left(|ii\rangle + |iii\rangle - |v\rangle - |vi\rangle\right) \qquad (4.21)$$

$$\left| E_2^{(2)} \right\rangle = \frac{3}{2}\left(|ii\rangle - |iii\rangle + |v\rangle - |vi\rangle\right) \qquad (4.22)$$

We note that the integral of $\left\langle E_1^{(1)}(j+)\middle|E_1^{(2)}(j-)\right\rangle$ is non-zero. This is because the construction of the $E_1^{(2)}(j-)$ state, by virtue of j being odd, produces a state that has the same symmetry structure as an $E_1^{(1)}(j+)$ state. This is because the E irreducible representation states, as constructed by the projection operators on even and odd j states, result in functions that do exhibit reflection symmetries, even though there isn't a definition of reflection symmetry to the E irreducible representations . This actually is consistent, because this symmetry is accidental for the E states, and emerges because there does exist a reflection symmetry only in a single given channel that is even or odd depending on whether j is even or odd. That this symmetry exists is not necessary for the definitions of the E irreducible representation states, but does produce two reflection planes, one along the x axis and one along the y axis in the E states. Therefore, the E states constructed here do exhibit reflections of

Using the projection operators to construct a states of odd j in the same way

- | +	+ | +	+ | +	- | +
- | +	- | -	+ | +	+ | -
$E_1^{(1)}(j+)$	$E_1^{(2)}(j+)$	$E_2^{(1)}(j+)$	$E_2^{(2)}(j+)$

as for the even j states gives functions with reflection symmetries of Note that

+ | +	- | +	- | +	+ | +
- | -	- | +	+ | -	+ | +
$E_1^{(1)}(j-)$	$E_1^{(2)}(j-)$	$E_2^{(1)}(j-)$	$E_2^{(2)}(j-)$

the reflection symmetries for the E_1 states are reversed for odd j from what they are for even j, and likewise for the E_2 states. To rectify this, we redefine the projections for the odd states by exchanging the projection definitions according to $E_1^{(1)}(j-) \leftrightarrow E_1^{(2)}(j-)$ $E_2^{(1)}(j-) \leftrightarrow E_2^{(2)}(j-)$. This prevents any state with a (1)

superscript mixing with a state of (2) superscript. The E states, regardless of even or odd j, then all have the reflection properties of

- | +	+ | +	+ | +	- | +
- | +	- | -	+ | +	+ | -
$E_1^{(1)}(j\pm)$	$E_1^{(2)}(j\pm)$	$E_2^{(1)}(j\pm)$	$E_2^{(2)}(j\pm)$

After this exchange, the final definitions are

$$\left|E_1^{(1)}(j+)\right\rangle = 2\left|i^+\right\rangle + \left|ii^+\right\rangle - \left|iii^+\right\rangle - 2\left|iv^+\right\rangle - \left|v^+\right\rangle + \left|vi^+\right\rangle \tag{4.23}$$

$$\left|E_1^{(2)}(j+)\right\rangle = \frac{3}{2}\left(\left|ii^+\right\rangle + \left|iii^+\right\rangle - \left|v^+\right\rangle - \left|vi^+\right\rangle\right) \tag{4.24}$$

$$\left|E_2^{(1)}(j+)\right\rangle = 2\left|i^+\right\rangle - \left|ii^+\right\rangle - \left|iii^+\right\rangle + 2\left|iv^+\right\rangle - \left|v^+\right\rangle - \left|vi^+\right\rangle \tag{4.25}$$

$$\left|E_2^{(2)}(j+)\right\rangle = \frac{3}{2}\left(\left|ii^+\right\rangle - \left|iii^+\right\rangle + \left|v^+\right\rangle - \left|vi^+\right\rangle\right) \tag{4.26}$$

$$\left|E_1^{(1)}(j-)\right\rangle = 2\left|i^-\right\rangle + \left|ii^-\right\rangle - \left|iii^-\right\rangle - 2\left|iv^-\right\rangle - \left|v^-\right\rangle + \left|vi^-\right\rangle \tag{4.27}$$

$$\left|E_1^{(2)}(j-)\right\rangle = \frac{3}{2}\left(\left|ii^-\right\rangle + \left|iii^-\right\rangle - \left|v^-\right\rangle - \left|vi^-\right\rangle\right) \tag{4.28}$$

$$\left|E_2^{(1)}(j-)\right\rangle = \frac{3}{2}\left(\left|ii^-\right\rangle - \left|iii^-\right\rangle + \left|v^-\right\rangle - \left|vi^-\right\rangle\right) \tag{4.29}$$

$$\left|E_2^{(2)}(j-)\right\rangle = 2\left|i^-\right\rangle - \left|ii^-\right\rangle - \left|iii^-\right\rangle + 2\left|iv^-\right\rangle - \left|v^-\right\rangle - \left|vi^-\right\rangle \tag{4.30}$$

Where the Roman kets have superscript labels of $+$ or $-$ to denote the choice of addition or subtraction in equation 4.10.

Examples of these functions is shown as stereographic projections in APH coordinates (see appendix B.3) in Figures 4.3 and 4.4. While it is true that the integrals do not need to be computed in order to construct the $E_x^{(2)}$ states, the integrals must be computed in order to normalize the symmetrized states and to calculate the potential energy matrices. However, this result means that only a twelfth of the full space must be integrated over.

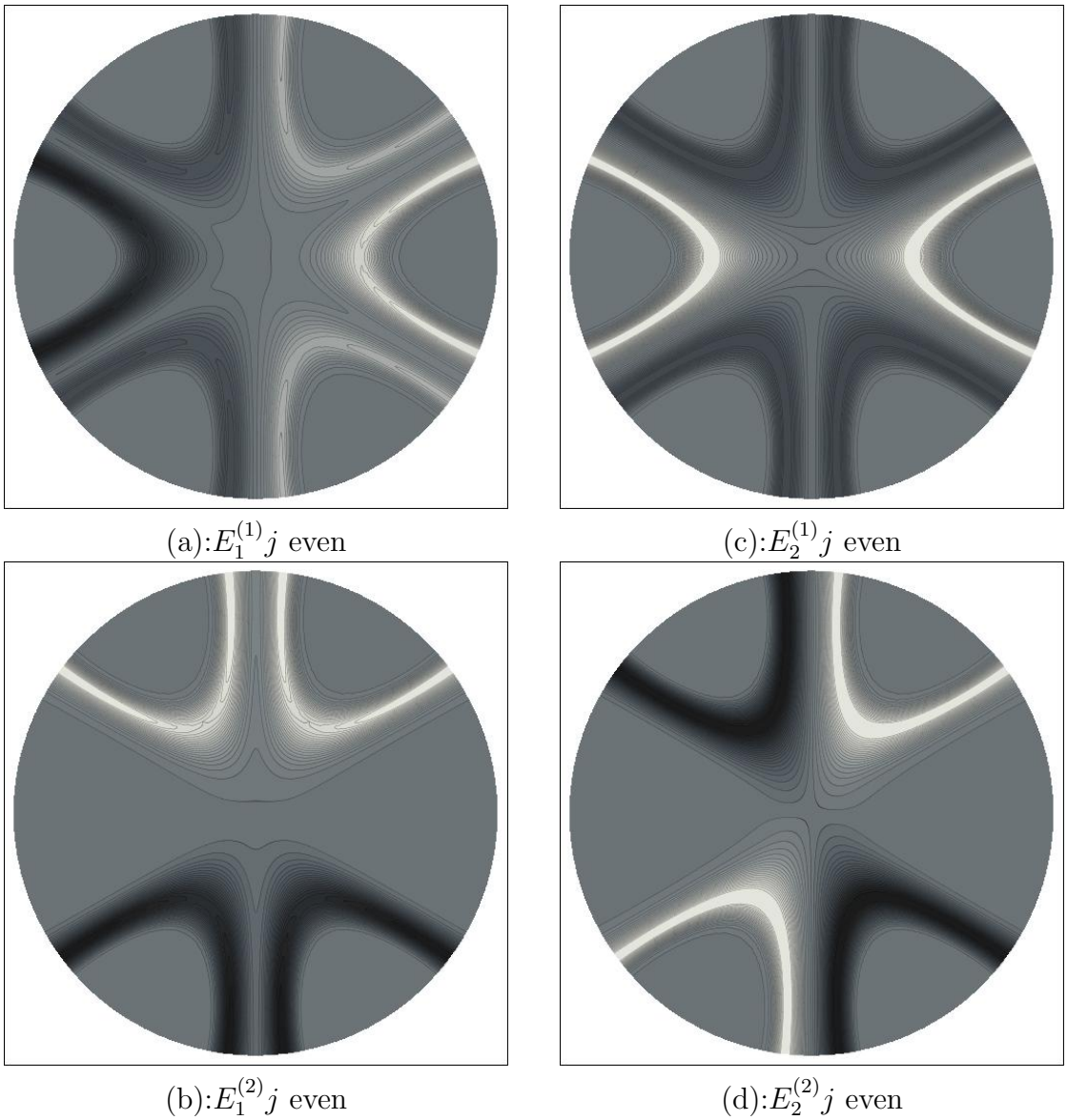

(a):$E_1^{(1)} j$ even (c):$E_2^{(1)} j$ even

(b):$E_1^{(2)} j$ even (d):$E_2^{(2)} j$ even

Figure 4.3: Example functions of the two-dimensional C_{6v} irreducible representations for even rotational j states. On the left are the orthogonal pair for the E_1 representation, on the right are the orthogonal pair for E_2. Note that for plots (a) and (c), the functions for $|i\rangle$ and $|iii\rangle$ aligned with channel A have greater amplitude than those for channels B and C, while they have zero amplitude in plots (b) and (d).

There are a few fine points that need to be made regarding the integrals between these states. The inclusion of m_3 in the above analysis is for completeness.

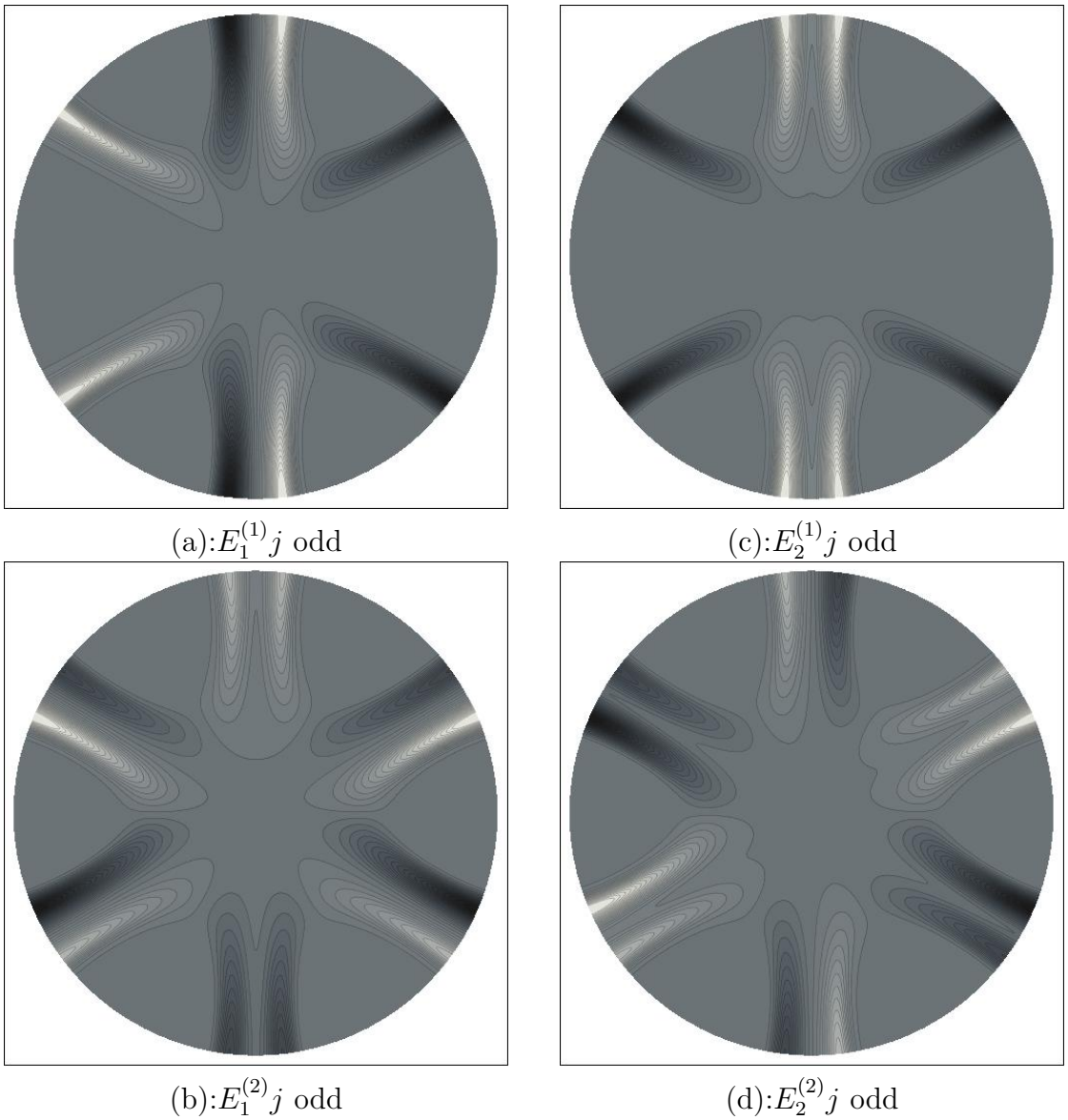

(a):$E_1^{(1)} j$ odd (c):$E_2^{(1)} j$ odd

(b):$E_1^{(2)} j$ odd (d):$E_2^{(2)} j$ odd

Figure 4.4: Example functions of the two-dimensional C_{6v} irreducible representations for odd rotational j states. The left side plots are the orthogonal pair for the E_1 representation, and the right side plots are the orthogonal pair for E_2. Like figure 4.3, note that the functions associated with channel A, $|i\rangle$ and $|iii\rangle$, in plots (a) and (c) have larger amplitude than the functions in channels B and C.

However, as we have described the Roman numeral states, the physical wavefunction only extends to $\pm\pi/2$ from the associated arrangement channel. This means that there is no overlap between function $|i\rangle$ and $|iv\rangle$, for example.

Furthermore, in the definition of the Roman numbered states, we have dropped any overlap between the adjacent Arabic states that constitute the Roman states. Thus, there is no overlap between $|1\rangle$ and $|12\rangle$, but this too is physically accurate, since $|1\rangle$ and $|12\rangle$ are simply two parts of the same function, and the reflection symmetry between them is a property of that function, not a property of the space and two different functions.

There is also no overlap between $|1\rangle$ and $|6\rangle$, as mentioned before. APH coordinates represents all of physical space twice, and a function centered on channel A only extends to a range in χ that is $\pm\pi/2$ from the channel. While $|1\rangle$ and $|6\rangle$ are directly related by the values of j and the parity, they have no overlap. This is true for each of the Arabic numbered functions. Function $|1\rangle$ has a domain in χ of $[0, \pi/2]$, $|2\rangle$ has a domain of $[-\pi/3, \pi/6]$, $|3\rangle$ has a domain of $[-\pi/6, \pi/3]$, and so on for each of them. The limitations on the ranges for each of these reduces the number of integrals that need to be performed to normalize the symmetrized states, or to get overlaps.

Just as we defined m_i for the integrals between the Roman numbered states, it is useful to define values for the Arabic numbered states in order to more clearly see which functions are included in integrals of the entire symmetry state. Let us define n_0 as the integral of an Arabic function with itself, n_1 the value of the integral with a function and the one immediately next to it as related by the σ_d symmetry (those related by σ_v, such as $|1\rangle$ and $|12\rangle$ are always zero), and so on. The only non-zero integrals are those between functions that have overlapping domains.

All of the normalizations for the symmetrized functions, and their overlaps, are explicitly determined in terms of the n values in appendix E.2. One integral of key

interest is that of the $E_1^{(1)}(j+)$ state and the $E_1^{(1)}(j-)$ state. As we saw in equation 4.7-a, the E_1 and E_2 irreducible representations are both represented twice by these twelve functions. We used this freedom to define two sets of E functions, one with even j and one with odd. However, the set of even j E_1 states are not necessarily orthogonal to the set of odd j E_1 states, and likewise for the E_2 even and odd j states. Group theory does not dictate that functions of the same irreducible representation must be orthogonal, and since the σ symmetry elements do not appear in the E representations, different symmetries with respect to j being even or odd do not cause these states to be orthogonal. When we constructed the $E_x^{(2)}$ functions, we were assured that they were orthogonal to the corresponding $E_x^{(1)}$ states of the same j symmetry, but this does not assure that they are orthogonal to the other E representation. The E_1 states of odd j and the E_1 states of even j can mix.

This is an important point to consider, for this is the source of any mixing between initial states with an even rotational quantum number, and a final state with an odd rotational quantum number, or the reverse. Such a transition is allowed by symmetry, and it is allowed specifically because each E irreducible representation is represented twice.

The benefit of using symmetrized basis functions is demonstrated most dramatically in the propagation stage of scattering. Since the basis functions and eigenfunctions of different irreducible representation are orthogonal and do not couple, the radial wavefunction can be propagated separately for each irreducible representation . For example, if we have 50 basis functions in a single channel, then we have 150 total basis functions for an even parity case. The propagation stage would then involve multiplying and inverting matrices that were 150×150.

However, in symmetrizing the system, if we have roughly half even j states and half odd j states, then the A_1 block is 25×25, the A_2 block is 25×25, and the two E_2 blocks are 50×50. Since the computational cost of the propagation is dominated by matrix-matrix multiplications, which scale as N^3, the symmetrized propagation is 54 times faster. But another improvement can be made. The two E_2 blocks are exactly degenerate energetically, and the energy values are the only relevant factors in the propagation, so only one of them must be propagated. With this, the computational savings increases to a factor of 72.

For ABB (A and B are different atoms) or ABC (all three atoms different) systems, there is not as much available symmetry to use to reduce the problem. An ABB system has a potential surface that belongs to the C_{2v} point group in APH coordinates, and so a comparable even parity calculation could be reduced to two one-dimensional irreducible representations , A_1 and A_2, or for odd parity, B_1 and B_2. But this still reduces the computational cost in propagation by a factor of about 8. An ABC system belongs to the C_2 point group, and exhibits only even or odd parity symmetry, and so in this case, if using the same example as above, the full 150×150 matrix would have to be propagated. While these cases are logistically much simpler than the AAA/C_{6v} case, they can be much more computationally intensive.

4.3 Basis Construction

The same methods employed for the replacement basis sets of the HNe_2 problem can be used in the construction of basis functions for a reactive scattering problem

in which there are three end channels. The relationship between Delves hyperspherical coordinates and the APH coordinates of Pack and Parker [8] can be used to produce states that represent the bound states for a full three-channel problem.

Here we look at the properties of the APH surface Hamiltonian in order to ensure that the constructed functions have proper physical properties and boundary conditions. For the three-dimensional problem, we are seeking solutions to the surface Hamiltonian as given in reference [8], equation 164, which is

$$\begin{aligned} H_{surf} = & \frac{-\hbar^2}{2\mu\rho_\xi^2}\left[\frac{4}{\sin(2\theta)}\frac{\partial}{\partial\theta}\sin(2\theta)\frac{\partial}{\partial\theta} + \frac{1}{\sin^2(\theta)}\frac{\partial^2}{\partial\chi^2}\right] \\ & + \frac{A+B}{2}\hbar^2 J(J+1) + \frac{15\hbar^2}{8\mu\rho_\xi^2} \\ & + \left[C - \frac{A+B}{2}\right]\hbar^2\Lambda^2 + V(\rho_\xi,\theta,\chi) \end{aligned} \tag{4.31}$$

where A, B, and C are defined as

$$A = \frac{1}{\mu\rho_\xi^2(1+\sin\theta)} \tag{4.32-a}$$

$$B = \frac{1}{2\mu\rho_\xi^2\sin^2\theta} \tag{4.32-b}$$

$$C = \frac{1}{\mu\rho_\xi^2(1-\sin\theta)} \tag{4.32-c}$$

We define solutions to the surface Hamiltonian of equation 4.31 as

$$H_{surf}\Phi_{t\Lambda}^{Jp}(\rho_\xi;\theta,\chi) = \mathcal{E}_{t\Lambda}^{Jp}(\rho_\xi)\Phi_{t\Lambda}^{Jp}(\rho_\xi;\theta,\chi) \tag{4.33}$$

which are normalized according to

$$\int_{-\pi}^{\pi} d\chi \int_{0}^{\pi/2} \sin 2\theta d\theta \Phi^{Jp'}_{t'\Lambda}(\theta,\chi;\rho_\xi)\Phi^{Jp}_{t\Lambda}(\theta,\chi;\rho_\xi) = \delta_{tt'}\delta_{pp'} \tag{4.34}$$

As an aside, the derivatives with respect to θ in equation 4.31 can be written as

$$\frac{1}{\sin(2\theta)}\frac{\partial}{\partial\theta}\sin(2\theta)\frac{\partial}{\partial\theta} = \frac{2}{\sin^{1/2}(2\theta)}\left(\frac{\partial^2}{\partial\theta^2}\right)\frac{\sin^{1/2}(2\theta)}{2} + \left(2 + \frac{\cos^2(2\theta)}{\sin^2(2\theta)}\right) \tag{4.35}$$

Note that since the range of θ is $[0, \pi/2]$, $\sin^{1/2}(2\theta)$ introduces no complexities. Making the replacement of equation 4.35 is often very useful, for if we define some new function

$$\Phi = \frac{2}{\sin^{1/2}(2\theta)}\bar{\Phi} \tag{4.36}$$

with an orthonormalization condition of

$$\int_{-\pi}^{\pi} d\chi \int_{0}^{\pi/2} d\theta \bar{\Phi}^{Jp'}_{t'\Lambda}(\theta,\chi;\rho_\xi)\bar{\Phi}^{Jp}_{t\Lambda}(\theta,\chi;\rho_\xi) = \delta_{tt'}\delta_{pp'} \tag{4.37}$$

then the surface Hamiltonian can be rewritten in terms of $\bar{\Phi}$ and contains only second derivatives with respect to θ. This is useful and often necessary for some algorithms that solve second order differential equations that require only a second derivative term be present and no first derivative term, such as Johnson's log-derivative method [16] or a Numerov method [14]. It may be possible to use a two-dimensional Numerov algorithm to numerically solve for the Φ eigenstates much more efficiently than existing methods, and the development of such an algorithm is planned for future work.

The surface Hamiltonian must be Hermitian, and being real, this means its matrix representation must be symmetric, so it is useful to see how the terms of equation 4.31 applied to the Φ functions behave under integration. Breaking the terms of equation 4.31 into groups as

$$H^{\theta}_{surf} = \frac{-\hbar^2}{2\mu\rho_\xi^2}\frac{4}{\sin(2\theta)}\frac{\partial}{\partial\theta}\sin(2\theta)\frac{\partial}{\partial\theta} \tag{4.38}$$

$$H^{\chi}_{surf} = \frac{-\hbar^2}{2\mu\rho_\xi^2}\frac{1}{\sin^2(\theta)}\frac{\partial^2}{\partial\chi^2} \tag{4.39}$$

$$H^{0}_{surf} = \frac{A+B}{2}\hbar^2 J(J+1) + \frac{15\hbar^2}{8\mu\rho_\xi^2} + \left[C - \frac{A+B}{2}\right]\hbar^2\Lambda^2 + V(\rho_\xi,\theta,\chi) \tag{4.40}$$

The integrals over $\left\langle \Phi_m \middle| H^0_{surf} \middle| \Phi_n \right\rangle$ clearly produce matrix elements of $\mathbf{H}^0_{surf}$ that are symmetric in indices m and n, as none of the terms in equation 4.40 alter the functions Φ in any way. For $[\mathbf{H}^{\theta}_{surf}]_{mn}$ we have

$$\begin{aligned}
\left[\mathbf{H}^{\theta}_{surf}\right]_{mn} &= \int_{-\pi}^{\pi} d\chi \int_0^{\pi/2} d\theta \sin(2\theta)\Phi_m \frac{4}{\sin 2\theta}\frac{\partial}{\partial\theta}\left(\sin 2\theta\frac{\partial}{\partial\theta}\Phi_n\right) \\
&= \int_{-\pi}^{\pi} d\chi \left[\Phi_m \sin 2\theta \Phi'_n\Big|_0^{\pi/2} - \int_0^{\pi/2} d\theta \Phi'_m \sin 2\theta \Phi'_n\right] \\
&= \int_{-\pi}^{\pi} d\chi \left[0 - \int_0^{\pi/2} \Phi'_m \sin 2\theta \Phi'_n d\theta\right] \\
&= -\left\langle \Phi'_m \middle| H^{\theta}_{surf} \middle| \Phi'_n \right\rangle = -\left\langle \Phi'_n \middle| H^{\theta}_{surf} \middle| \Phi'_m \right\rangle
\end{aligned} \tag{4.41}$$

where the primes refer to differentiation with respect to θ, and in the second line we have used integration by parts, where the surface term must be zero in order for H^{θ}_{surf} to be Hermitian. This condition means that

$$\Phi_m \sin 2\theta \Phi'_n\Big|_0^{\pi/2} = 0 \tag{4.42}$$

for all Φ, so any combination of $\Phi_m \Phi'_n$ must not blow up at $\theta = 0, \pi/2$ faster than $1/\theta$, since $\sin 2\theta$ approaches zero at these points only linearly. However, in order for the solution to be regular everywhere, it is necessary that the θ boundary conditions at $\theta = 0, \pi/2$ are such that Φ has either a zero value or a zero derivative.

The matrix elements for H^{χ}_{surf} are more simple,

$$\begin{aligned}
\left[\mathbf{H}^{\theta}_{surf}\right]_{mn} &= \int_0^{\pi/2} \frac{\sin 2\theta}{\sin^2\theta} \int_{-\pi}^{\pi} d\chi \Phi_m \frac{\partial^2}{\partial \chi^2} \Phi_n \\
&= \int_0^{\pi/2} \frac{\sin 2\theta}{\sin^2\theta} \left[\Phi_m \Phi'_n \Big|_{-\pi}^{\pi} - \int_{-\pi}^{\pi} \Phi'_m \Phi'_n d\chi \right] \\
&= \int_0^{\pi/2} \frac{\sin 2\theta}{\sin^2\theta} \left[0 - \int_{-\pi}^{\pi} \Phi'_m \Phi'_n d\chi \right] \\
&= -\left\langle \Phi'_m \middle| H^{\chi}_{surf} \middle| \Phi'_n \right\rangle = -\left\langle \Phi'_n \middle| H^{\chi}_{surf} \middle| \Phi'_m \right\rangle
\end{aligned} \tag{4.43}$$

where here the primes refer to differentiation with respect to χ and this time the surface term is identically zero because χ is a cyclic coordinate; $\chi = -\pi$ and $\chi = \pi$ are the same point in χ space, so assuming Φ to be single valued means $\Phi_m(\theta, \chi = -\pi)$ is the same as $\Phi_m(\theta, \chi = \pi)$.

If we can satisfy these boundary conditions, then we need only to calculate the first derivatives of Φ with respect to each coordinate. We will show in the following sections that the process of constructing these states from asymptotic states meets these boundary conditions automatically, and that the derivative information for the projected functions can be attained from knowledge of the derivatives of the asymptotic functions.

4.3.1 APH Bound State Construction

Next we wish to construct basis functions to represent continuum states. In the last section we developed the theory for projecting the asymptotic $\zeta(s_\tau)$ functions onto a constant ρ surface by taking limits as $S_\tau \to \infty$, and then using these functions as approximations to the bound $\Upsilon(\vartheta_\tau)$ functions. Now we wish to replace all of the basis functions with asymptotic type states, and by doing so we remove completely the need to calculate basis functions numerically at every propagation step.

The construction of the bound states in the case of three identical channels is an extension of how they are constructed for the single channel as described in section 3.2. For one channel, we used the two-body potential to solve for a vibrational function in the mass-scaled Jacobi coordinate s_τ, and then at each value of ρ as the propagation proceeded in Delves coordinates, a vibrational function in ϑ_τ was constructed by projecting the calculated function of s onto the Delves coordinate hypersurface.

To do this for three channels, there are some notable complications. First, the propagation is in APH coordinates, instead of Delves hyperspherical coordinates. This makes the projection step of the vibrational wavefunctions in Jacobi coordinates more difficult. A function of the Jacobi coordinate s projects on to the Delves hypersphere as a function of ϑ_τ and ϑ_τ only. To project on to the APH hypersphere, the resulting vibrational motion is a function of both θ and χ. Furthermore, because the motion in APH coordinates is not separable, the projected state must also include the coupled spherical harmonic functions, $\mathscr{Y}$ of 2.13, whereas in projecting from Jacobi to Delves coordinates used the same $\mathscr{Y}$ function an there was no change from one set of bases to another.

Secondly, there are three channels, and while it is easy to determine which diatomic vibrational state should be considered when close to the arrangement channels in APH coordinates, it is more difficult to make such a determination in intermediate regions of the APH hypersphere. In these regions, rather than differentiate between channels, effectively choosing which channel's vibrational state to use in constructing the surface function, it is more appropriate to create surface functions that are linear combinations of vibrational states for all channels. The vibrational functions decay to zero as s_τ increases, and so as ρ increases, the non-zero portions of the vibrational wavefunctions become increasingly localized around the arrangement channels. At large values of ρ, these functions approximate the bound-state surface functions very well, and there is negligible to no overlap between the vibrational states for different channels.

In moderately valued ρ regions, taking a linear combination of the vibrational functions is similar to solving the surface Hamiltonian for a pairwise potential, neglecting the three-body potential contribution. Constructing surface functions in this manner is an approximation that gets better as propagation in ρ progresses and the presence of the third atom becomes less significant.

In small ρ regions of the propagation, it is possible for the bound vibrational wavefunction to be non-zero in APH coordinates at a location where two atoms from another channel coalesce. This causes large inaccuracies in constructing the interaction matrix elements, because here the full three-body potential is very repulsive, but since the constructed vibrational wavefunction for one diatomic channel ignores the presence of a third atom, this repulsion is not considered. Thus, the potential matrix element can be much, much too large. This means that this method of constructing surface functions must only be used after ρ is large enough

that this effect is negligible. This problem also occurs for the continuum surface functions, but ways to assuage this will be discussed in the next section.

The symmetry and C_{6v} irreducible representation plays a role in how the linear combination of the bound state surface functions are constructed. As discussed in section 4.2, the parity and rotational j quantum number determine the behavior of some of the symmetry elements. If j is odd, then the surface function must belong to an irreducible representation that has a -1 character for σ_v reflections. The linear combination of vibrational states must consider the σ_d reflections of the irreducible representation , as well as the parity, in order to produce states of the correct symmetry. This can be seen more clearly in figure 4.2. The A1 irreducible representation symmetrized function must have even j and even parity, while the B1 irreducible representation must have even j and odd parity.

To evaluate the surface Hamiltonian in APH coordinates, it is necessary to construct matrix elements of the full three-body potential energy surface, and also to construct matrix elements of the kinetic energy operators for θ and χ. In solving the APH surface Hamiltonian numerically, the functions calculated are usually eigenfunctions of the surface Hamiltonian operator. In the constructed basis method, however, the functions are *not* eigenfunctions, and the kinetic terms must be calculated explicitly. It is necessary to get derivatives of these functions with respect to the APH surface coordinates θ and χ.

For the bound states, what we do know are the derivatives of these functions with respect to the Jacobi coordinate s_τ. The bound state vibrational functions are independent of S_τ, and so these derivatives are zero. What is necessary, then, to accurately represent the first and second derivatives of these functions with respect to θ and χ is knowledge of the first and second derivatives of the functions

with respect to s, and the first and second derivatives of s_τ with respect to θ and χ. Explicitly, we have

$$\frac{\partial^2 f}{\partial \theta^2} = \frac{\partial^2 f}{\partial s_\tau^2}\left(\frac{ds_\tau}{d\theta}\right)^2 + \frac{\partial f}{\partial s_\tau}\frac{d^2 s_\tau}{d\theta^2} + \frac{\partial^2 f}{\partial \Theta^2}\left(\frac{d\Theta}{d\theta}\right)^2 + \frac{\partial f}{\partial \Theta}\frac{d^2\Theta}{d\theta^2} \tag{4.44}$$

$$\frac{\partial^2 f}{\partial \chi^2} = \frac{\partial^2 f}{\partial s^2}\left(\frac{ds}{d\chi}\right)^2 + \frac{\partial f}{\partial s}\frac{d^2 s}{d\chi^2} + \frac{\partial^2 f}{\partial \Theta^2}\left(\frac{d\Theta}{d\chi}\right)^2 + \frac{\partial f}{\partial \Theta}\frac{d^2\Theta}{d\chi^2} \tag{4.45}$$

From equations 52(a-c) in reference [8], we have the relations for the mass-scaled Jacobi coordinates with respect to the APH coordinates,

$$s_\tau = \frac{\rho}{\sqrt{2}}\left(1 - \sin(\theta)\cos[2(\chi_i - \chi_{\tau i})]\right)^{1/2} \tag{4.46-a}$$

$$S_\tau = \frac{\rho}{\sqrt{2}}\left(1 + \sin(\theta)\cos[2(\chi_i - \chi_{\tau i})]\right)^{1/2} \tag{4.46-b}$$

$$\Theta_\tau = \arccos\left(\frac{\sin(\theta)\sin(2\chi)}{\left[1 - \sin^2(\theta)\cos^2(2\chi)\right]^{1/2}}\right) \tag{4.46-c}$$

We need the terms in equations 4.44 and 4.45 for the derivatives of s and Θ with respect to θ and χ. These are provided explicitly in appendix B.4.

The derivatives of the bound states with respect to s can be computed once and then by use of a spline, the function or its derivative can be found at any point

in APH coordinates. The second derivatives are analytic by virtue of the two-body Hamiltonian of equation 3.1, rewritten here for convenience,

$$H^{BC}\zeta_\nu(s) = \epsilon_\nu\zeta_\nu(s) = \left[\frac{-\hbar^2}{2\mu}\frac{\partial^2}{\partial s^2} + \frac{\hbar^2}{2\mu}\frac{j(j+1)}{s^2} + V^{BC}(s)\right]\zeta_\nu(s)$$

and so the second derivative of the ζ_ν functions can be found explicitly. The first derivatives are again found numerically by Blatt's method [17]. If the two-body Hamiltonian is solved by a Numerov method or something similar, the error of Blatt's method for the first derivatives is on the same order as the error of the solution function anyway, and so a more accurate or analytic derivative is unnecessary. The function and its derivatives are determined at a grid of s points and then splined. The spline coefficients are constant throughout the propagation and can be used repeatedly to determine the function or derivative values at any point in APH space.

These projections were used for the bound states in the HNe_2 expansion, but only after a certain value of ρ_ξ. The numerically solved $\Upsilon(\vartheta_\tau)$ functions were used up to $\rho_\xi = 30a_0$, and then the replacement functions were used afterward. In the present case, we do not have numeric solutions for Φ, and so must use these projected functions for the entire range for which ρ is propagated. This causes an issue with these functions behaving physically at short ρ distances. The projected function can get cut off, as shown in figure 4.5 which, when projected onto the APH hypersphere, can cause discontinuities in the surface function in cases where there is odd parity, and discontinuities in the surface function derivatives in cases of even parity.

A simple solution is to use a tangent projection instead of sine. A direct projection (shown in part a of figure 4.6) employs the relation $s_\tau = \rho_\xi \sin\vartheta_\tau$. If we

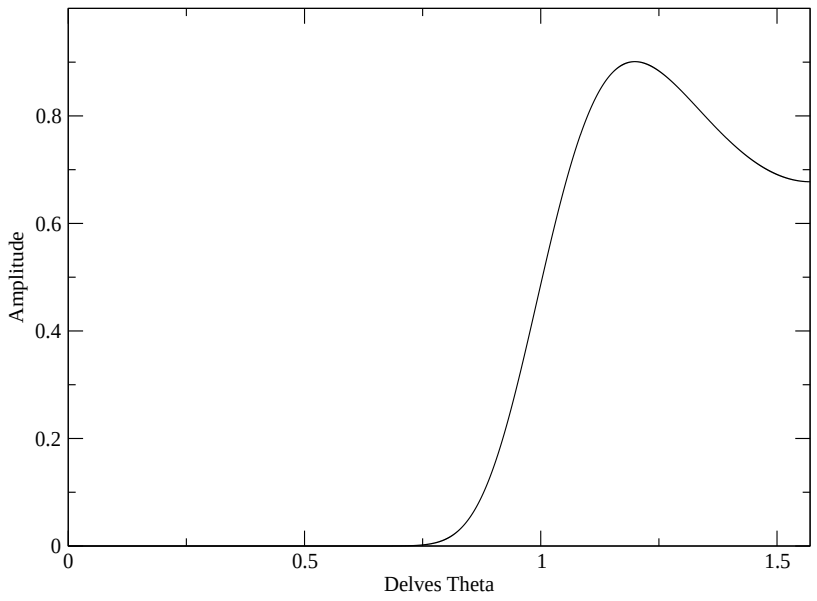

Figure 4.5: Plot of $\zeta(s_\tau)$ projected onto Delves hypersurface at $\rho_\xi = 8.0a_0$ with "direct" projection of $s_\tau = \rho_\xi \sin\vartheta_\tau$

instead use $s_\tau = \rho_\xi \tan\vartheta_\tau$, the entire domain of s_τ is mapped onto the hypersurface (as in part b of figure 4.6). At small ρ_ξ, this can drastically change the appearance of the function; for example, the same function as in figure 4.5 is plotted again with a tangent projection in figure 4.7.

This does not cause serious problems, however. For one, at a short ρ_ξ, the diatomic basis functions are not good physical representations anyway, since they are functions created by neglecting the three-body potential terms, which are non-negligible at this range. Secondly, provided a sufficient number of states are included, an optimized adiabatic basis can still be formed during the diagonalization process of the surface Hamiltonian.

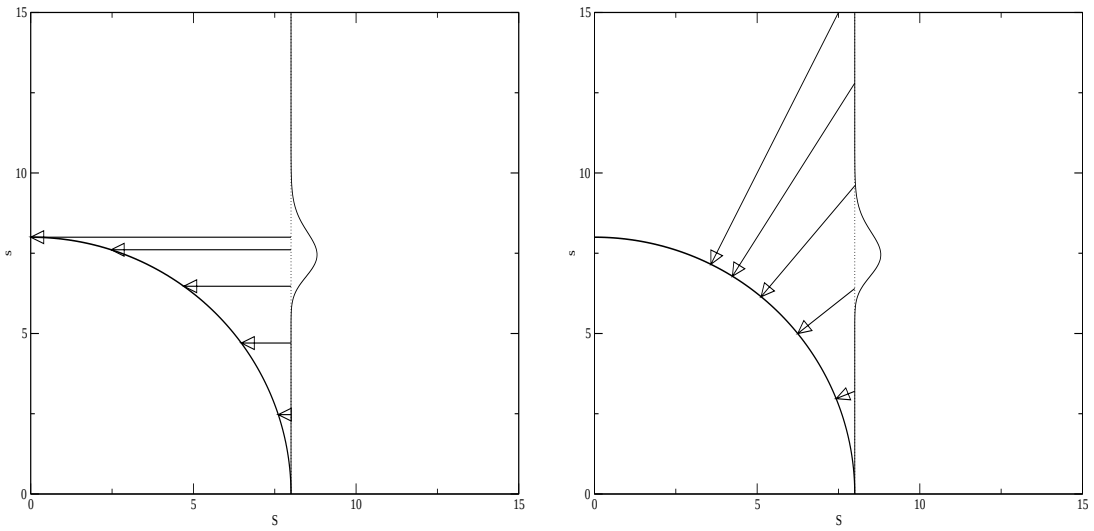

Figure 4.6: In figure a, a $s_\tau = \rho \sin \vartheta_\tau$ projection is used to project the asymptotic Jacobi functions onto the constant ρ hypersurface. In figure b, a $s_\tau = \rho \tan \vartheta_\tau$ projection is used in order to ensure that the entire domain of s_τ is projected onto the hypersurface and to avoid any discontinuities in the projected function.

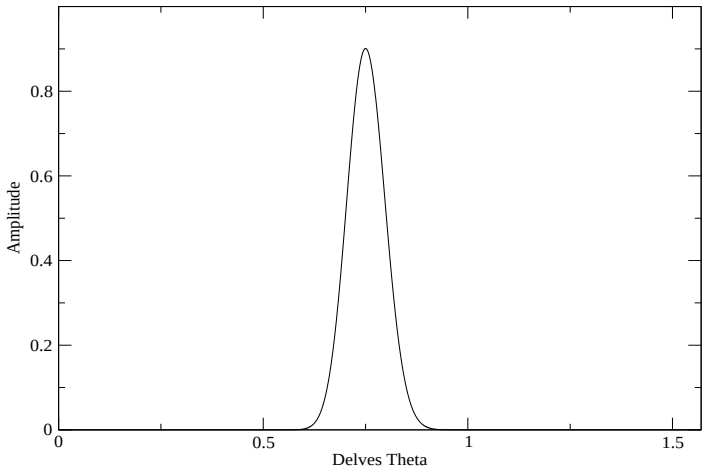

Figure 4.7: Plot of $\zeta(s_\tau)$ projected onto Delves hypersurface at $\rho_\xi = 8.0a_0$ with projection of $s_\tau = \rho_\xi \tan \vartheta_\tau$

At large ρ_ξ, because of the finite range of s_τ for which the bound states have amplitude, there is little difference in the two projections. Figure 4.8 shows the same state as those plotted in figure 4.6. but this at $100a_0$. At this distance, the two are nearly indistinguishable. We can now fully form the projected bound state for a single channel onto a Delves hypersurface. The complete description of the bound states must also include the coupled spherical harmonic functions, $\mathscr{Y}$, that were used in section 3.

A very important point to note is the distinction between space-fixed labels and body-fixed labels. Throughout this process, we have used space-fixed functions labeled by $\nu j \ell$ to describe the state. The intention, though, is to generate symmetry labeled Φ functions that are eigenfunctions of the APH surface Hamiltonian with

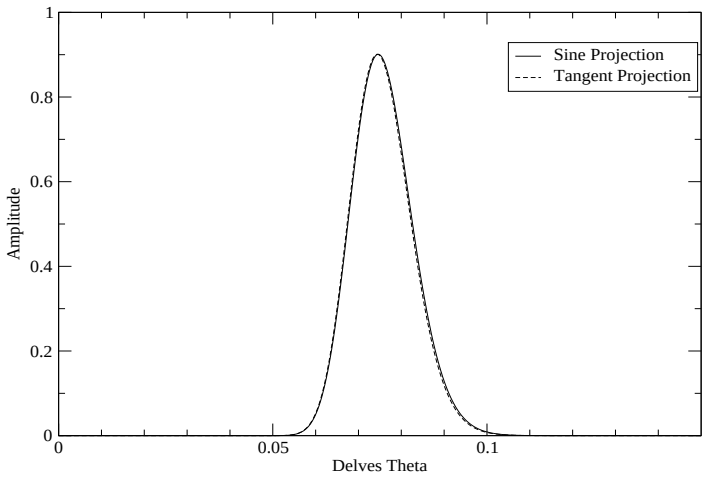

Figure 4.8: Plot of $\zeta(s_\tau)$ projected onto Delves hypersurface both with $s_\tau = \rho_\xi \sin\vartheta_\tau$ and $s_\tau = \rho_\xi \tan\vartheta_\tau$ at $\rho_\xi = 100.0a_0$. At this value of ρ, the two are nearly indistinguishable. Note that the domain of $\vartheta_\tau$plotted here is reduced to show the function more clearly.

body-fixed labels. There is not an incongruity here; these constructed φ states are simply to be used as basis functions. An alternate definition of $\mathscr{Y}$ can be used,

$$\mathscr{Y}_{j\ell}^{JM}(\hat{s},\hat{S}) = \left(\frac{2\ell+1}{2J+1}\right)^{1/2} \sum_{\Lambda} C(j\ell J;\Lambda 0\Lambda)\hat{P}_{j\Lambda}(\Theta_\tau)\hat{D}^{J}_{\Lambda,M}(\alpha_\tau,\beta_\tau,\gamma_\tau) \qquad (4.47)$$

where $\hat{P}$ is a normalized associated Legendre polynomial, and $\hat{D}^{J}_{\Lambda,M}(\alpha_\tau,\beta_\tau,\gamma_\tau)$ is the normalized Wigner rotation function that establishes the relationship between the space-fixed axes and the body-fixed axes for the respective angular momentum projections M and Λ. The ζ bound states do not depend on ℓ, and so we can generate a set of functions that are labeled by the body-fixed Λ, the projection of the total angular momentum on the body-fixed z axis without any difficulty, and indeed this is what is done. However, the next step is to symmetrize this basis to get functions not labeled by the channel τ, but by the irreducible representation Γ. In the symmetrization process, the functions are reflected or rotated in the APH internal coordinates, and for these Λ looses its physical meaning since we change the orientation of the function to the z axis by which it was defined. But in using the functions defined in internal (θ,χ) coordinates only, Λ is only a parameter in the APH surface Hamiltonian, and these are merely basis functions; we don't actually need to label them with anything at all. Therefore, in the final definition of the internal-only basis function, we ignore for the time the $\hat{D}$ function. However, in order to make the basis as physically representative as possible, the Λ on $\hat{P}_{j\Lambda}$ should match that in the APH surface Hamiltonian (equation 2.38.

The resultant basis function for a single channel is thus defined as

$$\varphi^{J\Lambda}_{\tau\nu j\xi}(\vartheta_\tau,\Theta;\rho_\xi) = \frac{1}{\sin(2\vartheta_\tau)}\zeta_{\tau\nu j}(\rho_\xi \tan\vartheta_\tau)\hat{P}_{j\Lambda}(\Theta_\tau) \qquad (4.48)$$

Noting that the Delves wavefunction expansion in equation 2.18 also includes a $1/sin2\vartheta_\tau$ term in the basis definition, it must be included in the projected basis here as well. This set of φ functions represents a set of channel specific basis functions. From here we can generate a symmetrized set of basis functions according to the theory set forth in section 4.2. This produces a set of functions, ϕ^B that are labeled by irreducible representation instead of by channel. But, it is exactly the same number of basis functions either way. The φ functions are not devoid of symmetry as it is, and as discussed in 4.2, whether j is odd or even affects which irreducible representations the function contributes to, as well as the parity, but we can define a generic symmetrizing operator, $\mathcal{S}(j, p, \tau, \Gamma)$ such that

$$\phi^{J\Lambda}_{\Gamma\nu j}(\theta, \chi; \rho_\xi) = \sum_\tau \mathcal{S}(j, p, \tau, \Gamma)\varphi^{J\Lambda}_{\tau\nu j} \tag{4.49}$$

where for simplicity we have omitted the coordinates on the right side, as the correlation between the coordinates between the Delves and APH systems is somewhat complex, but the relations are given in appendix B. However, for any given point in θ, χ we can evaluate the basis function as it is defined.

4.3.2 APH Continuum State Construction

A *continuum state* in this context refers to states of the three-atom system in which all three atoms can separate infinitely as opposed to a *bound state* in which the asymptotic system consists of a diatomic molecule and a separated atom. The latter should not be confused with the triatomic bound states where all three atoms are bound together, which is not discussed here.

The goal is to construct basis functions on the APH hyper-surface at constant ρ that represent the continuum states, and like the bound and quasibound states, it would be ideal to use functions that are as similar to the asymptotic ($\rho \to \infty$) continuum state functions as possible. The bound states were constructed from diatomic rovibrational states in mass-scaled Jacobi coordinates, and then as the propagation proceeds, are used to create bound states in APH coordinates by use of a simple coordinate transform. Constructing the continuum states in the same way has some complications:

1. Unlike the bound state basis functions, the continuum state functions do not become localized to any particular region as $\rho \to \infty$. Instead, they have amplitude over the entire domain of space. At no point can any region of space be ignored as having negligible contribution as can be done with scattering calculations involving bound states alone.

2. While the continuum basis functions can be labeled and associated with a specific channel, such basis functions from different channels can correspond to identical quantum numbers (i.e. J^2, Λ), and so identical asymptotic continuum states can be over-represented by the basis if continuum states from each channel are included.

3. The bound states, being derived from diatomic wavefunctions of two atoms associated with a given channel, ran the risk of being non-zero in the other channels where a different combination of two atoms coalesced. On the other hand, by definition the continuum states have amplitude throughout the whole space. If constructed as they were for the HNe_2 problem, i.e. for a single channel, they will certainly have amplitude in the highly repulsive regions of the other channels because the continuum functions in Delves

coordinates, as constructed, ignores the diatomic potentials for the other channels.

4. The continuum state basis functions cannot be represented easily in Jacobi coordinates. Were they constructed the same way as the bound and quasibound states, from solutions to the diatomic Hamiltonian, their energy spectrum would be continuous rather than discrete, thus forcing one to make explicit choices as to the diatomic energies to include, and the functions would oscillate indefinitely in the Jacobi s_τ coordinate, making it impossible to project them onto the APH hypersurface with any consistence.

Not all of these issues are highly problematic. Item 1 requires that all integrals involving the basis functions be over the whole spatial domain of a constant ρ surface. While theoretically trivial, in practice such integrals can be numerically cumbersome and very difficult to perform accurately. However, this difficulty can be assuaged with careful consideration of the function's properties and a well tailored integration grid as is explained in chapter 5.

Item 2 is solved by virtue of the symmetrization of the basis sets. Continuum functions from each channel are combined in linear combinations to produce symmetrized surface functions on the APH hypersphere.

Item 3 can be handled in multiple ways. One is to ignore it, and allow the diagonalization of the surface Hamiltonian (eqn 4.31) to produce eigenfunctions. For the propagation phase of the scattering calculation, it is not necessary to include the same number of eigenfunctions of equation 4.31 as we have basis functions, so increasing the number of basis functions and allowing the variational principle to optimize the low energy eigenfunctions is a viable and simple solution. However, it is also possible to tailor the continuum functions so that they have small amplitude

in the classically forbidden potential regions by multiplying them by a "killing" function, a function designed to reduce the amplitude near the highly repulsive regions of the potential but not affecting the rest of it. This function may take the form of a simple inverse tangent function of s_τ for each channel, or a function similar to the zero-energy diatomic wavefunction may be used, as was done for the single channel continuum states of HNe_2 (see section 3.3). The downside to either of these methods is that the numerical derivatives necessary for the surface Hamiltonian calculation can be much more complicated.

To address issue 4, we do know how to construct the continuum functions for a single channel in Delves coordinates, and the solution is given in equation 3.18 in section 3.3. Rewriting that definition here again we have

$$\phi_{\tau j\ell\nu\xi}(\vartheta_\tau) = \phi^0_j(\rho_\xi \sin\vartheta_\tau)\cos^{\ell+1}(\vartheta_\tau)\mathscr{P}_{j,\ell,\nu-nbqb}(\vartheta_\tau) \tag{4.50}$$

were again the ϕ^0 functions are the two-body, zero energy wavefunctions that replaced the $\sin^{j+1}(\vartheta_\tau)$ term in the zero-potential Delves solution (equation 3.16). These ϕ^0 functions are calculated as functions of s and then transformed, while the rest of the constituents of the continuum function are developed as functions of ϑ_τ. The zero-potential solution to the surface Hamiltonian in APH coordinates are not known analytically, so we must continue to use the Jacobi polynomial solutions. The coordinate transformations between Delves coordinates and APH coordinates, and between Jacobi coordinates and APH coordinates, are known analytically and can be applied without difficulty to transform the continuum functions into APH coordinates. To do so does, however, require some care in ensuring that the proper transformation between coordinate systems are applied to each constituent part of the constructed continuum function.

One way to do this is to apply the zero-energy, ϕ^0 function for each channel to the whole linear combination. Let's redefine the notation of the ϕ functions to include the channel index, τ, and drop the other indices for clarity. Further, let us separate the zero-energy part of the function from the rest, and thus define

$$\phi_\tau(\theta,\chi) = \phi^0_\tau(\theta,\chi)\phi^1_\tau(\theta,\chi) \tag{4.51}$$

where the coordinate transformation to APH has been assumed, and the ϕ^1_τ term represents everything in the ϕ_τ definition except the zero-energy function.

The continuum functions as defined in equation 4.51 do not behave correctly in the regions were the other channel lines lie, which is to say they ignore the repulsive potential of where two atoms would coalesce in a different channel. To account for this, we multiply this result by the product of the ϕ^0_τ functions for each channel. Calling the new APH continuum function φ, we have

$$\varphi^{JM}_{\tau\nu j\ell\xi}(\theta,\chi) = \left(\phi^0_j\right)_A \left(\phi^0_j\right)_B \left(\phi^0_j\right)_C \phi^1_{\tau j\nu\ell}\mathscr{Y}^{JM}_{\tau j\ell} \tag{4.52}$$

The φ function behaves correctly at each of the different channels, yet are still associated with a specific channel. Linear combinations of these states can be created to make symmetrized functions, just like the

To get the kinetic matrix elements of these functions, we must get their derivatives with respect to the APH coordinates θ and χ. This is done by taking the derivative of each component of $\varphi(\theta,\chi)$ as defined in equation 4.52. Like the derivatives for the HNe_2 problem, the ϕ^0 functions are functions of the mass-scaled Jacobi

coordinate s_τ, and the ϕ^1 functions are functions of the Delves hyperspherical coordinates for the associated channel. Thus we have

$$\begin{aligned}\frac{\partial \varphi_\tau}{\partial \theta} &= \frac{\partial}{\partial s}\left(\phi_A^0 \phi_B^0 \phi_C^0\right)\left(\frac{\partial s}{\partial \theta}\right)\phi_\tau^1 \mathscr{Y}_\tau^J \\ &+ \left(\phi_A^0 \phi_B^0 \phi_C^0\right)\frac{\partial}{\partial \vartheta_\tau}\left(\phi_\tau^1 \mathscr{Y}_{\tau j\ell}^J\right)\left(\frac{\partial \vartheta_\tau}{\partial \theta}\right) \\ &+ \left(\phi_A^0 \phi_B^0 \phi_C^0\right)\frac{\partial}{\partial \Theta}\left(\phi_\tau^1 \mathscr{Y}_{\tau j\ell}^J\right)\left(\frac{\partial \Theta}{\partial \theta}\right) \end{aligned} \tag{4.53}$$

with the derivative with respect to χ following the same form. The terms of Delves coordinates differentiated with respect to APH coordinates are given explicitly in appendix B.4. Only the $\mathscr{Y}$ functions in equation 4.53 depend on Θ, and derivatives of these functions are analytic. The ϕ^1 "vibrational" continuum functions contain the Jacobi Polynomials as functions of ϑ_τ, the derivatives of which can be found by recurrence relations, as shown in appendix D.

The second derivative terms can be found by further use of the differentiation chain rule. Once these are constructed from the already known quantities, then we can construct matrix elements of the APH surface Hamiltonian as given in equation 4.31.

Like with the bound states described in section 4.3.1, the φ^0 functions are calculated once in terms of the Jacobi s coordinate, and then splined so that the value of this function can be found where needed. The derivatives of these functions with respect to s_τ are also splined. All other terms in equation 4.53 are analytically known.

Another way to handle item 4 is to simply include more continuum states to the basis and employ the variational principle by constructing the Hamiltonian matrix with an excess of continuum functions and diagonalizing this to get eigenfunctions

that do behave physically. In this way, we use the zero-potential solutions to the Delves vibrational Hamiltonian, equation 2.20, with $V = 0$, and solutions given in equation 3.16, which are

$$\varphi^{C}_{j\ell n}(\vartheta_\tau) = \sin^{j+1}(\vartheta_\tau)\cos^{\ell+1}(\vartheta_\tau)\mathscr{P}_{j\ell n}(2\vartheta_\tau)$$

where the C superscript refers to a continuum state.

Including these states for each channel introduces linear dependency, since these states for a single channel alone constitute a complete basis. However, in creating the symmetrized basis functions, these states from each channel are included in the basis. If there is linear dependency, it can be removed by either forming an overlap matrix and looking for eigenvalues of this overlap matrix that are very small, thus indicating the corresponding eigenfunction to be linearly dependent, or by looking or eigenvalues of the Hamiltonian that are exceedingly large, which corresponds to states that behave non-physically in the highly repulsive potential regions. Either way, the basis set can then be truncated to just include the states with reasonable eigenvalues of either the overlap matrix or the Hamiltonian matrix.

In practice, this second method is much simpler to implement than the process of replacing the $\sin^{j+1}(\vartheta_\tau)$ terms as in equation 4.52. The functions are analytic, as are their derivatives, and can be calculated very quickly. For these reasons, after comparison, this was the method used.

4.4 Projections With Asymptotic-type States

The asymptotic states for the bound channels do not posses the symmetry of the full wavefunction, that is, they do not possess C_{6v} symmetry, but instead they

are functions of C_{2v} symmetry in APH coordinates. Naturally in other coordinate systems, they might belong to a different point group. However, a coordinate transformation can only change the point group to another that is isomorphic to the first, and so the concepts of this section still apply.

An asymptotic bound state for channel A is closely related to the functions discussed already that constitute the symmetry states. As shows in section 3.1, the two body constructed states approach the exact diatomic bound states as $S \to \infty$. So while the asymptotic-type states discussed in this section might not be exactly the asymptotic states, the symmetry relationships are the same and the physical representation is very similar, especially in moderate to large ρ regions.

An asymptotic state is labeled by its parity and rotational quantum number which completely define its symmetry in C_{2v}. The C_{2v} point group is of order four, whereas C_{6v} is of order twelve, and so only four functions need to be used to define it. Labeling these states by their channel, j, and parity, we can see that we have for an even (+) j, even (+) parity state on channel A,

$$A_{j+}^{p+} = |1\rangle + |6\rangle + |7\rangle + |12\rangle \tag{4.54}$$

or for a different channel, say

$$B_{j-}^{p+} = |9\rangle - |2\rangle + |3\rangle - |8\rangle \tag{4.55}$$

Plotted examples of these asymptotic functions for the A channel can be seen in figure 4.9

These asymptotic states consist of the same functions that the symmetry states do, and could themselves be used as a basis. The symmetrized basis has a great

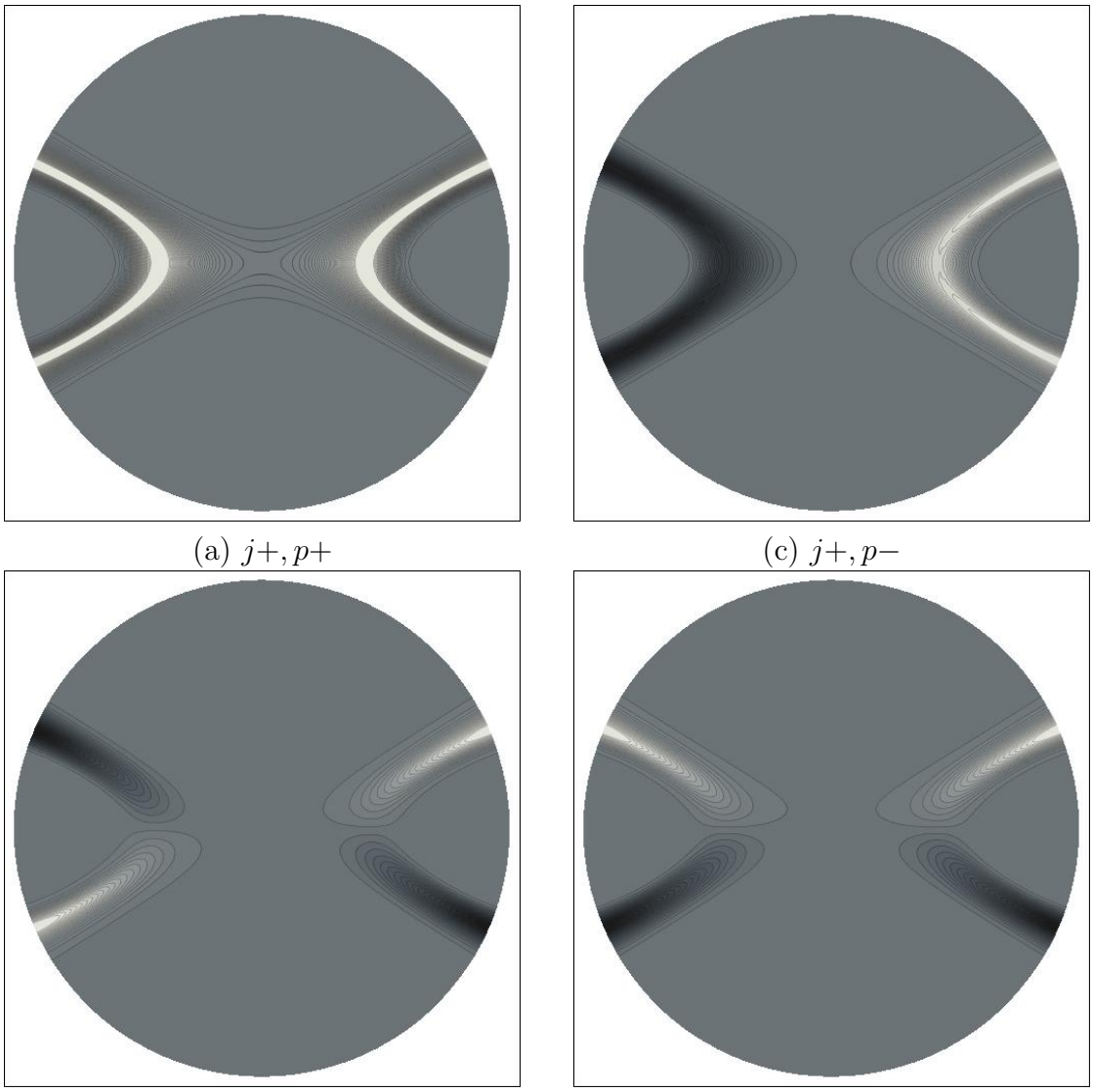

(a) $j+, p+$ (c) $j+, p-$

(b) $j-, p+$ (d) $j-, p-$

Figure 4.9: Example asymptotic functions for channel A and labeled by even or odd rotational j values and even or odd parity.

advantage that in most cases, it is obvious if integrals between states cancel due to symmetry, while it is not necessarily obvious with these asymptotic states.

It is therefore of interest to know how these functions relate to each other. The projections of each of the asymptotic states onto the symmetrized states is given in appendix E.3.

4.5 Propagation, Boundary Conditions, and Asymptotic Matching

Once the propagation has reached a point where the potential is effectively asymptotic, that is, where there are no longer three-body effects and the potential is only non-zero where two atoms become close, then the boundary conditions for the radial wavefunction, $\psi(\rho)$ can be applied, and scattering information can be extracted. Since the basis used for propagation, $\Phi(\theta, \chi; \rho_\xi) = \Phi_\xi$, is an adiabatic basis in that it diagonalizes the APH surface Hamiltonian at every ρ_ξ, we must transform this basis to the asymptotic basis set, which are the functions that describe the system beyond the range of the three-body interaction potential. In this basis, we can form $\psi^{asy}(\rho)$ which can be expressed in terms of the reactance matrix, $\mathbf{K}$ as

$$\psi^{asy}(\rho_\xi) = \mathbf{a}_\xi - \mathbf{b}_\xi \mathbf{K} \tag{4.56}$$

where $\mathbf{a}$ and $\mathbf{b}$ are known regular and irregular solutions to the radial Schrödinger equation. At an asymptotic region where the potential is ineffectual, all solutions to the Schrödinger equation can be expressed as a linear combination of the $\mathbf{a}$ and $\mathbf{b}$ solutions. The reactance matrix $\mathbf{K}$ contains all of the attainable scattering information.

The possible asymptotic states include the two-body, diatomic wavefunctions for each arrangement channel, and the continuum wavefunctions that describe three separated atoms. Let us call this asymptotic basis $\{\Xi\}_\xi$, which is defined at some ρ_ξ, and $\mathbf{\Xi}_\xi$ will represent a matrix of these states. We require a transformation from the adiabatic $\mathbf{\Phi}$ basis, evaluated at an asymptotic ρ_∞, to the asymptotic basis, such that

$$\mathbf{\Phi}(\theta, \chi; \rho_\infty) = \mathbf{\Xi}_\infty \mathbf{D}_\infty \tag{4.57}$$

Since studies of convergence would ask that asymptotic analysis be performed at many different values of ρ_∞, it is sensible to label each basis set and transformation matrix by a propagation step index rather than ∞.

$$\mathbf{\Phi}(\theta, \chi; \rho_\xi) = \mathbf{\Phi}_\xi = \mathbf{\Xi}_\xi \mathbf{D}_\xi \tag{4.58}$$

The set of $\{\Xi\}_\xi$ must be well defined. Since these would represent the system asymptotically and must represent all possible asymptotic states, this set of functions must include diatomic wavefunctions plus a free atom, and wavefunctions that describe three free atoms. These we call bound and continuum states, respectively, but not to be confused with three-body bound states. Thus the set can be written as

$$\{\Xi\}_\xi = \sum_{n_b} \Xi(E < 0) + \sum_{n_c} \Xi(E > 0) \tag{4.59}$$

How to form the Ξ functions will be discussed later in this section, but at present, if we assume these functions are well defined, then the propagated radial coefficients, $\psi(\rho) = \psi^{adia}$ that are defined in equation 4.6 can be transformed from the adiabatic

basis in which they are propagated, to the primitive basis by substituting equation 4.57 into the full wavefunction equation, such that

$$\begin{aligned} \mathbf{\Psi}_\xi &= \mathbf{\Phi}_\xi \psi_\xi^{adia} \\ \mathbf{\Psi}_\xi &= \mathbf{\Xi}_\xi \mathbf{D}_\xi \psi_\xi^{adia} \end{aligned} \tag{4.60}$$

In this $\mathbf{D}_\xi \psi^{\mathbf{adia}}$ provides a transformation only on the "final" states, since the row index of this matrix refers to the asymptotic primitive basis, and the column index is still the adiabatic propagation basis. To complete this appropriately we multiply on the right by $\mathbf{D^T}$, the transpose of $\mathbf{D}$,

$$\mathbf{\Psi}_\xi \mathbf{D}_\xi^{\mathbf{T}} = \mathbf{\Xi}_\xi \mathbf{D}_\xi^T \psi_\xi^{adia} \mathbf{D}_\xi^T \tag{4.61}$$

which gives $\mathbf{\Psi}$ fully in the asymptotic basis, and we can define a transformation between the sets of propagation coefficients,

$$\begin{aligned} [\psi_\xi{}^{asy}] &= [\mathbf{D}_\xi^T][\psi_\xi^{adia}][\mathbf{D}_\xi] \\ [\psi_\xi{}^{adia}] &= [\mathbf{D}_\xi][\psi_\xi^{asy}][\mathbf{D}_\xi^T] \end{aligned} \tag{4.62}$$

In using the Smooth Variable Discretized (SVD) Enhanced Renormalized Numerov algorithm[14] for the propagation, we calculate an R matrix rather than ψ^{adia}, where again the relation between them is given as

$$\mathbf{R}_\xi (\mathbf{I} - \mathbf{T}_\xi) \psi_\xi^{adia} = \mathbf{O}_{\xi,\xi+1} (\mathrm{I} - \mathbf{T}_{\xi+1}) \psi_{\xi+1}^{adia} \tag{4.63}$$

Using equation 4.62 to change to the asymptotic basis, we get

$$\mathbf{R}_\xi(\mathbf{I}-\mathbf{T}_\xi)\mathbf{D}_\xi^T\psi_\xi^{asy}\mathbf{D}_\xi = \mathbf{O}_{\xi,\xi+1}(\mathrm{I}-\mathbf{T}_\xi+1)\mathbf{D}_{\xi+1}^T\psi_{\xi+1}^{asy} \tag{4.64}$$

where $\mathbf{O}_{\xi,\xi+1}$ is the overlap matrix between the $\mathbf{\Phi}_\xi$ and $\mathbf{\Phi}_{\xi+1}$ bases. If we make the approximation that

$$\mathbf{D}_\xi\mathbf{D}_{\xi+1}^T \approx \mathrm{I} \tag{4.65}$$

then we can multiply on the right by $\mathbf{D}_{\xi+1}^T$ and use equation 4.56 to get

$$\mathbf{R}_\xi(\mathrm{I}-\mathbf{T}_\xi)\mathbf{D}_\xi^T(\mathbf{a}_\xi-\mathbf{b}_{\xi+\mathbf{1}}\mathbf{K}) = \mathbf{O}_{\xi,\xi+1}(\mathrm{I}-\mathbf{T}_{\xi+1})\mathbf{D}_{\xi+1}^T(\mathbf{a}_{\xi+1}-\mathbf{b}_{\xi+\mathbf{1}}\mathbf{K}) \tag{4.66}$$

This can be put in the form of

$$\mathbf{A} = \mathbf{B}\mathbf{K} \tag{4.67}$$

$$\mathbf{B} = \left[\mathbf{O}_{\xi,\xi+1}(\mathrm{I}-\mathbf{T}_{\xi+1})\mathbf{D}_{\xi+1}^T\mathbf{b}_{\xi+1} - \mathbf{R}_\xi(\mathrm{I}-\mathbf{T}_\xi)\mathbf{D}_\xi^T\mathbf{b}_\xi\right] \tag{4.68}$$

$$\mathbf{A} = \left[\mathbf{O}_{\xi,\xi+1}(\mathrm{I}-\mathbf{T}_{\xi+1})\mathbf{D}_{\xi+1}^T\mathbf{a}_{\xi+1} - \mathbf{R}_\xi(\mathrm{I}-\mathbf{T}_\xi)\mathbf{D}_\xi^T\mathbf{a}_\xi\right] \tag{4.69}$$

From here $\mathbf{K}$ can be solved for easily with linear algebra methods.

While this procedure is not new, there are some notes of interest that are relevant to the current problem. It must be observed that for the above transformations by the $\mathbf{D}$ matrix, which is dimensioned as $N_{adia} \times N_{asy}$, it is assumed that $\mathbf{D}$ is square and orthogonal (or unitary if complex functions are used). For this to be true, it is necessary that both the adiabatic basis and the asymptotic basis are sets of orthonormalized functions, and that there are equal numbers of each of them. This is not generally true; there could be more or less of either. In such a case, the generalized inverse of $\mathbf{D}$ would need to be used instead of $\mathbf{D}^T$.

If $N_{asy} < N_{adia}$, then more functions are being propagated than are necessary for the desired scattering information, and either N_{adia} should be reduced to save computation, or N_{asy} should be increased.

Colavecchia et al.[14] address the situation where there $N_{asy} > N_{adia}$, noting that asymptotically, and for a given channel, the adiabatic bound states approach the asymptotic bound states. If the indices of $\mathbf{D}$ represent states that are ordered by energy, then $\mathbf{D}$ would exhibit an $n_b \times n_b$ block that would approach the unit matrix. Furthermore, it is stated that the coupling between continuum and bound states is approximately zero for all combinations of asymptotic and adiabatic functions. With these provisions, they use $\mathbf{D}^T$ as an inverse, and show that this is effective as well as much more efficient than propagating an adiabatic basis that is as large as the asymptotic basis.

One other issue to address is the validity of $\mathbf{D_\xi D_{\xi+1}}^T \approx \mathrm{I}$. In practice, calculations on the HNe_2 system showed that at asymptotic ρ values used, the off-diagonal elements of $\mathbf{D_\xi D_{\xi+1}}^T$ at ρ up to $100a_0$ reached values of 0.01-0.03. While it is possible in theory to solve for $\mathbf{K}$ without making this approximation, attempts to numerically solve equation 4.64 for $\mathbf{K}$ either as a form of Sylvester's equation or by iterative processes were unsuccessful. The $\mathbf{a}$ and $\mathbf{b}$ matrices are composed of either tiny or huge numbers, depending on whether asymptotic channels were open or closed energetically, and too much accuracy was lost to get any converged result for $\mathbf{K}$. This approximation does improve, though, as the further one propagates.

4.5.1 Asymptotic Bound State Definitions

For the bound states, the asymptotic functions are the two-body diatomic wavefunctions, which are labeled by $\tau\nu j\ell$, where τ labels the arrangement channel,

and ν and j label the rovibrational state of the diatom, and ℓ labels the orbital angular momentum of the free atom about the center of mass of the diatom. The radial wave functions that correspond to these states asymptotically are the regular and irregular Riccati-Bessel functions for open states. Previous calculations [18, 19, 20], have shown that these functions are best described in a Jacobi coordinate system where s_τ measures the internuclear distance of the diatom, and S_τ is so large that there is no interaction between the third atom and the diatom. In a Jacobi coordinate matching scheme, $\mathbf{a}, \mathbf{b}$ are defined as

$$\begin{aligned} \mathbf{a}(\mathbf{S_f})_{fi} &= \delta_{fi} k_f^{1/2} S_f j_{\ell_f}(k_f S_f) \\ \mathbf{b}(\mathbf{S_f})_{fi} &= \delta_{fi} k_f^{1/2} S_f y_{\ell_f}(k_f S_f) \end{aligned} \tag{4.70}$$

and for closed states the radial functions in Jacobi use regular and irregular Modified Bessel functions

$$\begin{aligned} \mathbf{a}(S_f)_{fi} &= \delta_{fi} \left(k_f S_f \frac{\pi}{2k_f} \right)^{1/2} I_{\ell_f+1/2}(k_f S_f) \\ \mathbf{b}(S_f)_{fi} &= \delta_{fi} \left(k_f S_f \frac{\pi}{2k_f} \right)^{1/2} K_{\ell_f+1/2}(k_f S_f) \end{aligned} \tag{4.71}$$

Attempts have been made define these states in hyperspherical coordinates [21, 22, 13], but the resultant transition probabilities between states exhibited oscillations as a function of ρ. These oscillations diminished as ρ_∞ was increased,

but one had to propagate to much greater distances than if Jacobi coordinates were used. In Delves coordinates, we have for open states

$$\mathbf{a}(\rho)_{fi} = \delta_{fi} k_f^{1/2} \rho j_{\ell_f}(k_f \rho) \tag{4.72}$$

$$\mathbf{b}(\rho)_{fi} = \delta_{fi} k_f^{1/2} \rho y_{\ell_f}(k_f \rho) \tag{4.73}$$

and for closed states,

$$\mathbf{a}(\rho)_{fi} = \delta_{fi} \left(k_f \rho \frac{\pi}{2k_f} \right)^{1/2} I_{\ell_f+1/2}(k_f \rho) \tag{4.74}$$

$$\mathbf{b}(\rho)_{fi} = \delta_{fi} \left(k_f \rho \frac{\pi}{2k_f} \right)^{1/2} K_{\ell_f+1/2}(k_f \rho) \tag{4.75}$$

In either the Jacobi or the Delves equations above, the δ_{fi} is provided by the integrals performed on the respective orthonormal asymptotic basis sets.

Where continuum states are possible, however, it is desirable to propagate in hyperspherical coordinates, so to improve on bound state asymptotic matching, Kuppermann and Kaye introduced[23] a mixed boundary condition where by the bound states are expressed in Jacobi coordinates but are projected onto a hyperspherical surface for matching. Colavecchia et al.[14] showed that applying this method did not remove the oscillations in the transition probabilities entirely, but did reduce them significantly, and converged results were possible without the need to propagate to very large distances.

In a mixed boundary condition, the functions are matched at a constant ρ as in the Delves equations of 4.73 and 4.75, but the integrations give the projection

of Jacobi asymptotic states, e.g. $\sqrt{k_f} j_{\ell_f}(S_f) \Xi_f^{Jac}(s_f)$, onto a constant ρ surface with a Delves coordinate asymptotic basis, $\Xi_f^{Del}(\rho)$, which gives

$$\begin{aligned}
\mathbf{a}_f i &= \sqrt{k_f} \int_0^{\pi/2} \rho \cos(\vartheta_{\tau f}) d\vartheta_{\tau f} \zeta_i^{Jac}(\rho \sin \vartheta_{\tau f}) \Xi_f^{Del}(\vartheta_{\tau f}) j_{\ell_f}(k_f \rho \cos \vartheta_{\tau f}) \\
\mathbf{b}_f i &= \sqrt{k_f} \int_0^{\pi/2} \rho \cos(\vartheta_{\tau f}) d\vartheta_{\tau f} \zeta_i(\rho \sin \vartheta_{\tau f}) \Xi_f^{Del}(\vartheta_{\tau f}) y_{\ell_f}(k_f \rho \cos \vartheta_{\tau f})
\end{aligned} \tag{4.76}$$

for the open states. The closed states not changed from the standard definition. As ρ becomes large, the Ξ^{Jac} and Ξ^{Del} functions approach being identical, and the integral approaches the delta function times j or y evaluated at $S_f = \rho$. However, at moderate ρ values, this is effectively an overlap matrix that attempts to express the Jacobi asymptotic boundary conditions in terms of the Delves functions; two different orthonormal sets that span slightly different spaces.

In the present case of scattering in APH coordinates, this same mixed boundary procedure is used for the open bound states, but instead of matching onto a Delves hypersurface, we match onto an APH one. This requires a double integral over θ and χ in lieu of the single integral over ϑ_τ, but this does not add significant complexity as one simply projects the asymptotic Jacobi diatom wavefunctions, $\zeta_{\nu j \ell}(s_\tau)$ onto a constant ρ APH hypersurface in θ and χ. Otherwise, the $\mathbf{a}_{fi}$ and $\mathbf{b}_{fi}$ matrices are formed identically to the Delves case.

Since this method of mixed boundary conditions provides the benefit of propagating in hyperspherical coordinates along with significant improvement in the calculated bound state transitions, we choose to use it here also. The bound diatomic wavefunctions in each channel are calculated in Jacobi coordinates for the entire range of $s_\tau$for which they have amplitude, and these are labeled by good diatomic rovibrational quantum numbers.

4.5.2 Asymptotic Continuum State Definitions

Defining asymptotic continuum states is not as simple as the bound states. Hyperspherical coordinate definitions of the continuum states is desirable because if one were to define them in Jacobi coordinates, the continuum wavefunctions in $s_\tau$have amplitude to $s_\tau \to \infty$, making integration difficult, and have a continuous energy spectrum. If defined in hyperspherical coordinates, these states are defined by angles and thus have a finite range of amplitude and a discrete energy spectrum. Asymptotically, the Delves continuum states approach the energy[13]

$$\lim_{\rho\to\infty} \rho^2 \mathcal{E}_{\nu j\ell} = \frac{\hbar^2(\lambda+2)^2}{2\mu} \tag{4.77}$$

where λ is Smith's grand angular momentum [11] and is defined as $\lambda = 2\nu + j + \ell$. The radial functions become a linear combination of Bessel functions as

$$[\mathbf{a}(\rho)]_{fi} = \delta_{fi}\left(\frac{\pi\rho}{2}\right)^{1/2} J_{\lambda+2}(k\rho) \tag{4.78-a}$$

$$[\mathbf{b}(\rho)]_{fi} = \delta_{fi}\left(\frac{\pi\rho}{2}\right)^{1/2} Y_{\lambda+2}(k\rho) \tag{4.78-b}$$

where J and K are the integer-order regular and irregular Bessel functions, and

$$k^2 = \frac{2\mu E}{\hbar^2} \tag{4.79}$$

For closed states, we replace J and Y with the modified Bessel functions I and K. The asymptotic Delves continuum functions are well defined; equation 3.16, rewritten here,

$$\phi^C_{j\ell n}(\vartheta_\tau) = \sin^{j+1}(\vartheta_\tau)\cos^{\ell+1}(\vartheta_\tau)\mathscr{P}_{j\ell n}(2\vartheta_\tau)$$

for the "vibrational" ϑ_τ coordinate, and the $\mathscr{Y}$ rotational functions for the other coordinates. In APH coordinates, however, these motions are not separable in θ and χ. Furthermore, the asymptotic condition on the continuum states is not simply a zero potential case; for this the APH wavefunctions are well defined hyperspherical harmonics. But instead we have a case where exists diatomic potentials for all values of ρ. No matter how large ρ becomes, there are regions of (θ, χ) space where two of the atoms may become close, and at the point where they coalesce the potential becomes effectively infinite. As $\rho \to \infty$, the regions of non-zero diatomic potential on the (θ, χ) hypersphere become infinitesimally small, but a physical continuum state should still be zero at the points of diatom coalescence.

Furthermore, excluding the diatomic potentials from the definition of the asymptotic continuum states, thereby using a zero potential hyperspherical harmonic definition, leads to asymptotic continuum states that are not orthogonal to the asymptotic bound states. Since it is the masses of the atoms that determine the location of the channels, and proper continuum states of definite quantum numbers that are orthogonal to the bound states must be influenced by the diatomic potentials, an analytic solution that satisfies these conditions may not be possible.

One possible solution is to use the adiabatic states that correspond to energies greater than zero asymptotically. These have the advantage that they are by definition orthogonal to the adiabatic bound states, and as noted previously, at large ρ, the adiabatic bound states approach the asymptotic bound states. The adiabatic continuum states do have a difficulty in that they are linear combinations of the symmetrized primitive basis functions, the $\phi(\theta, \chi)$ functions defined in equation 4.49. The symmetrized ϕ functions have a definite λ label, but the Φ do not. It is possible to use these still, but this would result in the $\mathbf{a}_{fi}$ and $\mathbf{b}_{fi}$

in equations 4.78-a,4.78-b to be non-diagonal. If the transformation coefficients are kept that relate the symmetrized ϕ basis to the Φ basis, then these could be used to determine the off-diagonal elements, but the asymptotic states would still require a definite λ to be meaningful.

Another possibility is to simply use the symmetrized ϕ states that correspond to the asymptotic continuum states. While these do provide functions with a definite λ, these states are not orthogonal to each other. Continuum states for a single channel, $\varphi_\tau(\theta, \chi)$ defined in section 4.3.2, each span the entire space and continuum states from different channels overlap for all values of ρ. These cannot then be used as an orthogonal asymptotic basis, and again $\mathbf{a}_{fi}$ and $\mathbf{b}_{fi}$ are non-diagonal matrices.

A third option is to use the continuum functions for a single channel only. This is still physically realistic; a continuum state represents a state in which all three atoms can separate to infinity, and we don't need asymptotic continuum states that are defined for each channel. Furthermore, if the zero potential states are used as the asymptotic definition, then these functions are simple to compute, have a definite λ value, and are orthonormal to each other. They are not, however, orthogonal to the bound states. If matching is performed at a large value of ρ, however, than the overlap with the bound states is small, and as has been done before[24], one can approximate orthogonality. At this time, this is the method we choose to employ.

4.5.3 Adiabatic to Asymptotic Transformation

At the end of propagation we must construct the D matrix defined in equation 4.57. This is done by an integration,

$$\mathbf{D}_m n = \left\langle \Phi_{t\Lambda}^{Jp} \middle| \Xi_{\tau\nu j\ell} \right\rangle \tag{4.80}$$

If $J \neq 0$, this is where the space-fixed to body-fixed transformations become relevant. In constructing the Φ functions from the symmetrized basis, as noted in section 4.3.1, we did not include the Wigner $\hat{D}$ functions. Instead we constructed functions of internal coordinates only that were physically motivated by the asymptotic states, but did not correspond to a specific set of body-fixed axes. In the definition of APH coordinates, the body-fixed axes are determined by maximizing the moment of inertia along the $\hat{z}_{bf}$ axis, while simultaneously minimizing it in the $\hat{x}_{bf}$. Using this to define the Euler angles $\alpha_Q, \beta_Q, \gamma_Q$ for the APH wavefunction expansion in equation 4.6, and for each asymptotic function we define $\alpha_\tau, \beta_\tau, \gamma_\tau$ for the asymptotic state definition in body-fixed coordinates, we can then use the relation

$$\hat{D}^J_{\Lambda M}(\alpha_Q, \beta_Q, \gamma_Q) = \sum_\Omega D^J_{\Lambda\Omega}(0, \beta_{Q\tau}, 0) \hat{D}^J_{\Omega M}(\alpha_\tau, \beta_\tau, \gamma_\tau) \tag{4.81}$$

to label all of the states in the same set of body-fixed axes for the integration. The rotation from the τ set of axes to the Q set of axes, $\beta_{Q\tau}$ is given by[8]

$$\begin{aligned} \sin\beta_{Q\tau} &= \frac{s_\tau \sin\chi_\tau \sin\Theta_\tau}{Q} \\ \cos\beta_{Q\tau} &= \frac{S_\tau \cos\chi_\tau + s_\tau \sin\chi_\tau \cos\Theta_\tau}{Q} \end{aligned} \tag{4.82}$$

Chapter 5

Integration of the APH Hypersphere Surface

One of the prime difficulties of using multidimensional basis functions to expand the full scattering Hamiltonian is find ways to perform accurate integrals as efficiently as possible. In this section, we discuss how these difficulties arise and some methods to assuage them.

In the present case of a three atom system, the basis functions are defined at specific, constant values of the hyperradius, ρ. With the center of mass motion removed from consideration and ρ held fixed at some ρ_ξ, five coordinates remain, and it is over these coordinates that the basis functions, or surface functions, are defined.

In the previous sections, these surface functions were developed as functions of the APH surface coordinates (θ, χ), and the Euler angles (α, β, γ). The Wigner $D(\alpha, \beta, \gamma)$ functions serve to represent the system's rotational motion, and the integrals over these functions can be done analytically. What is left is to perform integrals over the internal APH surface coordinates of θ and χ, which have domains of $[0, \pi/2]$ and $[0, 2\pi)$, respectively.

The physical behavior of the system in APH coordinates is highly non-separable, which is why great care has been taken in the formulation of surface basis functions, but this also means that the integrals over the APH hypersurface (θ, χ at some fixed ρ_ξ) is impossible to separate into one-dimensional integrals. Though the functions are separable in Delves' or Jacobi coordinates, from which the constructed basis functions were created and then projected onto APH coordinates, and the primitive functions of a given channel could be projected back to these coordinates and integrated analytically, the integrals between functions of different channels cannot be done analytically. If only two-body bound state primitive basis functions are being used, then at sufficiently large ρ_ξ values, there would be no overlap between channels. But, the continuum state primitive functions would always produce cross terms between channels. A two-dimensional integration scheme is necessary.

That the continuum functions have amplitude over the entire domain of the internal space, in any coordinate system, is one of the principle difficulties of collision-induced dissociation scattering. A scattering calculation without possibility of three-body break-up has final states that are always an atom plus a diatom, and the maintained close proximity of two of the atoms for all values of ρ (or S_τ) mean that the amplitude of basis functions and/or eigenfunctions is restricted to some localized piece of space. Hence, integrals over these functions could be focused or even constricted entirely to this localized area, and numeric integration could be done quickly and without excessive computation power. In a Jacobi coordinate system, for instance, such functions could be simply represented as functions of s_τ and Θ_τ, both with finite domains since the bound states do not have amplitude far beyond the two-body potential well. The continuum functions,

however, are not similarly localized. At large, or even just moderate values of ρ, this adds the complication that the integration must accommodate the entire space while still sufficiently focusing on the localized regions where the bound state functions exist such that they, too, are integrated accurately. This can require very large numbers of integration points or very complicated fitting schemes, as well as a lot of computation time.

Fortunately, as we saw in section 4.2, taking advantage of the system's symmetries can simplify the integration process. For a homonuclear triatomic system, an integral over a mere 1/12 of χ's $[0, 2\pi)$ domain is needed for the one-dimensional irreducible representations of A_1, A_2, B_1, B_2, and integrating only a quarter of the surface is sufficient for the two-dimensional irreducible representations , E_1 and E_2. Knowing that the integral of two functions belonging to different irreducible representations must be zero, we need only consider the integrals between functions of the same irreducible representation . As such, the rotational and reflective symmetries of the one-dimensional irreducible representations enable integrals over χ to be performed from $[0, \pi/6)$ to give exactly 1/12 of the value of the total integral. Likewise for E_1 and E_2, integrating from $[0, \pi/4)$ gives a quarter of the total integral.

5.1 Direct Square Integration by Quadrature

The least elegant and least efficient method to integrate these spaces is by simply defining quadrature points in both θ and χ coordinates, finding the integrand values at these points, and then summing the product of the integrand values with the quadrature weights. A simple, evenly distributed grid may work well at short values of ρ_ξ, but at larger values, it can be very ineffective. Specifically, in regards

to the aforementioned point of bound state localization, as ρ increases, the region where the bound state functions have amplitude becomes a smaller and smaller region on the hypersphere. While the domains of θ and χ do not change, the larger ρ_ξ is, the more physical space is covered by the hypersphere. Eventually, an evenly distributed grid will have so few points in the bound state regions that there is no hope of accurate integration. Or, there will be no points at all in this region, and all integrals will evaluate to zero.

There is merit, though, in a square grid of integration points. It is very easy to implement, very easy to increase the number of points, and is enormously useful for checking other, more complicated schemes. Also, at small values of ρ_ξ where no basis functions are constricted to small regions of space, a simple square grid is effective at getting accurate integrals. Yet even still, it might take many more quadrature points than other methods.

5.2 Static Jacobi Grid

In this method, a rectilinear grid in Jacobi s_τ and Θ_τ, and then the grid is projected onto the APH hypersurface at each value of ρ_ξ. Each rectangular integration element in s_τ, Θ_τ space has a set of Gauss-Legendre quadrature points forming a grid in each direction. In this work, we used a 6×6 grid. The Gauss-Legendre integration weights are scaled appropriately to the width and height of the rectangle element. When this is projected onto the APH hypersurface, the rectangle becomes a general quadrilateral in θ, χ space. A linear transformation is used to place the quadrature points in the APH quadrilateral and to scale the integration weights according to the new shape of the element.

The constant Θ_τ grid distribution was determined by the maximum rotational state used in the asymptotic basis set. A *points-per-wavelength* parameter was established that determined how many elements in the Θ_τ direction should be established with 6 points per element such that integrals over these functions squared could be performed accurately.

In the s_τ direction, the constant grid was determined by the diatomic potential, and again the defining parameter was a requisite number of points per wavelength (p_w). First, the energy difference, ΔE_{max}, between the highest rotational ($j = j_{max}$) barrier peak to the depth of the $j = 0$ diatomic well minimum was calculated. The first line of constant s_τ was set at the well minimum. The ΔE_{max} was then used to calculate a local wavelength, λ_s, at this point. With p_e points per integration element, the distance to the next constant s_τ value Δs_τ is determined by

$$\Delta s_\tau = \lambda_s \frac{p_e}{p_w} \tag{5.1}$$

if 12 points per wavelength are required, with 6 points per element, the next constant s_τ line is a half wavelength away from the well minimum. This was done in both directions. At the next outward step, the same peak energy was used, but the potential was re-evaluated, so ΔE_1 is less than ΔE_{max}. The wavelength was recomputed, and a new Δs_τ determines the second outward constant s_τ line. This process was repeated until $s_\tau >= \rho_{max}$, the largest ρ value for which the basis is generated. The inward process is the same as the outward until the classical turning point is reached for the maximum barrier energy, and then a set number of constant s_τ elements was used in the classically forbidden region.

Examples of the resultant grids are shown for $\rho = 5a_0, 10a_0, 15a_0, 55a_0$ in figures 5.1-5.4

In figures 5.3 and 5.4 the well region is visible by a more dense band of points that follows the well minimum in s_τ.

One other modification to this grid was made, which was to determine the largest vibrational state of the continuum functions and determine how many points would be necessary to integrate it accurately. Then an estimation was made on the largest distance in s_τ for which the bound or quasibound states had amplitude. Beyond this distance, a fixed number of constant s_τ values was used, regardless of how large ρ became. Since the continuum states do not increase their oscillations as ρ increases, and the diatomic well part of the potential diminishes in size on the hypersphere for large ρ, we reach a point were no additional integration elements are ever necessary. This allows us to propagate to very large ρ values, but always use the same number of integration points.

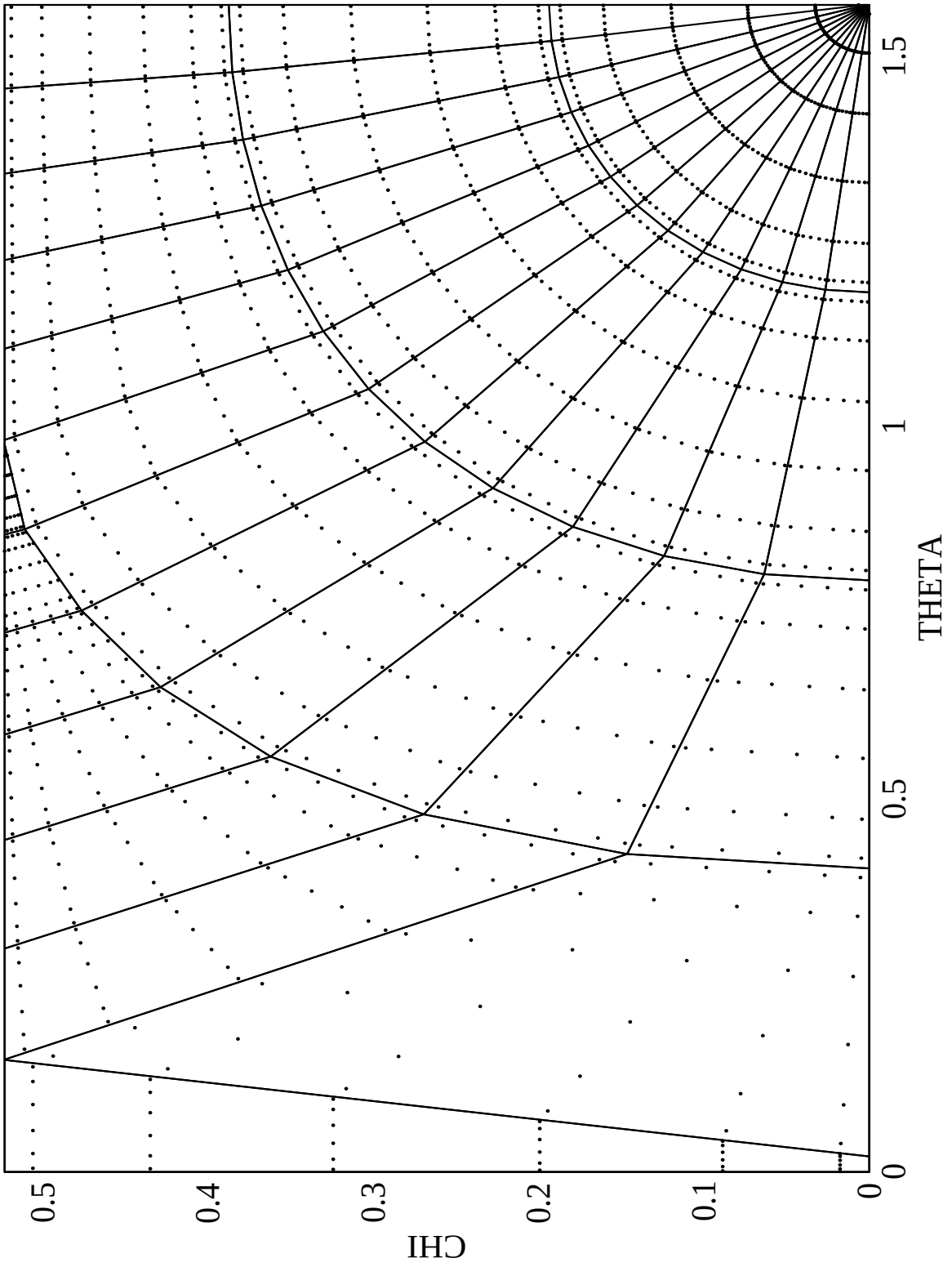

Figure 5.1: Static Jacobi grid for integration projected onto the APH hypersurface at $\rho = 5a_0$.

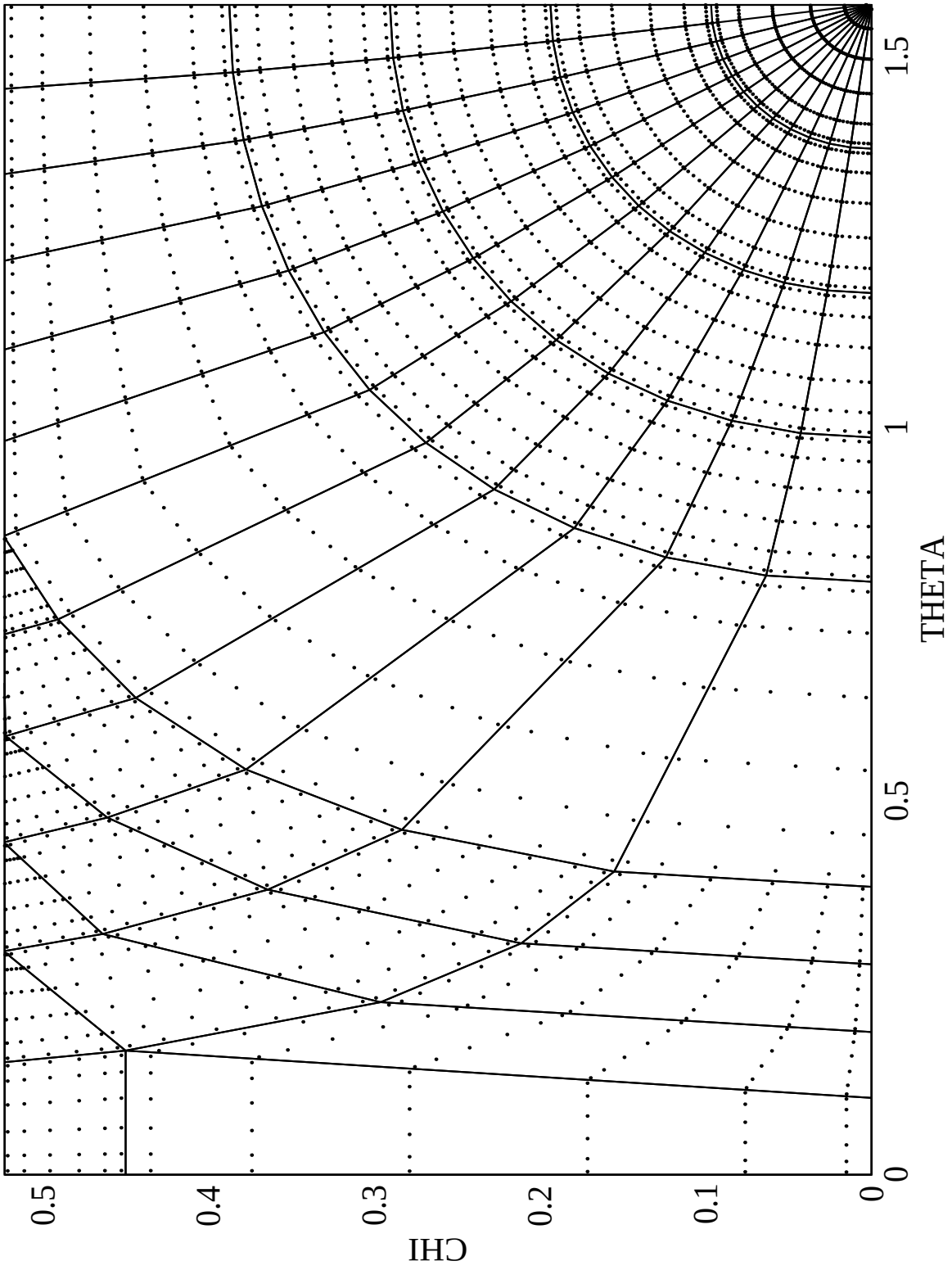

Figure 5.2: Static Jacobi grid for integration projected onto the APH hypersurface at $\rho = 10a_0$.

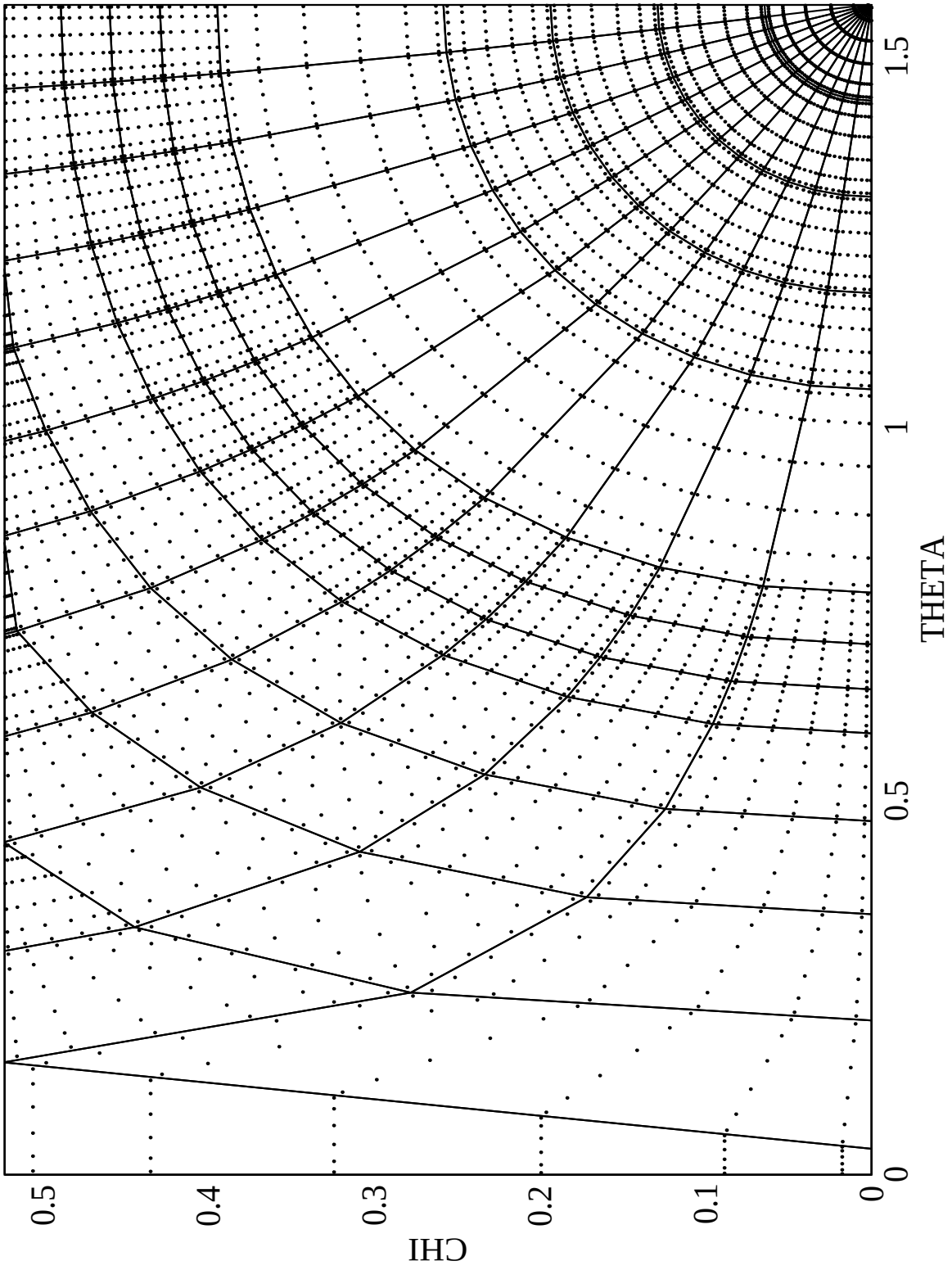

Figure 5.3: Static Jacobi grid for integration projected onto the APH hypersurface at $\rho = 15a_0$.

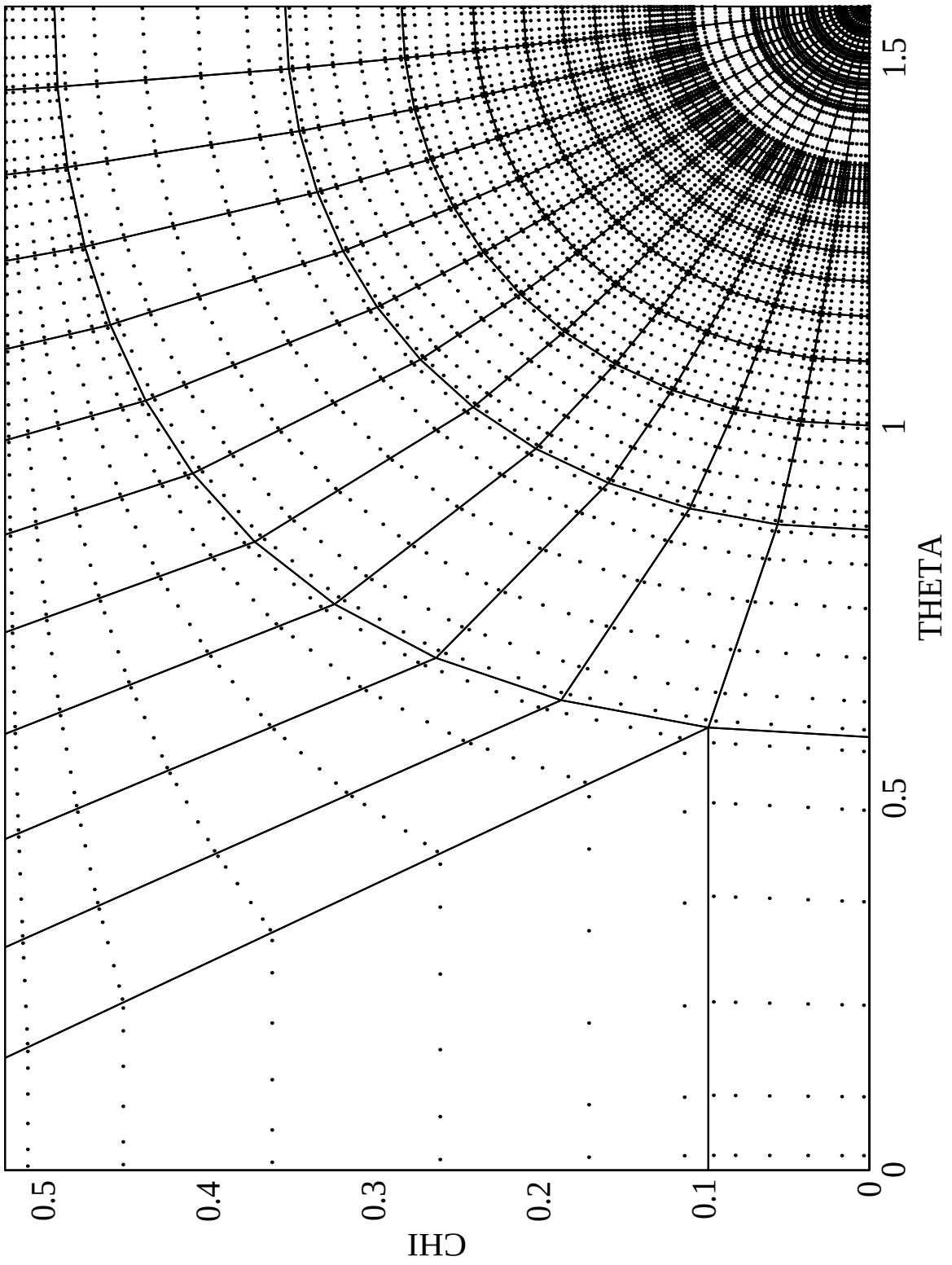

Figure 5.4: Static Jacobi grid for integration projected onto the APH hypersurface at $\rho = 55a_0$.

Chapter 6

Results of H_3 calculations

Scattering calculations were performed on the H_3 system in order to test the validity of the method. Comparisons were made against the calculations done for reference [8], and both calculations use the Porter-Karplus[25] H_3 potential energy surface. It should be noted that this potential is not highly accurate, but many calculations have been done on this potential surface so it is an excellent choice for testing.

There are specific criteria to be met in order to validate the theory of chapters 3,4, and 5,

1. The basis set described can be used effectively to reproduce known energy correlation diagrams for a given system

2. The basis set consistently includes quasibound states regardless of energy. However, this criteria is met automatically by the process of constructing the basis set.

3. The basis set can adequately represent continuum state functions

4. The basis set faithfully represents the symmetry of the system and can allow for the problem to be reduced solving a single irreducible representation at a time.

5. The integration method is sufficient to the task of accurately calculating integrals, but is also sufficiently efficient to allow the scattering calculation to be performed in a reasonable time period.

6.1 Energy Correlations

In regards to item 1, one of the most crucial tests is the output of the eigenvalues of the surface Hamiltonian of equation 4.31. In the energy correlation diagrams, we are looking for three things in particular: behavior that corroborates that from energy correlation diagrams in other calculations, correct asymptotic eigenvalues, and degeneracy between states from different irreducible representations .

In regards to the first in this list, we compare the energy correlation diagrams in figures 6.1 and 6.2 to the results published in reference [8]. The energy correlation diagrams are plots of the eigenenergies of the surface Hamiltonian, defined in equation 4.31 and reprinted here,

$$\begin{aligned} H_{surf} = & \frac{-\hbar^2}{2\mu\rho_\xi^2}\left[\frac{4}{\sin(2\theta)}\frac{\partial}{\partial\theta}\sin(2\theta)\frac{\partial}{\partial\theta} + \frac{1}{\sin^2(\theta)}\frac{\partial^2}{\partial\chi^2}\right] \\ & + \frac{A+B}{2}\hbar^2 J(J+1) + \frac{15\hbar^2}{8\mu\rho_\xi^2} \\ & + \left[C - \frac{A+B}{2}\right]\hbar^2\Lambda^2 + V(\rho_\xi, \theta, \chi) \end{aligned}$$

If the eigenenergies of this equation are poor, then there is little hope that the basis set is performing well enough to conduct a scattering calculation.

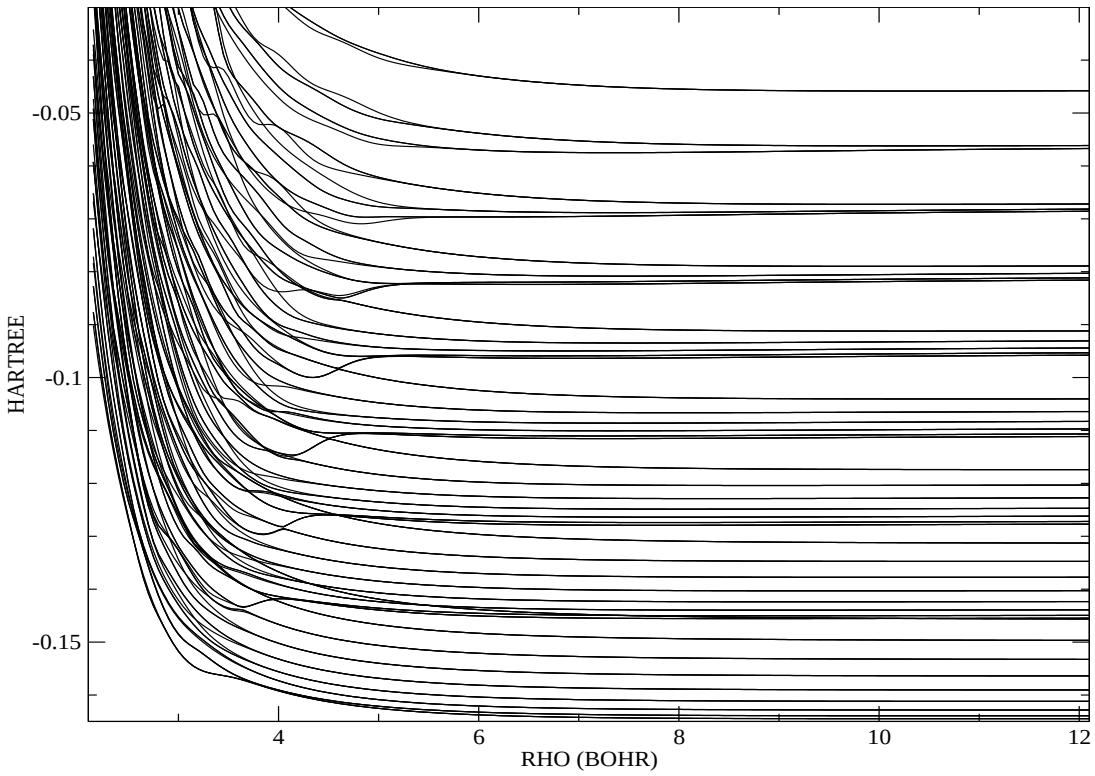

Figure 6.1: Energy correlation diagram for the H_3 system using the Porter-Karplus[25] potential energy surface. In this plot are all even parity irreducible representations : A_1, A_2, $E_2^{(1)}$, and $E_2^{(2)}$ In the calculation that produced this data, all single-channel φ states included up to $\lambda_{max} = 16$, where $\lambda = 2\nu + j + \ell$. Many of these states are degenerate or very nearly so.

In figures 6.1 and 6.2, we see plotted the energy correlation in atomic units (Hartrees) as a function of ρ in Bohr.

In looking at the plots in figures 6.1 and 6.2, we see behaviors that correspond with figure 6 in reference [8]. The short-ρ belly of the ground state is very clearly reproduced, as well as the locations of the first several avoided crossings.

Next, we look at the values of the energy correlation diagrams in comparison to the asymptotic energies. In table 6.1 is a comparison between the asymptotic

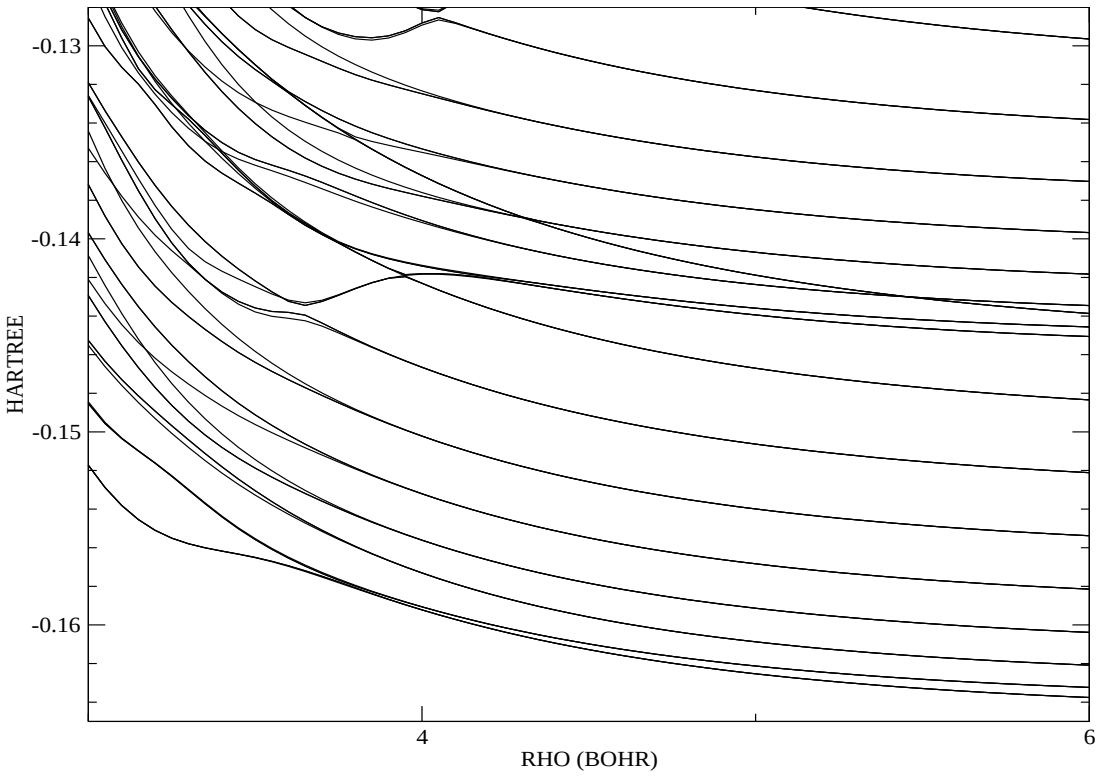

Figure 6.2: Energy correlation diagram for the H_3 system using the Porter-Karplus[25] potential energy surface. This plot is a blow-up of figure 6.1

energy values as calculated in three different ways. The first column are the eigenvalues for a given ν and j for the solutions to the Jacobi rovibrational Hamiltonian in equation 2.14. In the second column are the eigenenergies energies found by applying the Delves rovibrational Hamiltonian, given in equation 2.20 to the Jacobi eigenfunctions as projected onto the constant $\rho = 12.1$ Bohr. This Delves Hamiltonian matrix was then diagonalized. The intention behind this test was to see how much the projection process changed the function. Since the constant ρ surface is not a constant S_τ surface, there is some difference between the two functions at any finite value of ρ. The constant $S_\tau$surface is tangent to the constant ρ surface. In the last column are the values of the APH surface Hamiltonian at 12.1

(ν, j)	E_J	E_D	E_A
(0,0)	-0.164400	-.164146	-.164476
(0,1)	-0.163869	-.163602	-.163926
(0,2)	-0.162782	-.162494	-.162671
(1,0)	-0.145242	-.144511	-.145035
(1,1)	-0.144716	-.143971	-.144509
(1,2)	-0.143678	-.142917	-.143464
(2,0)	-0.127272	-.126085	-.126945
(2,1)	-0.126767	-.125574	-.126444
(2,2)	-0.125786	-.124557	-.125445

Table 6.1: Asymptotic energies. The first column is the Jacobi two-body rovibrational energies, the second column is the Delves two-body rovibrational energies at 12.1 Bohr, and the third column is the corresponding limits for the APH eigenenergies at 12.1 Bohr.

Bohr. Technically, because of mixing between even and odd j states, these values do not have a (ν, j) set of quantum numbers. But, for a $J_{total} = 0$ case, at at a sufficiently large value of ρ, these can be sorted by appearance, as will be shown in the next section.

The numbers given in table 6.1 are from a calculation with only functions corresponding to these quantum numbers given as a basis. This small of a basis does not perform well at short ρ distances where the three-body contribution to the total potential energy is significant. But, at large ρ values (12.1 is sufficiently large for H_3 that the three body terms are negligible), even this small of a basis does fairly well as is demonstrated in table 6.1.

Between this agreement and tests done for convergence, on these energies, this data also lends confidence that the integration procedure is sufficient, thus satisfying criteria 5.

6.2 Symmetrized Eigenfunctions

For a system of three identical particles, the potential energy surface in APH coordinates exhibits a C_{6v} point group symmetry, as shown in figure

The lowest energy A_1 irreducible representation eigenfunction is plotted in figure 6.3, and the lowest A_2 irreducible representation eigenfunction in figure 6.4 for $\rho = 2.1, 4.6, 7.1, 9.6$ Bohr. As ρ increases, we can see that the amplitude of the eigenfunction becomes centralized around the different arrangement channels located at 0, 60, 120, 180, 240, and 300 degrees on the circle. Note that the A_2 functions have negative reflection symmetry about each channel, corresponding to an odd j rotational state, whereas for the A_1 functions correspond to an even rotational state.

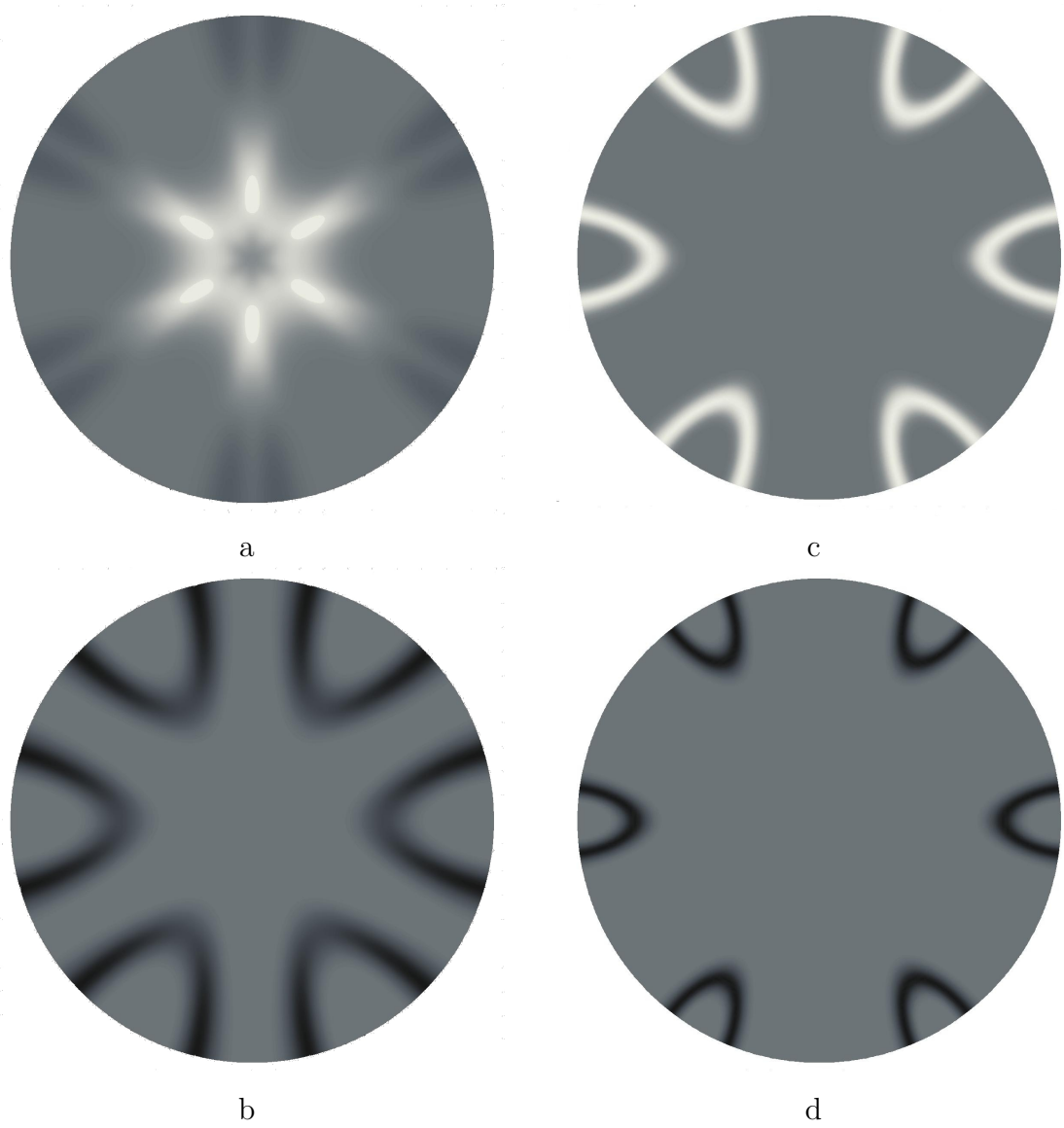

Figure 6.3: Lowest A_1 eigenfunctions at ρ values a,b,c,d = 2.1, 4.6, 7.1, 9.6 Bohr respectively. The overall phase of the functions is arbitrary, so the function will change sign at some sectors, as shown by the switching of positive amplitude (white) and negative (black). See appendix B.3 for more explanation of APH surface plots.

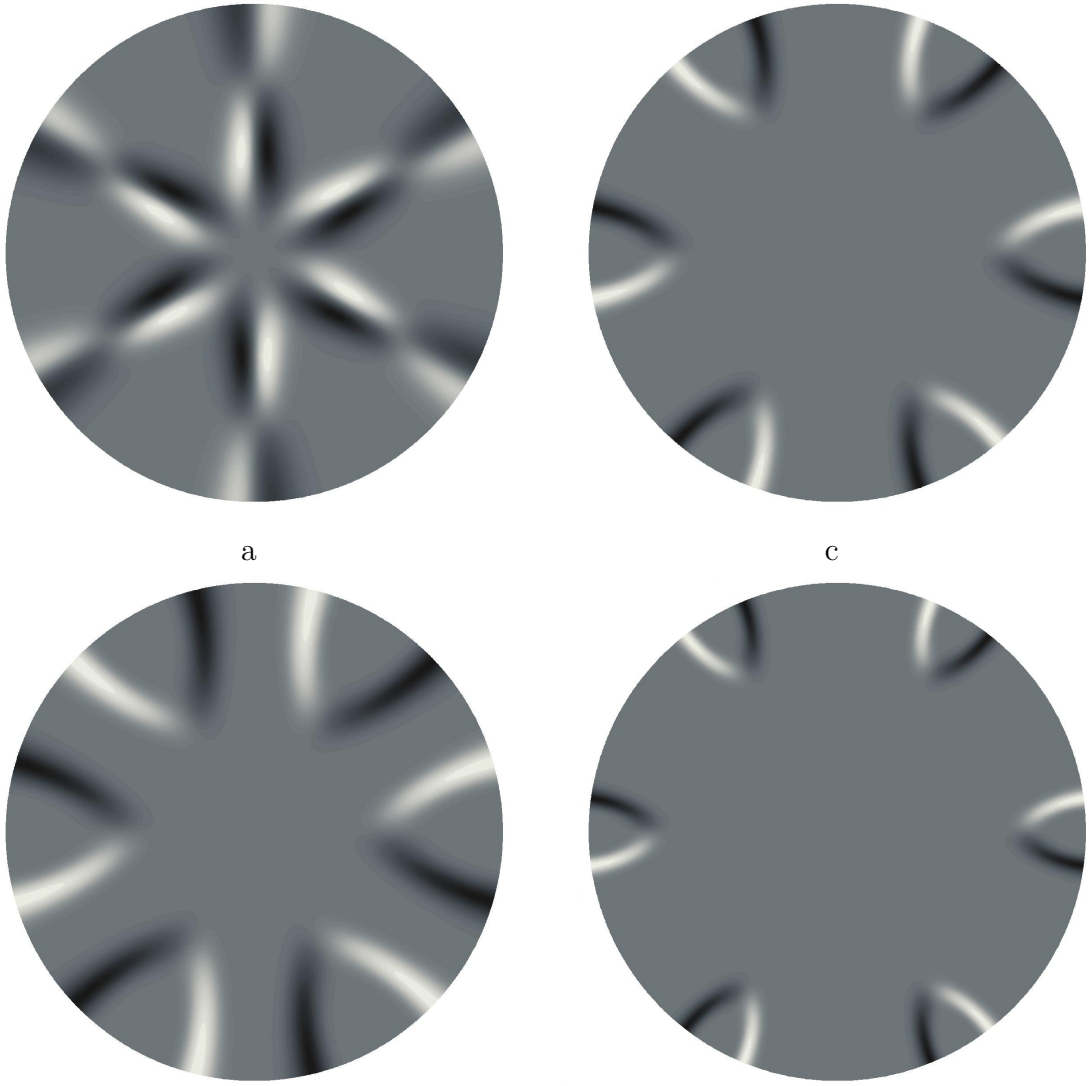

Figure 6.4: Lowest A_2 eigenfunctions at ρ values a,b,c,d = 2.1, 4.6, 7.1, 9.6 Bohr respectively.

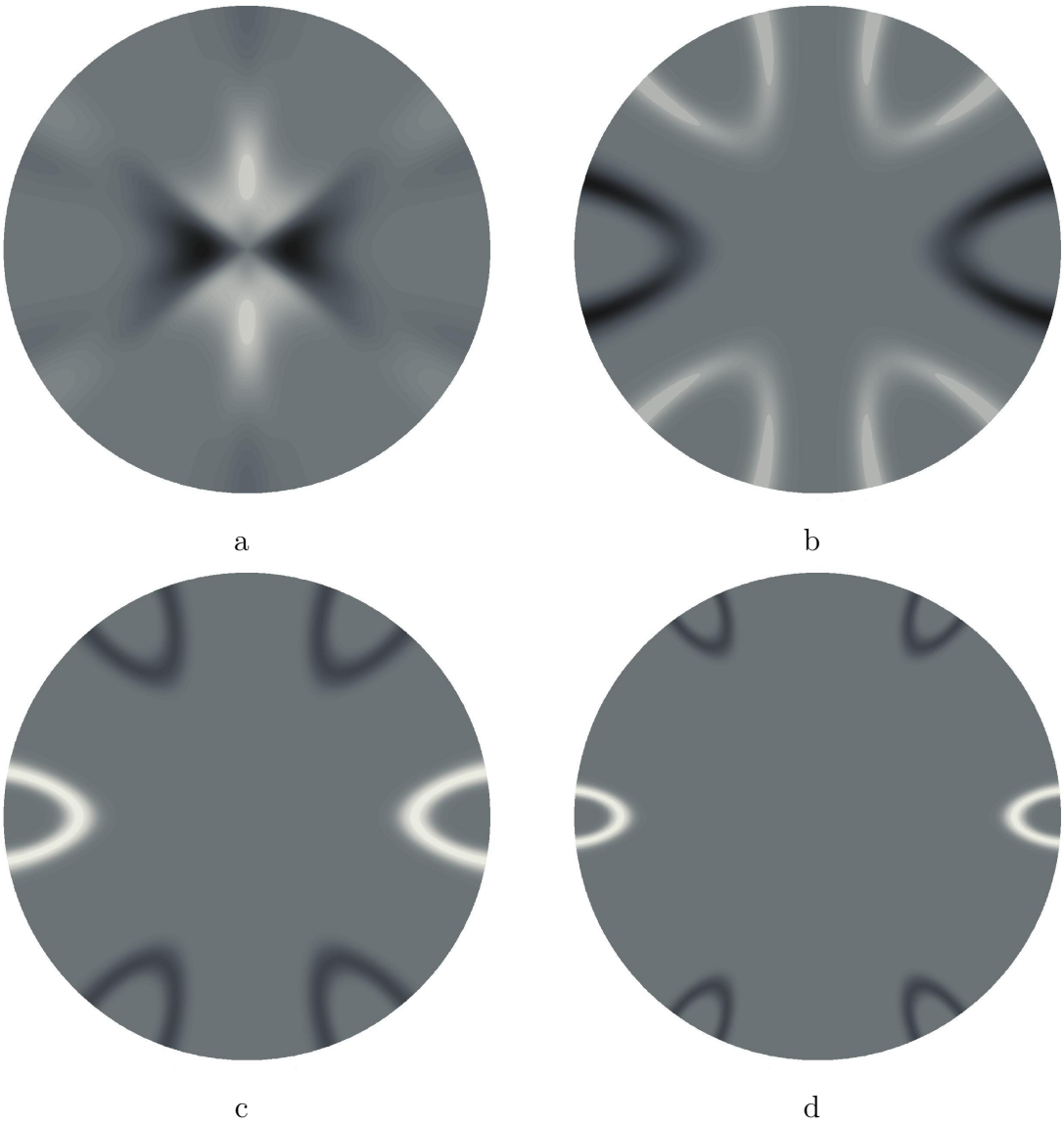

Figure 6.5: Lowest $E_2^{(1)}$ eigenfunctions at ρ values a,b,c,d = 2.1, 4.6, 7.1, 12.1 Bohr respectively.

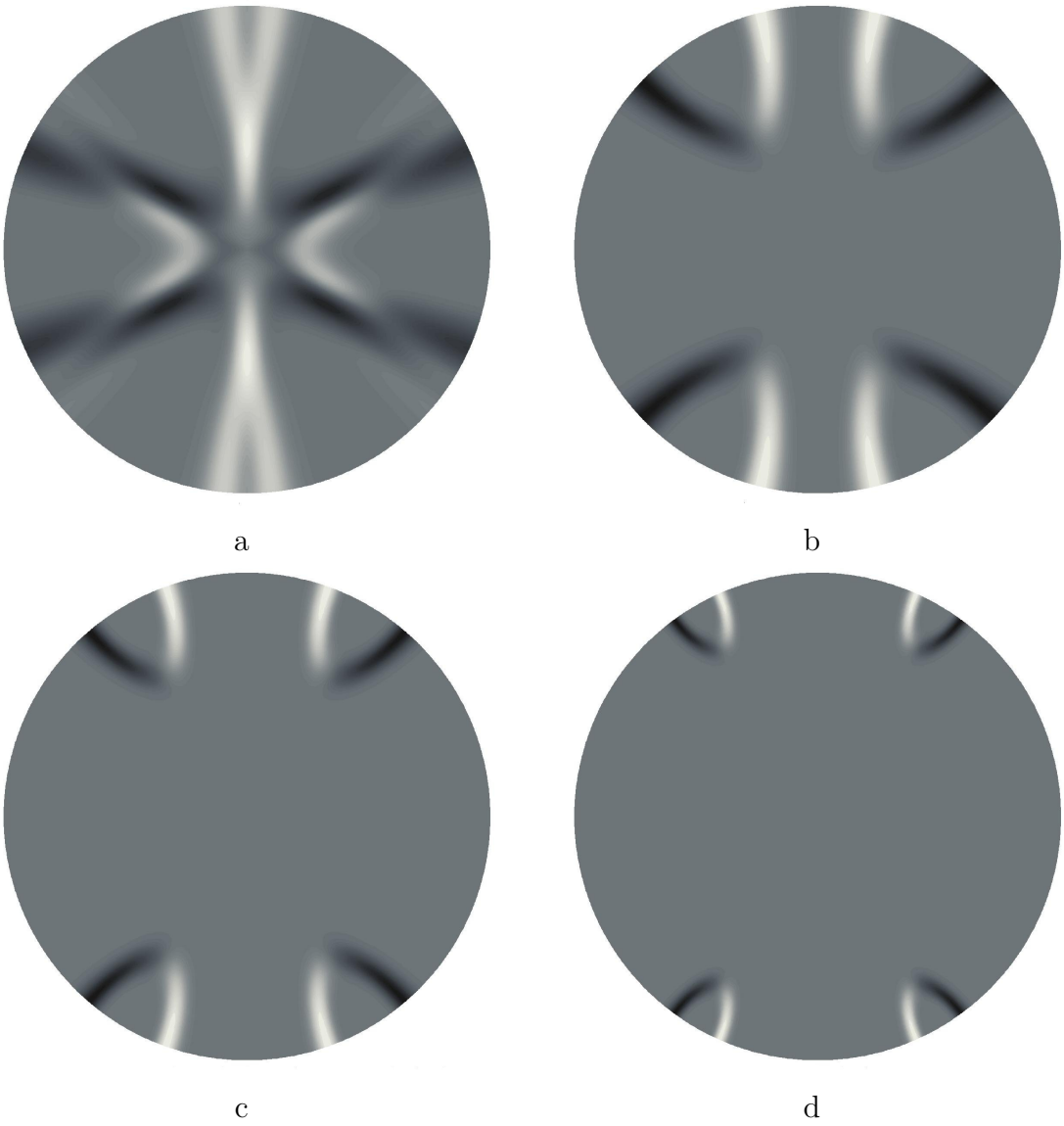

Figure 6.6: Second Lowest $E_2^{(1)}$ eigenfunctions at ρ values a,b,c,d = 2.1, 4.6, 7.1, 12.1 Bohr respectively.

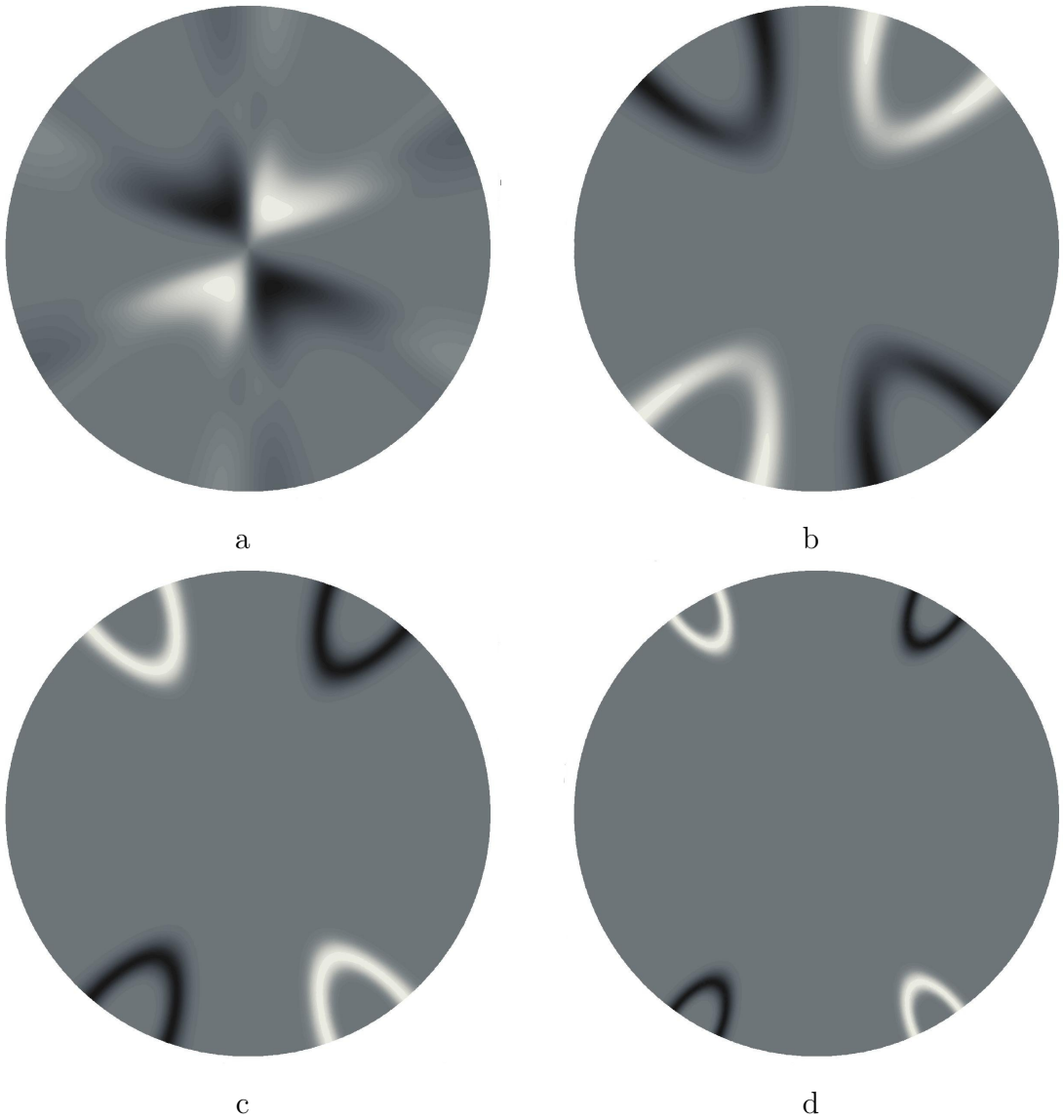

Figure 6.7: Lowest $E_2^{(2)}$ eigenfunctions at ρ values a,b,c,d = 2.1, 4.6, 7.1, 12.1 Bohr respectively.

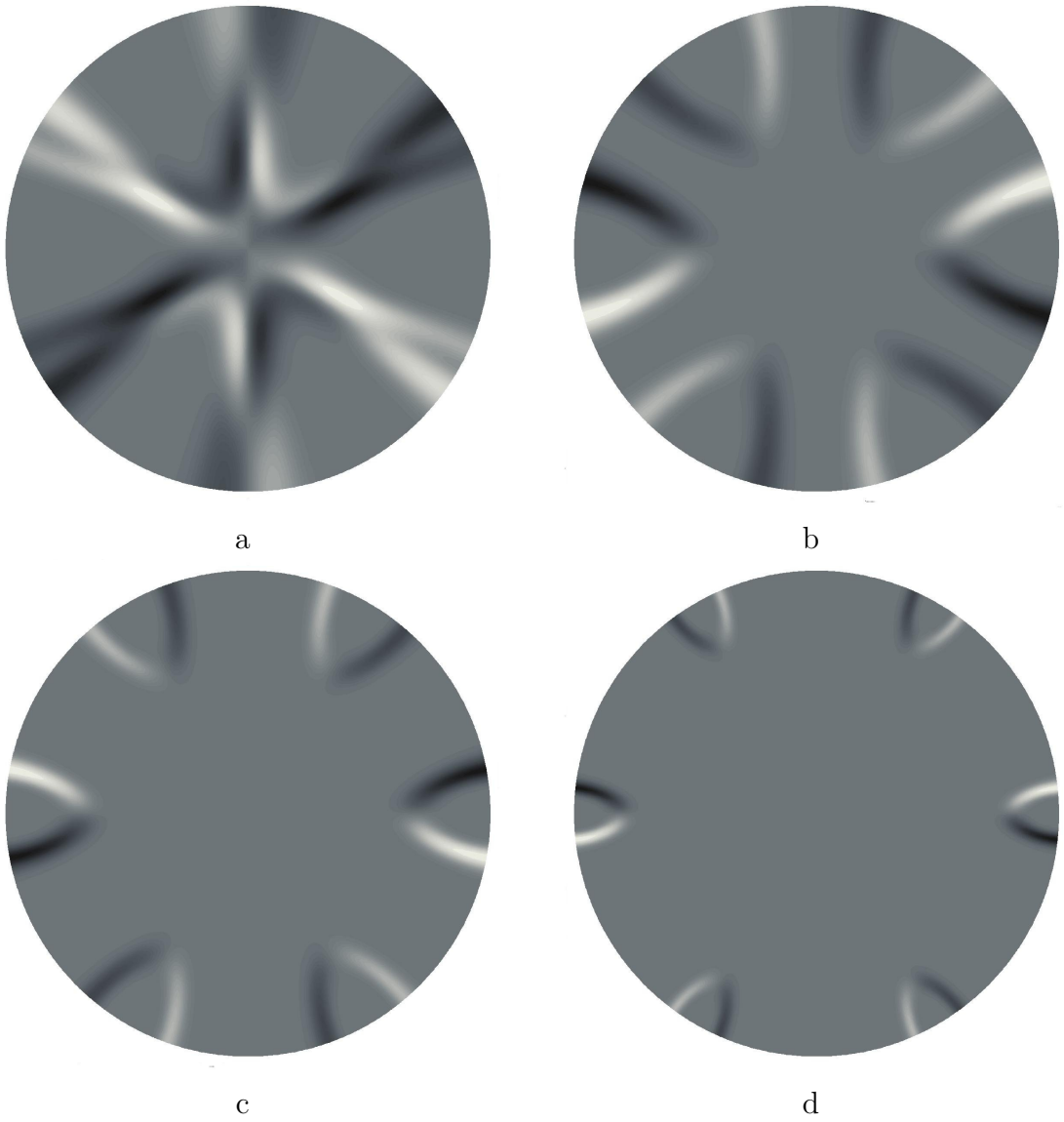

Figure 6.8: Second lowest $E_2^{(2)}$ eigenfunctions at ρ values a,b,c,d = 2.1, 4.6, 7.1, 12.1 Bohr respectively.

6.3 Representation of Continuum States

The ultimate goal of this project was to construct a basis for scattering that would efficiently allow for three-body breakup states. The basis functions representing the continuum states must have amplitude over the entire constant ρ hypersurface, obey the physical boundary conditions, and be orthogonal to the bound and quasibound states.

In this section we present the continuum state basis functions developed by the methods described in section 4.3. These states are the eigenstates of the APH surface Hamiltonian that have positive energy, and by virtue of diagonalizing the surface Hamiltonian matrix, these states are orthonormal to the bound and quasibound states, as required. Lastly, since the primitive basis functions used to construct the eigenstates are themselves asymptotic solutions of the system, we are guaranteed to have physical behavior at the boundaries.

In figures 6.9-6.12 are plots of the first continuum states for the labeled irreducible representations . The continuum states have amplitude over the entire region of the constant ρ hyper-surface, showing that the continuum functions are in fact able to be represented by the basis.

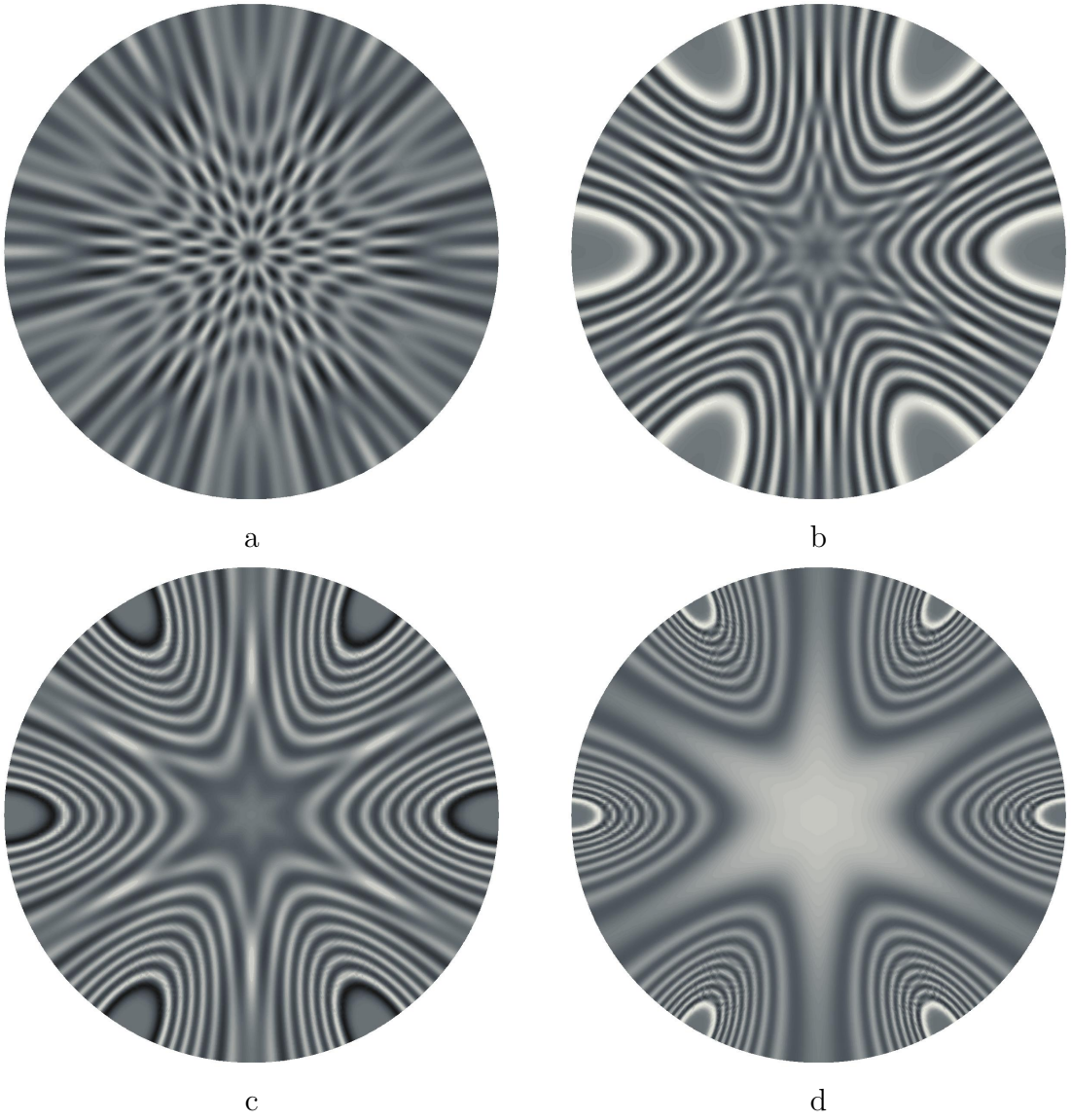

Figure 6.9: First continuum state for A_1 irreducible representation at ρ values of a,b,c,d = 2.1, 4.6, 7.1, 12.1 Bohr

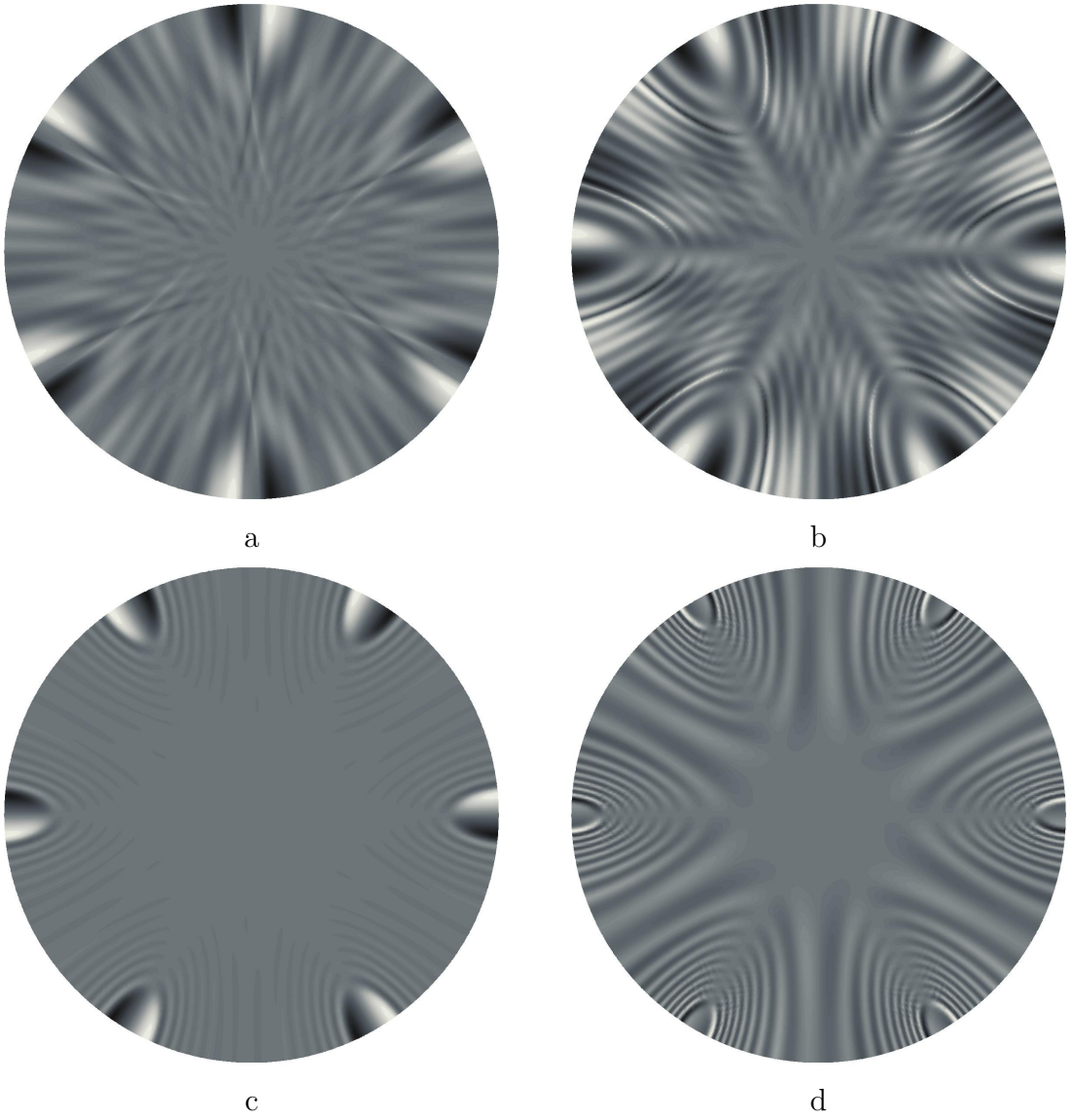

Figure 6.10: First continuum state for A_2 irreducible representation at ρ values of a,b,c,d = 2.1, 4.6, 7.1, 12.1 Bohr

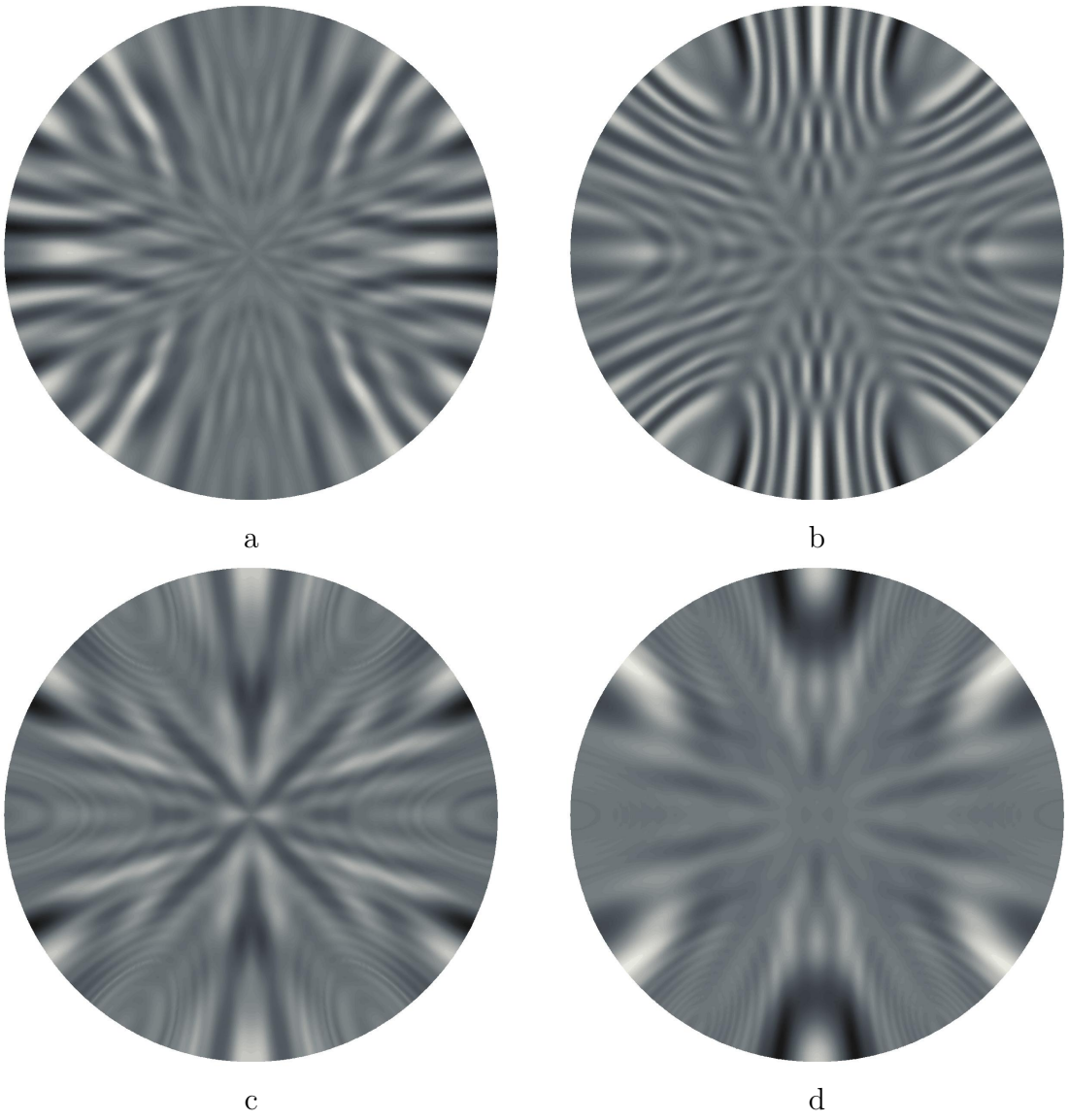

Figure 6.11: First continuum state for $E_2^{(1)}$ irreducible representation at ρ values of a,b,c,d = 2.1, 4.6, 7.1, 12.1 Bohr

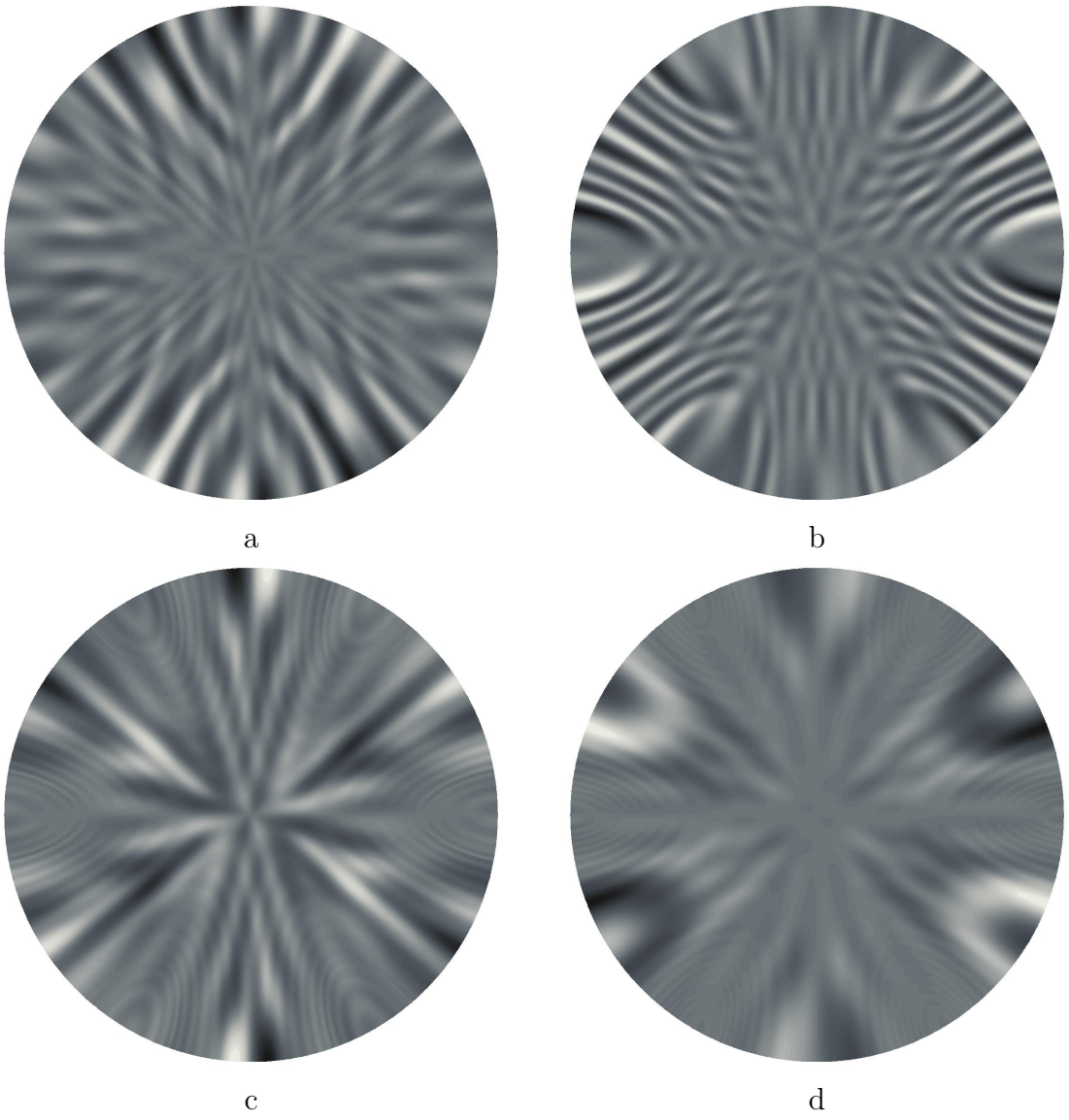

Figure 6.12: First continuum state for $E_2^{(1)}$ irreducible representation at ρ values of a,b,c,d = 2.1, 4.6, 7.1, 12.1 Bohr

6.4 Conclusion

The criteria enumerated at the beginning of the chapter have been shown to be satisfied, and the goal of generating basis functions that can represent general collision-induced dissociation or three-body breakup processes has been successful.

With a given three-body potential energy surface, this process can be applied to most any three-atom system. Depending on the number of bound states and the collision energy, some calculations may still be computationally very expensive, however, much of the process of generating these basis functions can be easily parallelized for multiprocessor systems or clusters. Very little shared memory is required for calculations at different sectors, as each $\rho_\xi$sector's basis functions can be computed independently of every other sector. Even the processes of projecting asymptotic states to generate symmetrized primitives and the matrix generation and diagonalization naturally lend themselves to parallel calculation. Furthermore, with the integration scheme introduced in chapter 5, the number of integration points increases with ρ until a maximum is reached and then it remains constant, so it does not become more expensive to calculate basis functions at values of ρ of many thousands or millions of Bohr. Propagating to such distances may be necessary for some systems, such as He_3, where the two-body bound state extends to several hundred Bohr, and the three-body asymptotic region may not be reached until ρ is much, much larger than as is necessary for H_3 or Li_3. It is expected that much research can be produced with this methodology and the corresponding set of scattering codes that have been developed to implement it.

Appendix A

Notation

The following symbols are used throughout this document.

Labels

- τ : index specifying a specific three-body arrangement channel
- ξ : index specifying propagation sector
- j : space-fixed rotational angular momentum of diatomic molecule
- ℓ : space-fixed orbital angular momentum of an atom about a diatom
- ν : two-body vibrational quantum number
- J_{total} : total three-body angular momentum
- M : space-fixed projection of total angular momentum, J_{total}
- Λ : body-fixed projection of total angular momentum, J_{total}

Symmetry

- C_2 : point group symmetry of APH surface Hamiltonaian for system of three atoms of different masses
- C_{2v} : point group symmetry of APH surface Hamiltonian for system of three atoms where two have the same mass and one is different
- C_{6v} : symmetry point group of APH surface Hamiltonian for system of three atoms of identical mass
- D_{3h} : symmetry point group, isomorphic to C_{6v}, for doubled Delves' hyperspherical coordinates with threee identical atoms
- C_s : symmetry Point group of space with three atoms
- Γ : irreducible representation label of a given point group
- σ_v : reflection in plane containing primary rotation axis
- σ_d : reflection in plane containing primary rotation axis, but of a different class than σ_v
- σ_h : reflection in plane orthogonal to primary rotation axis
- C_n : nth order rotational symmetry
- S_n : nth order improper rotational symmetry, a C_n rotation followed by a reflection in plane orthogonal to rotation axis
- i : inversion symmetry

Coordinates

- α, β, γ : Euler Angles
- r_τ : Jacobi coordinate, distance between two atoms forming a diatom
- R_τ : Jacobi coordinate, distance from center of mass of diatom to third atom
- s_τ : Jacobi Mass-Scaled coordinate, scaled of r_τ
- S_τ : Jacobi Mass-Scaled coordinate, scaled of R_τ
- Θ_τ : angle between Jacobi $\mathbf{s}$ and $\mathbf{S}$ vectors. Also part of Delves' hyperspherical coordinates
- ϑ_τ : Delves' theta coordinate, specific to an arragement channel and so either implicitly or explicitly labeled by τ, etc.
- ρ : APH and Delves' hyperradius coordinate
- θ : APH theta coordinate, defined in appendix B
- χ : APH coordinate, defined in appendix B

Functions

- Ψ : solution full three-body differential equation, coordinate independent
- Φ : solutions of APH surface Hamiltonian
- Υ : solutions of Delves' surface Hamiltonian in ϑ_τ
- ζ : solutions of the Jacobi coordinate s diatomic vibrational Hamiltonian

- φ : either a 2D or 5D function, depending on inclusion of Euler angles. φ refers to a constructed basis function specific to a single channel. The φ functions are not orthonormal.
- ϕ : symmetrized non-orthogonal linear combinations of φ functions
- $D^J_{M\Lambda}$: Wigner rotation functions, $\hat{D}^J_{M\Lambda}$ are normalized
- P^m_l : associated Legendre Polynomials, $\hat{P}^m_l$ are normalized
- Y^m_l : spherical harmonic functions, $\hat{Y}^m_l$ are normalized
- $\mathscr{Y}^{JM}_{j\ell}$: coupled angular momentum functions; linear combinations of spherical harmonics, normalized
- $\mathscr{P}^{j\ell}_n$: Jacobi Polynomials, $\hat{\mathscr{P}}^{j\ell}_n$ are normalized

Acronyms

- **CID** : Collision-Induced Dissociation
- **3BR** : Three-Body Recombination
- **APH** : Adiabatically-adjusting Principle-axis Hyperspherical
- **FEM** : Finite Element Method
- **DAF** : Distributed Approximating Functionals
- **DVR** : Discrete Variable Representation

Appendix B

Coordinate Systems

Here we describe the coordinate systems used in this paper. There are multiple ways in which the positions of three atoms can be described, and each has advantages in illuminating physical properties.

B.1 Jacobi Coordinates

For three atoms, there are three different sets of Jacobi coordinates that can be employed. For Jacobi coordinate set "A", a vector $\mathbf{r}_A$ is defined between the centers of mass of atoms B and C. Then, the vector $\mathbf{R}_A$ is defined from the center of mass of the BC diatom to the atom A. Likewise for the "B" set, a vector $\mathbf{r}_B$ is defined between atoms A and C, and a vector $\mathbf{R}_B$ is defined from the center of mass of the AC diatom to the B atom.

It is almost always more useful, however, to work with Mass-Scaled Jacobi coordinates. With standard Jacobi coordinates, the kinetic energy terms for $\mathbf{R}$

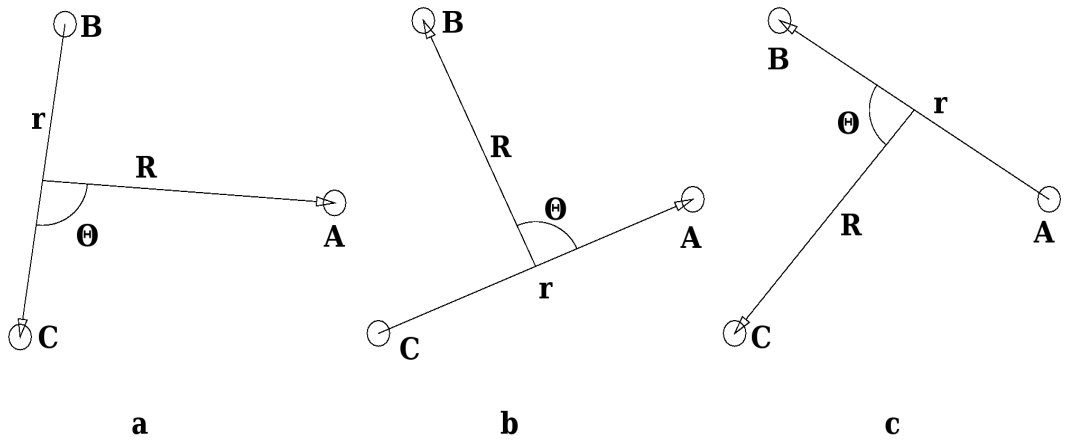

Figure B.1: Diagrams of the three sets of Jacobi coordinates. Diagrams a, b, and c represent the Jacobi coordinates associated with arrangement channels A, B, and C, respectively.

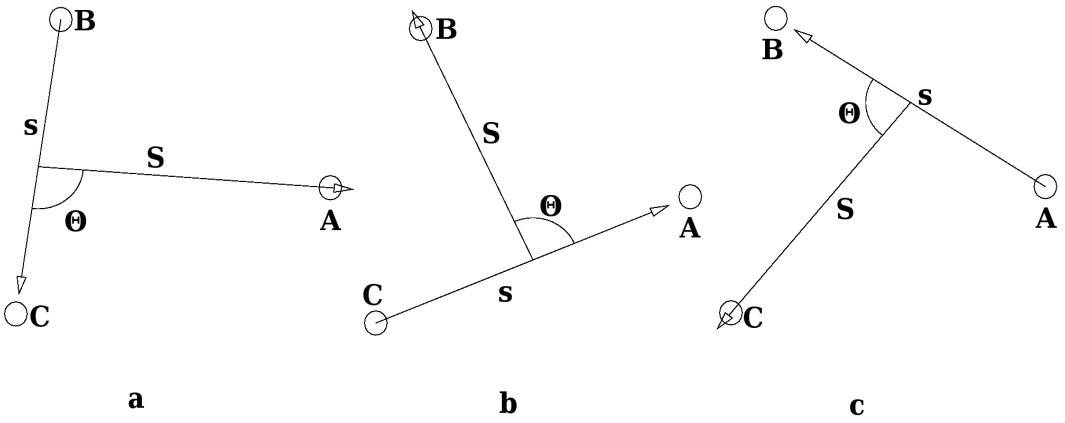

Figure B.2: Diagrams of the three sets of Mass-Scaled Jacobi coordinates. Diagrams a, b, and c represent the Jacobi coordinates associated with arrangement channels A, B, and C, respectively. Note that with mass-scaling, the s vector length is shorter than r, and the S vector length is longer than R.

and **r** have different mass factors. In mass-scaled coordinates, there is a single reduced mass factor defined as

$$\mu = \left[\frac{m_A m_B m_C}{m_A + m_B + m_C}\right]^{1/2} \tag{2.1}$$

and the new coordinates S and s are defined as

$$\begin{aligned} \mathbf{s}_\tau &= d_\tau^{-1}\mathbf{r}_\tau \\ \mathbf{S}_\tau &= d_\tau \mathbf{R}_\tau \end{aligned} \tag{2.2}$$

where $\tau = A, B, C$, and d_τ is

$$d_\tau = \left[\frac{m_\tau}{\mu}\left(1 - \frac{m_\tau}{m_A + m_B + m_C}\right)\right]^{1/2} \tag{2.3}$$

With this definition, the kinetic energy operator has the same reduced mass for both the ∇_S^2 and ∇_s^2 terms so that

$$T = -\frac{\hbar^2}{2\mu}(\nabla_{S_\tau}^2 + \nabla_{s_\tau}^2) \tag{2.4}$$

Jacobi coordinates are especially useful in ranges where two atoms are close together and the third is moderately to distantly removed. In such a case it is convenient to use $\mathbf{s}$ to describe the "diatom" and have $\mathbf{S}$ point to the third, farther away atom.

B.2 Delves Hyperspherical Coordinates

The Delves hyperspherical coordinate system [12] is related to the Jacobi coordinate system in a direct and simple way. Instead of coordinates s_τ and S_τ that are vectors describing the positions of the atoms, the Delves coordinates are ρ and ϑ_τ,

which are the polar equivalent of $S_\tau$and $s_\tau$if one considers the magnitudes of S_τ and s_τ as Cartesian coordinates. We then have the simple relation,

$$s_\tau = \rho \sin \vartheta_\tau \tag{2.5}$$

$$S_\tau = \rho \cos \vartheta_\tau \tag{2.6}$$

which leads to the simple inverse relationship

$$\rho = \sqrt{s_\tau^2 + S_\tau^2} \tag{2.7}$$

$$\tan \vartheta_\tau = \frac{s_\tau}{S_\tau} \tag{2.8}$$

The third internal coordinate, Θ_τ, is the same coordinate for both the Jacobi and Delves coordinate systems. We see that $\vartheta_\tau$is also labeled by the same arrangement channel τ as S_τ and s_τ are labeled by, as the value of $\vartheta_\tau$will depend on which set of mass-scaled Jacobi coordinates one is using. The hyperradius,ρ, however, is independent of arrangement channel, and is the same for all sets of S_τ and s_τ coordinates.

B.3 Adiabatically Adjusting Principle-Axis Hyperspherical (APH) Coordinates

The ρ coordinate remains unchanged from Delves' hyperspherical coordinates, however, the internal hyperangles are defined for θ and χ (in terms of mass-scaled Jacobi coordinates) as

$$\tan\theta = \frac{\left[(S_\tau^2 - s_\tau^2)^2 + (2\mathbf{S}_\tau \cdot \mathbf{s}_\tau)^2\right]^{1/2}}{2S_\tau s_\tau \sin(\Theta_\tau)} \tag{2.9}$$

with inverse relationships given as

$$s_\tau = \frac{\rho}{\sqrt{2}}\left[1 - \sin\theta\cos(2(\chi_i - \chi_{\tau i}))\right]^{1/2} \tag{2.10}$$

$$S_\tau = \frac{\rho}{\sqrt{2}}\left[1 + \sin\theta\cos(2(\chi_i - \chi_{\tau i}))\right]^{1/2} \tag{2.11}$$

$$\cos\Theta_\tau = \frac{\sin\theta\sin(2(\chi_i - \chi_{\tau i}))}{\left[1 - \sin^2\theta\cos^2(2(\chi_i - \chi_{\tau i}))\right]^{1/2}} \tag{2.12}$$

We know that the angle Θ_τ is the angle between the $\mathbf{S}$ and $\mathbf{s}$ vectors, and so we have the relation,

$$\mathbf{S}_\tau \cdot \mathbf{s}_\tau = S_\tau s_\tau \cos(\Theta_\tau) \tag{2.13}$$

Furthermore, from equation 2.12, we can see that the denominator can be written as

$$\left[1 - \sin^2\theta\cos^2(2(\chi_i - \chi_{\tau i}))\right]^{1/2} = \frac{2}{\rho^2} s_\tau S_\tau \tag{2.14}$$

such that

$$\cos(\Theta_\tau) = \frac{\rho^2\sin\theta\sin(2(\chi_i - \chi_{\tau i}))}{2S_\tau s_\tau} \tag{2.15}$$

$$S_\tau s_\tau \cos(\Theta_\tau) = \frac{\rho^2}{2}\sin(\theta)\sin(2(\chi_i - \chi_{\tau i})) \tag{2.16}$$

$$\mathbf{S}_\tau \cdot \mathbf{s}_\tau = \frac{\rho^2}{2}\sin(\theta)\sin(2(\chi_i - \chi_{\tau i})) \tag{2.17}$$

It can be difficult to visualize how hyperspherical coordinates represent the physical system, so it is helpful to see plots of how the Jacobi and Delves coordinate systems project into the APH coordinate system. In figures B.3, B.4, B.5, and B.6, are plots of the s_τ, S_τ, ϑ_τ, and $\Theta_\tau$coordinates for the Jacobi and Delves systems on an APH hypersurface of constant $\rho = 1$ Bohr. These plots are stereographic projections, where the x and y values are given in terms of APH coordinates as $x = \tan(\theta/2)\cos(\chi)$ and $y = \tan(\theta/2)\sin(\chi)$. The value of $\tan(\theta/2)$ behaves as a radius in these two dimensional plots, and χ behaves as a standard polar system angular coordinate.

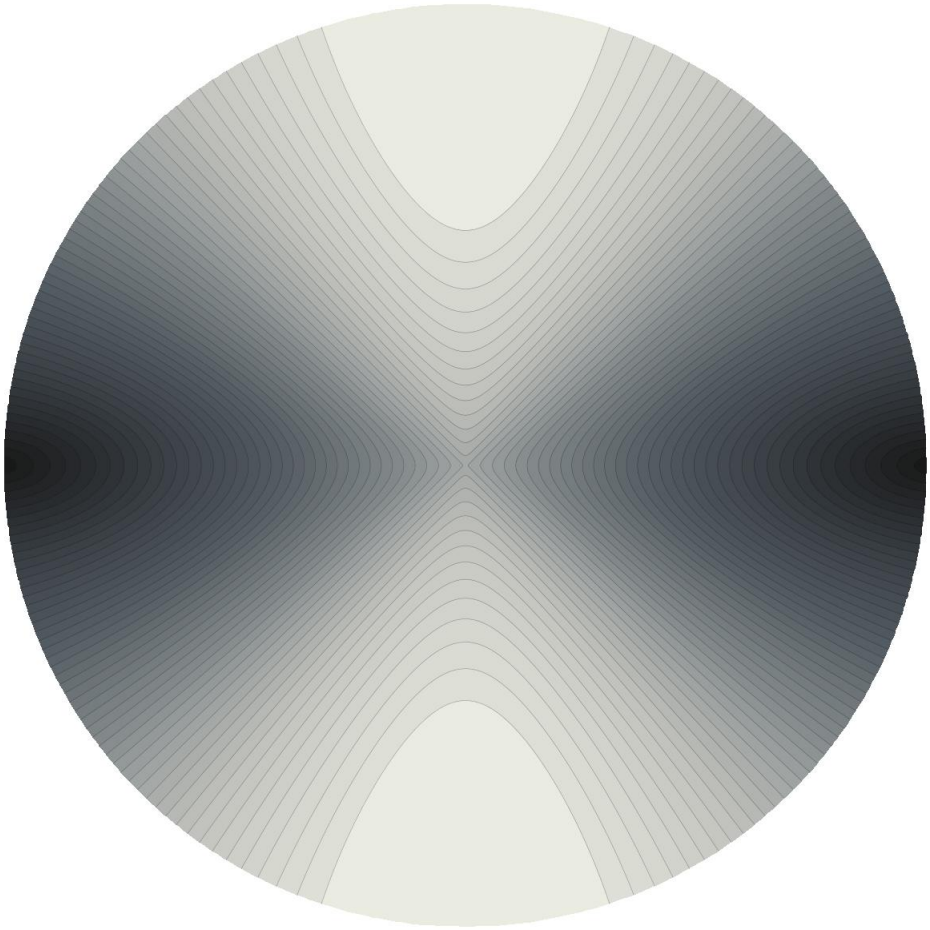

Figure B.3: Stereographic constant $\rho = 1$ plot of the Jacobi mass scaled $s_\tau$variable for channel A. In this plot, $x = \tan(\theta/2)\cos(\chi), y = \tan(\theta/2)\sin(\chi)$. The range of s_A is from 0 to 1 Bohr, and each contour shows a 0.02 Bohr change in s_A, and s_A increases from black to white. APH θ is zero at the center of the circle, and $\pi/2$ at the circumference. $\chi = 0$ is along the positive x axis. The $s_A = 0$ at the $\chi = 0, \theta = \pi/2$ and $\chi = \pi, \theta = \pi/2$ positions, represented by the black regions, and $s_A = 1$ at $\chi = \pi/2, \theta = \pi/2$, $\chi = 3\pi/2, \theta = \pi/2$ which are shown in white.

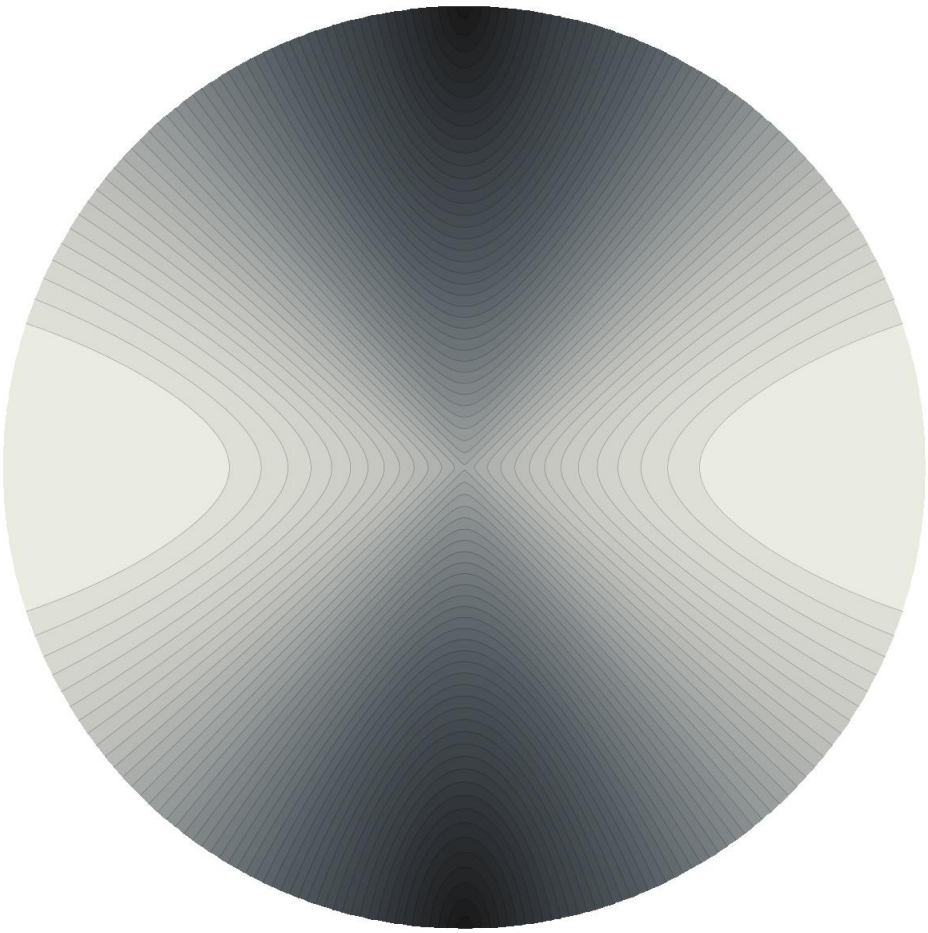

Figure B.4: Stereographic constant $\rho = 1$ plot of the Jacobi mass scaled $S_\tau$variable for channel A. In this plot, $x = \tan(\theta/2)\cos(\chi), y = \tan(\theta/2)\sin(\chi)$. The range of S_A is from 0 to 1 Bohr, and each contour shows a 0.02 Bohr change in S_A, and S_A increases from black to white. APH θ is zero at the center of the circle, and $\pi/2$ at the circumference. $\chi = 0$ is along the positive x axis. The $S_A = 0$ at the $\chi = \pi/2, \theta = \pi/2$ and $\chi = 3\pi/2, \theta = \pi/2$ positions, represented by the black regions, and $S_A = 1$ at $\chi = 0, \theta = \pi/2$, $\chi = \pi, \theta = \pi/2$ which are shown in white.

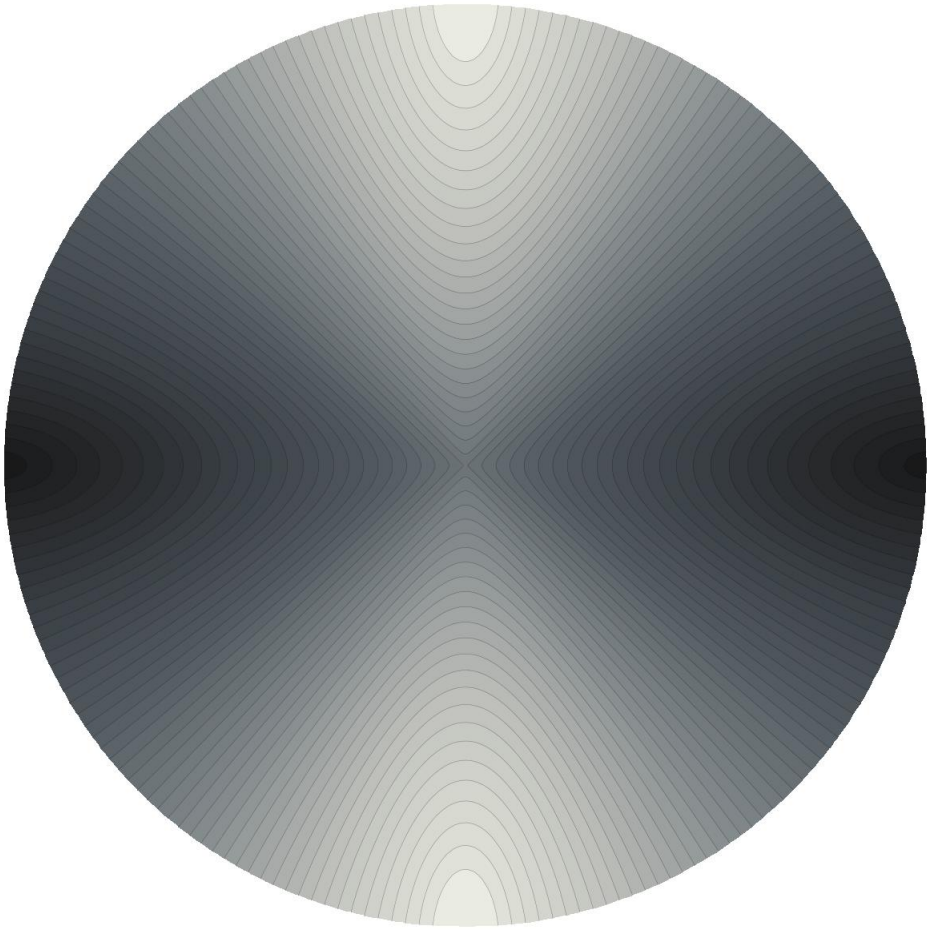

Figure B.5: Stereographic constant $\rho = 1$ plot of the Delves $\vartheta_\tau$coordinate for channel A. In this plot, $x = \tan(\theta/2)\cos(\chi), y = \tan(\theta/2)\sin(\chi)$. The ϑ_τ coordinate ranges from 0 to $\pi/2$, increasing in this plot from black to white. The contours show increments in ϑ_τ of $\pi/100$.

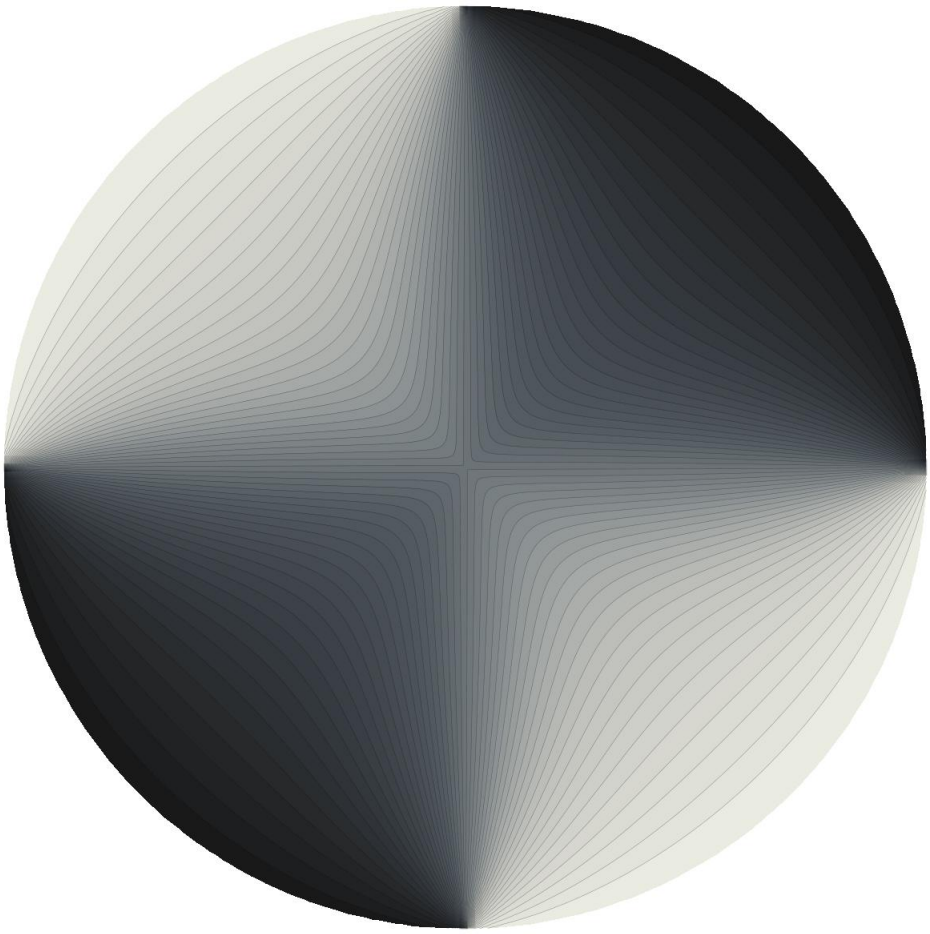

Figure B.6: Stereographic constant $\rho = 1$ plot of the Delves and Jacobi $\Theta_\tau$coordinate for channel A. In this plot, $x = \tan(\theta/2)\cos(\chi), y = \tan(\theta/2)\sin(\chi)$. The Θ_τ coordinate ranges from 0 to π, increasing in this plot from black to white. The contours show increments in Θ_τ of $\pi/50$. As $\Theta_\tau$changes, the two atoms defining the Jacobi $s_\tau$coordinate are rotating. Following a single constant $s_\tau$contour in figure B.3 from one point on the circle edge to another corresponds to Θ_τ changing by 180 degrees; the two atoms have switched position by a rotation.

B.4 Derivatives in Coordinate Transformations

In the process of transforming the derivative of a function with respect to one set of coordinates into a new set of coordinates, terms arise through the differentiation chain rule that are derivatives of the old set of coordinates with respect to the new. These are provided here for completeness, and to show how formulas used in computer code were developed.

B.4.1 Derivatives of Jacobi Coordinates with Respect to APH Coordinates

We use the relation of the Jacobi coordinates for a specified channel in terms of APH coordinates as

$$s = \frac{\rho}{\sqrt{2}} \left[1 - \sin(\theta)\cos(2(\chi_i - \chi_{i\tau}))\right] \tag{2.18}$$

$$S = \frac{\rho}{\sqrt{2}} \left[1 + \sin(\theta)\cos(2(\chi_i - \chi_{i\tau}))\right] \tag{2.19}$$

Where χ_τ is the value of χ for the τ channel.

Setting $\chi = \chi_i - \chi_{\tau i}$ for simplicity, these terms are easily calculated by chain-rule derivatives to give

$$\frac{ds}{d\theta} = \frac{-\rho\cos(\theta)\cos(2\chi)}{\sqrt{8}\left(1 - \sin(\theta)\cos(2\chi)\right)^{1/2}} \tag{2.20-a}$$

$$\frac{d^2s}{d\theta^2} = \frac{\rho\sin(\theta)\cos(2\chi)}{\sqrt{8}\left(1 - \sin(\theta)\cos(2\chi)\right)^{1/2}} - \frac{\rho\cos^2(\theta)\cos^2(2\chi)}{\sqrt{32}\left(1 - \sin(\theta)\cos(2\chi)\right)^{3/2}} \tag{2.20-b}$$

$$\frac{ds}{d\chi} = \frac{\rho\sin(\theta)\sin(2\chi)}{\sqrt{2}\left(1 - \sin(\theta)\cos(2\chi)\right)^{1/2}} \tag{2.20-c}$$

$$\frac{d^2s}{d\chi^2} = \frac{\rho\sqrt{2}\sin(\theta)\cos(2\chi)}{(1-\sin(\theta)\cos(2\chi))^{1/2}} - \frac{\rho\sin^2(\theta)\sin^2(2\chi)}{\sqrt{2}\,(1-\sin(\theta)\cos(2\chi))^{3/2}} \tag{2.20-d}$$

Equations 2.20-a-2.20-d are analytic, and can be calculated for any given point as needed. Similar formulas can be found for the derivatives of S with respect to θ and χ, but again they are never needed because the vibrational bound states are not functions of S.

Likewise, for S we have,

$$\frac{dS}{d\theta} = \frac{\rho\cos(\theta)\cos(2\chi)}{\sqrt{8}\,(1+\sin(\theta)\cos(2\chi))^{1/2}} \tag{2.21-a}$$

$$\frac{d^2S}{d\theta^2} = -\frac{\rho\sin(\theta)\cos(2\chi)}{\sqrt{8}\,(1+\sin(\theta)\cos(2\chi))^{1/2}} - \frac{\rho\cos^2(\theta)\cos^2(2\chi)}{\sqrt{32}\,(1+\sin(\theta)\cos(2\chi))^{3/2}} \tag{2.21-b}$$

$$\frac{dS}{d\chi} = -\frac{\rho\sin(\theta)\sin(2\chi)}{\sqrt{2}\,(1+\sin(\theta)\cos(2\chi))^{1/2}} \tag{2.21-c}$$

$$\frac{d^2S}{d\chi^2} = -\frac{\rho\sqrt{2}\sin(\theta)\cos(2\chi)}{(1+\sin(\theta)\cos(2\chi))^{1/2}} - \frac{\rho\sin^2(\theta)\sin^2(2\chi)}{\sqrt{2}\,(1+\sin(\theta)\cos(2\chi))^{3/2}} \tag{2.21-d}$$

B.4.2 Derivatives of Delves' coordinates With Respect To APH Coordinates

The continuum state construction also requires the Delves' Hyperspherical coordinate derivatives with respect to the APH coordinates, since the constructed continuum state functions include the Jacobi Polynomials as functions of Delves' theta, θ_d. Since any value of ϑ_τ or s and S require a specified channel, we again simplify the equations with $\chi = \chi_i - \chi_{i\tau}$, and recognize that the value of χ is

channel dependent. Furthermore, since we will always have the derivatives of the Jacobi coordinates with respect to the APH coordinates, also, it is convenient and computationally simpler to formulate the derivatives in Delves' coordinates in terms of the Jacobi coordinates. From reference [8], we have the definitions

$$\tan\vartheta_\tau = \left(\frac{s}{S}\right) \tag{2.22}$$

Applying the chain rule of derivatives to this equation gives

$$\begin{aligned}
\frac{d\tan\vartheta_\tau}{d\theta} &= \frac{1}{S}\frac{ds}{d\theta} - \frac{s}{S^2}\frac{dS}{d\theta} \\
\sec^2\vartheta_\tau\frac{d\vartheta_\tau}{d\theta} &= \frac{1}{S}\frac{ds}{d\theta} - \frac{\tan\vartheta_\tau}{S}\frac{dS}{d\theta} \\
\frac{d\vartheta_\tau}{d\theta} &= \left[\frac{\cos\vartheta_\tau}{\rho}\frac{ds}{d\theta} - \frac{\sin\vartheta_\tau}{\rho}\frac{dS}{d\theta}\right]
\end{aligned} \tag{2.23}$$

and likewise for χ,

$$\frac{d\vartheta_\tau}{d\chi} = \left[\frac{\cos\vartheta_\tau}{\rho}\frac{ds}{d\chi} - \frac{\sin\vartheta_\tau}{\rho}\frac{dS}{d\chi}\right] \tag{2.24}$$

and for second derivatives, we have

$$\frac{d^2\vartheta_\tau}{d\theta^2} = \frac{d}{d\theta}\left[\frac{S}{\rho^2}\frac{ds}{d\theta} - \frac{s}{\rho^2}\frac{dS}{d\theta}\right] \tag{2.25}$$

$$= \frac{1}{\rho^2}\left[S\frac{d^2s}{d\theta^2} - s\frac{d^2S}{d\theta^2}\right] \tag{2.26}$$

$$= \frac{1}{\rho}\left[\cos(\vartheta_\tau)\frac{d^2s}{d\theta^2} - \sin(\vartheta_\tau)\frac{d^2S}{d\theta^2}\right] \tag{2.27}$$

and for *chi* we have the same form,

$$\frac{d^2\vartheta_\tau}{d\chi^2} = \frac{1}{\rho}\left[\cos(\vartheta_\tau)\frac{d^2s}{d\chi^2} - \sin(\vartheta_\tau)\frac{d^2S}{d\chi^2}\right] \tag{2.28}$$

We must also have the derivatives of Θ_τ with respect to the APH coordinates. The Delves' bending angle Θ_τ is channel dependent, so again we must understand that all terms of χ that appear are in relation to the channel specified. Θ_τ is defined in APH coordinates as

$$\cos(\Theta_\tau) = \left(\frac{\sin(\theta)\sin(2\chi)}{\left(1 - \sin^2(\theta)\cos^2(2\chi)\right)^{1/2}} \right) \tag{2.29}$$

With some algebraic manipulation, we can alter this relationship to give simpler derivative terms. From equation 2.9, we can write

$$\sin(\Theta_\tau) = \frac{\left[(S_\tau^2 - s_\tau^2)^2 + (2\mathbf{S}_\tau \cdot \mathbf{s}_\tau)^2\right]^{1/2}}{2S_\tau s_\tau \tan(\theta)} \tag{2.30}$$

Using the definitions of the mass-scaled Jacobi coordinates in terms of APH coordinates given in equations 2.10 and 2.11, we can write

$$(S^2 - s^2)^2 = \rho^4 \sin^2(\theta)\cos^2(2\chi) \tag{2.31}$$

and from equation 2.29 we can write

$$(2\mathbf{S} \cdot \mathbf{s})^2 = 2Ss\cos(\Theta_\tau) = \rho^4 \sin^2(\theta)\sin^2(2\chi) \tag{2.32}$$

to give

$$\sin(\Theta_\tau) = \frac{\rho^2 \sin(\theta)}{2Ss\tan(\theta)} \tag{2.33}$$

Noting that equation 2.29 can be written as

$$\cos(\Theta_\tau) = \frac{\rho^2 \sin(\theta)\sin(2\chi)}{2Ss} \tag{2.34}$$

we can now write

$$\frac{\sin(\Theta_\tau)}{\cos(\Theta_\tau)} = \frac{2\rho^2 Ss}{2\rho^2 Ss\tan(\theta)\sin(2\chi)} \tag{2.35}$$

so that

$$\tan(\Theta_\tau) = \frac{1}{\tan(\theta)\sin(2\chi)} \tag{2.36}$$

With this form of this equation, we can get simple derivative terms. Since Θ is an orthogonal coordinate to $\mathbf{S}$, $\mathbf{s}$, and ρ, changes in theta do not depend on changes of these coordinates. What we have done in the above simplification is attempt to remove as many orthogonal terms from the definition of Θ as possible. From here we can get derivative terms of Θ with respect to θ and χ

$$\frac{d}{d\theta}\tan(\Theta_\tau) = \frac{d}{d\theta}\frac{1}{\tan(\theta)\sin(2\chi)} \tag{2.37-a}$$

$$\sec^2(\Theta_\tau)\frac{d\Theta_\tau}{d\theta} = \frac{-1}{\sin(2\chi)\cos(\theta)\sin(\theta)\tan(\theta)} \tag{2.37-b}$$

$$\sec^2(\Theta_\tau)\frac{d\Theta_\tau}{d\theta} = \frac{-\tan(\Theta_\tau)}{\cos(\theta)\sin(\theta)} \tag{2.37-c}$$

$$\frac{d\Theta_\tau}{d\theta} = \frac{-\cos^2(\Theta_\tau)\tan(\Theta_\tau)}{\cos(\theta)\sin(\theta)} \tag{2.37-d}$$

This is a relatively simple expression for the derivative, and it is easy to compute. We also have for χ,

$$\sec^2(\Theta_\tau)\frac{d\Theta_\tau}{d\chi} = \frac{d}{d\chi}\frac{1}{\tan\theta\sin(2\chi)} \tag{2.38-a}$$

$$= \frac{-2}{\tan\theta\tan(2\chi)\sin(2\chi)} \tag{2.38-b}$$

$$= \frac{-2}{\tan(2\chi)}\tan(\Theta_\tau) \tag{2.38-c}$$

$$\frac{d\Theta_\tau}{d\chi} = \frac{-2\sin(\Theta_\tau)\cos(\Theta_\tau)}{\tan(2\chi)} \tag{2.38-d}$$

As for second derivatives of Θ with respect to θ and χ, we have

$$\frac{d^2}{d\theta^2}\tan(\Theta_\tau) = \frac{d^2}{d\theta^2}\frac{1}{\tan(\theta)\sin(2\chi)} \tag{2.39-a}$$

$$\frac{d}{d\theta}\left[\sec^2(\Theta_\tau)\frac{d\Theta_\tau}{d\theta}\right] = \frac{d}{d\theta}\left[\frac{-\tan(\Theta_\tau)}{\cos(\theta)\sin(\theta)}\right] \tag{2.39-b}$$

Working with just the left side now, we have,

$$\begin{aligned}\frac{d}{d\theta}\left[\sec^2(\Theta_\tau)\frac{d\Theta_\tau}{d\theta}\right] &= 2\sec^2(\Theta_\tau)\tan(\Theta_\tau)\left(\frac{d\Theta_\tau}{d\theta}\right)^2 + \sec^2(\Theta_\tau)\frac{d^2\Theta_\tau}{d\theta^2} \\ &= \sec^2(\Theta_\tau)\left[2\tan(\Theta_\tau)\left(\frac{d\Theta_\tau}{d\theta}\right)^2 + \frac{d^2\Theta_\tau}{d\theta^2}\right] \end{aligned} \tag{2.39-c}$$

and now the right side of equation 2.39-b,

$$\frac{d}{d\theta}\left[\frac{-\tan(\Theta_\tau)}{\cos(\theta)\sin(\theta)}\right] = \tan\Theta_\tau\frac{d}{d\theta}\frac{-1}{\sin\theta\cos\theta} + \frac{-1}{\sin\theta\cos\theta}\frac{d}{d\theta}\tan(\Theta_\tau) \tag{2.39-d}$$

$$= \left(\frac{1}{\sin^2\theta} - \frac{1}{\cos^2\theta}\right)\tan(\Theta_\tau) + \frac{\tan(\Theta_\tau)}{\cos^2\theta\sin^2\theta} \tag{2.39-e}$$

$$= \tan(\Theta_\tau)\left[\frac{1}{\sin^2\theta\cos^2\theta} + \frac{\cos^2\theta - \sin^2\theta}{\cos^2\theta\sin^2\theta}\right] \tag{2.39-f}$$

$$= \tan(\Theta_\tau)\left[\frac{2}{\sin^2\theta}\right] \tag{2.39-g}$$

recombining equations 2.39-c and 2.39-g gives

$$\sec^2(\Theta_\tau)\left[2\tan(\Theta_\tau)\left(\frac{d\Theta_\tau}{d\theta}\right)^2 + \frac{d^2\Theta_\tau}{d\theta^2}\right] = \tan(\Theta_\tau)\left[\frac{2}{\sin^2\theta}\right] \tag{2.39-h}$$

$$\frac{d^2\Theta_\tau}{d\theta^2} = \frac{2\cos^2(\Theta_\tau)\tan(\Theta_\tau)}{\sin^2\theta} - 2\tan(\Theta_\tau)\left(\frac{d\Theta_\tau}{d\theta}\right)^2 \tag{2.39-i}$$

For the derivatives with respect to χ, a simpler form is found by directly differentiating equation 2.38-d,

$$\frac{d^2\Theta_\tau}{d\chi^2} = \frac{d}{d\chi}\left[\frac{-2\sin(\Theta_\tau)\cos(\Theta_\tau)}{\tan(2\chi)}\right] \tag{2.40-a}$$

$$\frac{d^2\Theta_\tau}{d\chi^2} = \left[\frac{\sin^2(\Theta_\tau) - \cos^2(\Theta_\tau)}{\tan(2\chi)}\right]\frac{d\Theta_\tau}{d\chi} + \frac{\sin(\Theta_\tau)\cos(\Theta_\tau)}{\cos^2(2\chi)} \tag{2.40-b}$$

Appendix C

Symmetry Operations as Matrices

To show a smaller example than the 12 function basis set used in section 4.2, consider a C_{2v} system with a symmetry plot that looks like figure C.1. The numbers in each quadrant of the image could represent basis functions, and a representation of C_{2v} symmetry using these functions would be of dimension four.

To find the character table, we apply the symmetry operations to these four functions and observe if any of them stay the same or become inverted. In matrix

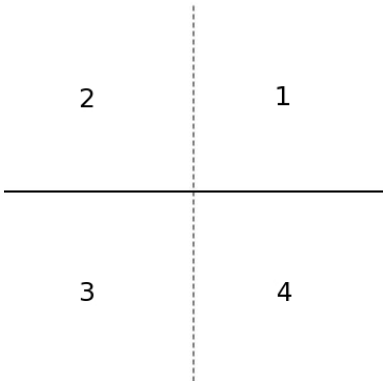

Figure C.1: C_{2v} symmetry example. The solid and dashed line represent two different reflection planes. There exists a C_2 rotation symmetry about the axis defined by the intersection of the reflection planes, i.e. perpendicular to the plane of the page.

notation, we define matrices that represent the operators. A C_2 rotation would move $|1\rangle$ to $|3\rangle$, and $|2\rangle$ to $|4\rangle$, etc., so the C_2 operation would appear as

$$C_2 \begin{pmatrix} |1\rangle \\ |2\rangle \\ |3\rangle \\ |4\rangle \end{pmatrix} = \begin{pmatrix} 0 & 0 & 1 & 0 \\ 0 & 0 & 0 & 1 \\ 1 & 0 & 0 & 0 \\ 0 & 1 & 0 & 0 \end{pmatrix} \begin{pmatrix} |1\rangle \\ |2\rangle \\ |3\rangle \\ |4\rangle \end{pmatrix} = \begin{pmatrix} |3\rangle \\ |4\rangle \\ |1\rangle \\ |2\rangle \end{pmatrix} \tag{3.1}$$

The character of the C_2 rotation defined in equation 3.1, as with the character of any matrix, is defined as the sum of the diagonal elements. In this case we can see that the character of the C_2 rotation is zero. The identity operation, E, which changes the positions of none of the basis functions, is the identity matrix, and therefore always has a character equal to the dimension of the representation.

Appendix D

Jacobi Polynomials and Delves' Continuum Functions

The constructed continuum state functions used throughout this paper contain the Jacobi polynomials. The Jacobi polynomials are terms in the analytic solution to the zero potential three-body Hamiltonian in Delves' hyperspherical coordinates. This appendix contains relevant information regrading these functions.

The Jacobi polynomial has three indices, generically called α, β, and ν. In this paper, these correspond to the Delves' coordinate rotational and vibrational quantum numbers of j, ℓ, and n, respectively. (Where n is $\nu - n_{bqb}$, and n_{bqb} is the number of bound and quasibound states. See note on continuum state vibrational ordering in section 3.3.)

Further information on the Jacobi polynomials can be found in references [26] and [27].

The Jacobi polynomials are the solutions to the Jacobi differential equation,

$$(1-x^2)\frac{d^2y}{dx^2} + [\beta - \alpha - (\alpha+\beta+2)x]\frac{dy}{dx} + n(n+\alpha+\beta+1)y = 0 \qquad (4.1)$$

and they are defined on the range of $[-1, 1]$.

The Jacobi polynomial recursion relation is defined as

$$\begin{aligned}
&2(n+1)(n+\alpha+\beta+1)(2n+\alpha+\beta)\mathscr{P}_{n+1}^{\alpha,\beta}(x) \\
&= \left[(2n+\alpha+\beta+1)(\alpha^2-\beta^2)+x(2n+\alpha+\beta)_3\right]\mathscr{P}_n^{\alpha,\beta}(x) \\
&- 2(n+\alpha)(n+\beta)(2n+\alpha+\beta+2)\mathscr{P}_{n-1}^{\alpha,\beta}(x)
\end{aligned} \tag{4.2}$$

where the term $(2n+\alpha+\beta)_3$ employs the Pochhammer symbol and evaluates as

$$(x)_k = x(x+1)(x+2)\ldots(x+k-1) \tag{4.3}$$

for a total of k terms.

The derivative formula is given as

$$\frac{d}{dx}\mathscr{P}_n^{\alpha\beta}(x) = \frac{1}{2}(\alpha+\beta+n+1)\mathscr{P}_{n-1}^{\alpha+1,\beta+1}(x) \tag{4.4}$$

Defining a new function $u(x)$ as,

$$u(x) = (1-x)^{(\alpha+1)/2}(1+x)^{(\beta+1)/2}\mathscr{P}_n^{\alpha,\beta}(x) \tag{4.5}$$

then the Jacobi differential equation can be transformed into

$$\frac{d^2u}{dx^2} + \left[\frac{1}{4}\frac{1-\alpha^2}{(1-x)^2} + \frac{1}{4}\frac{1-\beta^2}{(1+x)^2} + \frac{n(n+\alpha+\beta+1)+\frac{1}{2}(\alpha+1)(\beta+1)}{1-x^2}\right]u = 0 \tag{4.6}$$

Next if we make a coordinate transformation of $x = \cos(\theta)$, and making use of the half-angle formulas $\sin(\theta/2) = \sqrt{(1-\cos(\theta))/2}$ and $\cos(\theta/2) = \sqrt{(1+\cos(\theta))/2}$, we get

$$\frac{d^2u(\theta)}{d\theta^2} + \left[\frac{\frac{1}{4}-\alpha^2}{4\sin^2(\theta/2)} + \frac{\frac{1}{4}-\beta^2}{4\cos^2(\theta/2)} + \frac{1}{4}\left(2n+\alpha+\beta+1\right)^2\right] u(\theta) = 0 \tag{4.7}$$

with

$$u(\theta) = \sin^{\alpha+1/2}(\theta/2)\cos^{\beta+1/2}(\theta/2)\mathscr{P}_n^{\alpha,\beta}(\cos(\theta)) \tag{4.8}$$

Lastly, if we make the following substitutions,

$$\vartheta_\tau = \theta/2 \tag{4.9}$$

$$\alpha = j + 1/2 \tag{4.10}$$

$$\beta = \ell + 1/2 \tag{4.11}$$

then we arrive with a form of

$$\frac{d^2u}{d\vartheta_\tau^2} - \left[\frac{j(j+1)}{\sin^2(\vartheta_\tau)} + \frac{\ell(\ell+1)}{\cos^2(\vartheta_\tau)} - (2n+j+\ell+2)^2\right] u(\vartheta_\tau) = 0 \tag{4.12}$$

with

$$u(\vartheta_\tau) = \sin^{j+1}(\vartheta_\tau)\cos^{\ell+1}(\vartheta_\tau)\mathscr{P}_n^{j+1/2,\ell+1/2}(\cos(2\vartheta_\tau)) \tag{4.13}$$

This last definition corresponds directly with the form of equation 2.20. Note that now the domain of ϑ_τ for which $u(\vartheta_\tau)$ is defined is $[0, \pi/2]$, corresponding to the physical range of Delves' coordinates ϑ_τ. Also, the last term in square brackets of equation 4.12 can be simplified. We know that $\lambda = 2n + j + \ell$, so we can see that the eigenvalue is $(\lambda+2)^2$, as expected from equation 49 in reference [13].

Appendix E

Integrals Of Symmetrized Basis Surface Functions and Asymptotic Functions

This section contains integrals for the normalization of the symmetrized constructed basis functions and also overlaps with asymptotic states.

The states in this appendix are defined as follows. Note that the symmetrized states maintain labels for even or odd rotational quantum numbers, j, and for even or odd parity. These labels are redundant for the one-dimensional irreducible representations , since whether they are even or odd is determined by the character tables. The one exception is j for the E irreducible representations , which does not have a symmetry element to define whether j is even or odd. The inclusion of this

notation is for clarity; it shows some of the physical properties of the symmetrized states.

$$\begin{aligned}\left|(A_1)^{p+}_{j+}\right\rangle &= |1\rangle + |2\rangle + |3\rangle + |4\rangle + |5\rangle + |6\rangle \\ &\quad + |7\rangle + |8\rangle + |9\rangle + |10\rangle + |11\rangle + |12\rangle \qquad (5.1)\\ \left|(A_2)^{p+}_{j-}\right\rangle &= |1\rangle - |2\rangle + |3\rangle - |4\rangle + |5\rangle - |6\rangle \\ &\quad + |7\rangle - |8\rangle + |9\rangle - |10\rangle + |11\rangle - |12\rangle \qquad (5.2)\\ \left|(B_1)^{p-}_{j+}\right\rangle &= |1\rangle - |2\rangle - |3\rangle + |4\rangle + |5\rangle - |6\rangle \\ &\quad - |7\rangle + |8\rangle + |9\rangle - |10\rangle - |11\rangle + |12\rangle \qquad (5.3)\\ \left|(B_2)^{p-}_{j-}\right\rangle &= |1\rangle + |2\rangle - |3\rangle - |4\rangle + |5\rangle + |6\rangle \\ &\quad - |7\rangle - |8\rangle + |9\rangle + |10\rangle - |11\rangle - |12\rangle \qquad (5.4)\end{aligned}$$

$$\begin{aligned}\left|(E^{(1)}_1)^{p-}_{j+}\right\rangle &= 2\,|1\rangle + |2\rangle + |3\rangle - |4\rangle - |5\rangle - 2\,|6\rangle \\ &\quad - 2\,|7\rangle - |8\rangle - |9\rangle + |10\rangle + |11\rangle + 2\,|12\rangle \qquad (5.5)\\ \left|(E^{(2)}_1)^{p-}_{j+}\right\rangle &= \frac{3}{2}(|2\rangle + |3\rangle + |4\rangle + |5\rangle \\ &\quad - |8\rangle - |9\rangle - |10\rangle - |11\rangle) \qquad (5.6)\\ \left|(E^{(1)}_2)^{p-}_{j+}\right\rangle &= 2\,|1\rangle - |2\rangle - |3\rangle - |4\rangle - |5\rangle + 2\,|6\rangle \\ &\quad + 2\,|7\rangle - |8\rangle - |9\rangle - |10\rangle - |11\rangle + 2\,|12\rangle \qquad (5.7)\\ \left|(E^{(2)}_2)^{p-}_{j+}\right\rangle &= \frac{3}{2}(|2\rangle + |3\rangle + |4\rangle + |5\rangle \\ &\quad - |8\rangle - |9\rangle - |10\rangle - |11\rangle) \qquad (5.8)\end{aligned}$$

$$\left|(E_1^{(1)})_{j-}^{p-}\right\rangle = \frac{3}{2}(-|2\rangle + |3\rangle - |4\rangle + |5\rangle + |8\rangle - |9\rangle + |10\rangle - |11\rangle) \tag{5.9}$$

$$\left|(E_1^{(2)})_{j-}^{p-}\right\rangle = 2|1\rangle - |2\rangle + |3\rangle + |4\rangle - |5\rangle + 2|6\rangle - 2|7\rangle + |8\rangle - |9\rangle - |10\rangle + |11\rangle - 2|12\rangle \tag{5.10}$$

$$\left|(E_2^{(1)})_{j-}^{p-}\right\rangle = \frac{3}{2}(-|2\rangle + |3\rangle + |4\rangle - |5\rangle - |8\rangle + |9\rangle + |10\rangle - |11\rangle) \tag{5.11}$$

$$\left|(E_2^{(2)})_{j-}^{p-}\right\rangle = 2|1\rangle + |2\rangle - |3\rangle + |4\rangle - |5\rangle - 2|6\rangle + 2|7\rangle + |8\rangle - |9\rangle + |10\rangle - |11\rangle - 2|12\rangle \tag{5.12}$$

And the asymptotic-type states,

$$\left|A_{j+}^{p+}\right\rangle = |1\rangle + |6\rangle + |7\rangle + |12\rangle \tag{5.13}$$

$$\left|A_{j+}^{p-}\right\rangle = |1\rangle - |6\rangle - |7\rangle + |12\rangle \tag{5.14}$$

$$\left|A_{j-}^{p+}\right\rangle = |1\rangle - |6\rangle + |7\rangle - |12\rangle \tag{5.15}$$

$$\left|A_{j-}^{p-}\right\rangle = |1\rangle + |6\rangle - |7\rangle - |12\rangle \tag{5.16}$$

$$\left|B_{j+}^{p+}\right\rangle = |9\rangle + |2\rangle + |3\rangle + |8\rangle \tag{5.17}$$

$$\left|B_{j+}^{p-}\right\rangle = |9\rangle - |2\rangle - |3\rangle + |8\rangle \tag{5.18}$$

$$\left|B_{j-}^{p+}\right\rangle = |9\rangle - |2\rangle + |3\rangle - |8\rangle \tag{5.19}$$

$$\left|B_{j-}^{p-}\right\rangle = |9\rangle + |2\rangle - |3\rangle - |8\rangle \tag{5.20}$$

$$\left|C_{j+}^{p+}\right\rangle = |5\rangle + |10\rangle + |11\rangle + |4\rangle \tag{5.21}$$

$$\left|C_{j+}^{p-}\right\rangle = |5\rangle - |10\rangle - |11\rangle + |4\rangle \tag{5.22}$$

$$\left|C_{j-}^{p+}\right\rangle = |5\rangle - |10\rangle + |11\rangle - |4\rangle \tag{5.23}$$

$$\left|C_{j-}^{p-}\right\rangle = |5\rangle + |10\rangle - |11\rangle - |4\rangle \tag{5.24}$$

E.1 Integral Definitions

Not all of the numbered functions overlap with each other. This section explicitly defines the n numbers, and which overlaps between the numbered functions are non-zero. The overlap of a function with itself is n_0. The others are defined as

$$\begin{aligned} n_1 &= \langle 1|2\rangle = \langle 3|4\rangle = \langle 5|6\rangle \\ &= \langle 7|8\rangle = \langle 9|10\rangle = \langle 11|12\rangle \end{aligned} \tag{5.25}$$

$$\begin{aligned} n_2 &= \langle 1|3\rangle = \langle 2|4\rangle = \langle 3|5\rangle \\ &= \langle 4|6\rangle = \langle 5|7\rangle = \langle 6|8\rangle \\ &= \langle 7|9\rangle = \langle 8|10\rangle = \langle 9|11\rangle \\ &= \langle 10|12\rangle = \langle 11|1\rangle = \langle 12|2\rangle \end{aligned} \tag{5.26}$$

$$\begin{aligned} n_3 &= \langle 1|4\rangle = \langle 2|11\rangle = \langle 3|6\rangle \\ &= \langle 5|8\rangle = \langle 7|10\rangle = \langle 9|12\rangle \end{aligned} \tag{5.27}$$

All other integrals are zero.

E.2 Symmetrized Function Normalizations and Overlaps

This section contains the results of integrals between each of the symmetrized states. From this we can get normalizations in terms of the n_0,n_1,n_2, and n_3 numbers. The definitions of these numbers is given in appendix E.1. While most of these numbers are zero, knowing those that are not in terms of the n_i numbers allows the values of the integrals to be determined very quickly. Note also that overlaps between even and odd j states for functions of E_1 symmetry are not zero, and the same is true for E_2. This is notable because it is only through these elements that any coupling between even and odd rotational asymptotic states can occur.

$$\left\langle (A_1)^{p+}_{j+} \middle| (A_1)^{p+}_{j+} \right\rangle = 12.0n_0 + 12.0n_1 + 12.0n_2 + 12.0n_3 \qquad \neq 0 \qquad (5.28)$$

$$\left\langle (A_1)^{p+}_{j+} \middle| (A_2)^{p+}_{j-} \right\rangle = 0.0n_0 + 0.0n_1 + 0.0n_2 + 0.0n_3 \qquad = 0 \qquad (5.29)$$

$$\left\langle (A_1)^{p+}_{j+} \middle| (B_1)^{p-}_{j+} \right\rangle = 0.0n_0 + 0.0n_1 + 0.0n_2 + 0.0n_3 \qquad = 0 \qquad (5.30)$$

$$\left\langle (A_1)^{p+}_{j+} \middle| (B_2)^{p-}_{j-} \right\rangle = 0.0n_0 + 0.0n_1 + 0.0n_2 + 0.0n_3 \qquad = 0 \qquad (5.31)$$

$$\left\langle (A_1)^{p+}_{j+} \middle| (E_1^{(1)})^{p-}_{j+} \right\rangle = 0.0n_0 + 0.0n_1 + 0.0n_2 + 0.0n_3 \qquad = 0 \qquad (5.32)$$

$$\left\langle (A_1)^{p+}_{j+} \middle| (E_1^{(2)})^{p-}_{j+} \right\rangle = 0.0n_0 + 0.0n_1 + 0.0n_2 + 0.0n_3 \qquad = 0 \qquad (5.33)$$

$$\left\langle (A_1)^{p+}_{j+} \middle| (E_1^{(1)})^{p-}_{j-} \right\rangle = 0.0n_0 + 0.0n_1 + 0.0n_2 + 0.0n_3 \qquad = 0 \qquad (5.34)$$

$$\left\langle (A_1)^{p+}_{j+} \middle| (E_1^{(2)})^{p-}_{j-} \right\rangle = 0.0n_0 + 0.0n_1 + 0.0n_2 + 0.0n_3 \qquad = 0 \qquad (5.35)$$

$$\left\langle (A_1)^{p+}_{j+} \middle| (E_2^{(1)})^{p+}_{j+} \right\rangle = 0.0n_0 + 0.0n_1 + 0.0n_2 + 0.0n_3 \qquad = 0 \qquad (5.36)$$

$$\left\langle (A_1)^{p+}_{j+} \middle| (E_2^{(2)})^{p+}_{j+} \right\rangle = 0.0n_0 + 0.0n_1 + 0.0n_2 + 0.0n_3 \qquad = 0 \qquad (5.37)$$

$$\left\langle (A_1)^{p+}_{j+} \middle| (E_2^{(1)})^{p+}_{j-} \right\rangle = 0.0n_0 + 0.0n_1 + 0.0n_2 + 0.0n_3 \qquad = 0 \qquad (5.38)$$

$$\left\langle (A_1)^{p+}_{j+} \middle| (E_2^{(2)})^{p+}_{j-} \right\rangle = 0.0n_0 + 0.0n_1 + 0.0n_2 + 0.0n_3 \qquad = 0 \qquad (5.39)$$

$$\left\langle (A_2)^{p+}_{j-} \middle| (A_2)^{p+}_{j-} \right\rangle = 12.0n_0 - 12.0n_1 + 12.0n_2 - 12.0n_3 \qquad \neq 0 \qquad (5.40)$$

$$\left\langle (A_2)^{p+}_{j-} \middle| (B_1)^{p-}_{j+} \right\rangle = 0.0n_0 + 0.0n_1 + 0.0n_2 + 0.0n_3 \qquad = 0 \qquad (5.41)$$

$$\left\langle (A_2)^{p+}_{j-} \middle| (B_2)^{p-}_{j-} \right\rangle = 0.0n_0 + 0.0n_1 + 0.0n_2 + 0.0n_3 \qquad = 0 \qquad (5.42)$$

$$\left\langle (A_2)^{p+}_{j-} \middle| (E_1^{(1)})^{p-}_{j+} \right\rangle = 0.0n_0 + 0.0n_1 + 0.0n_2 + 0.0n_3 \qquad = 0 \qquad (5.43)$$

$$\left\langle (A_2)^{p+}_{j-} \middle| (E_1^{(2)})^{p-}_{j+} \right\rangle = 0.0n_0 + 0.0n_1 + 0.0n_2 + 0.0n_3 \qquad = 0 \qquad (5.44)$$

$$\left\langle (A_2)^{p+}_{j-} \middle| (E_1^{(1)})^{p-}_{j-} \right\rangle = 0.0n_0 + 0.0n_1 + 0.0n_2 + 0.0n_3 \qquad = 0 \qquad (5.45)$$

$$\left\langle (A_2)^{p+}_{j-} \middle| (E_1^{(2)})^{p-}_{j-} \right\rangle = 0.0n_0 + 0.0n_1 + 0.0n_2 + 0.0n_3 \qquad = 0 \qquad (5.46)$$

$$\left\langle (A_2)^{p+}_{j-} \middle| (E_2^{(1)})^{p+}_{j+} \right\rangle = 0.0n_0 + 0.0n_1 + 0.0n_2 + 0.0n_3 \qquad = 0 \qquad (5.47)$$

$$\left\langle (A_2)^{p+}_{j-} \middle| (E_2^{(2)})^{p+}_{j+} \right\rangle = 0.0n_0 + 0.0n_1 + 0.0n_2 + 0.0n_3 \qquad = 0 \qquad (5.48)$$

$$\left\langle (A_2)^{p+}_{j-} \middle| (E_2^{(1)})^{p+}_{j-} \right\rangle = 0.0n_0 + 0.0n_1 + 0.0n_2 + 0.0n_3 \qquad = 0 \qquad (5.49)$$

$$\left\langle (A_2)^{p+}_{j-} \middle| (E_2^{(2)})^{p+}_{j-} \right\rangle = 0.0n_0 + 0.0n_1 + 0.0n_2 + 0.0n_3 \qquad = 0 \qquad (5.50)$$

$$\left\langle (B_1)^{p-}_{j+} \middle| (B_1)^{p-}_{j+} \right\rangle = 12.0n_0 - 12.0n_1 - 12.0n_2 + 12.0n_3 \qquad \neq 0 \qquad (5.51)$$

$$\left\langle (B_1)^{p-}_{j+} \middle| (B_2)^{p-}_{j-} \right\rangle = 0.0n_0 + 0.0n_1 + 0.0n_2 + 0.0n_3 \qquad = 0 \qquad (5.52)$$

$$\left\langle (B_1)^{p-}_{j+} \middle| (E_1^{(1)})^{p-}_{j+} \right\rangle = 0.0n_0 + 0.0n_1 + 0.0n_2 + 0.0n_3 \qquad = 0 \qquad (5.53)$$

$$\left\langle (B_1)^{p-}_{j+} \middle| (E_1^{(2)})^{p-}_{j+} \right\rangle = 0.0n_0 + 0.0n_1 + 0.0n_2 + 0.0n_3 \qquad = 0 \qquad (5.54)$$

$$\left\langle (B_1)^{p-}_{j+} \middle| (E_1^{(1)})^{p-}_{j-} \right\rangle = 0.0n_0 + 0.0n_1 + 0.0n_2 + 0.0n_3 \qquad = 0 \qquad (5.55)$$

$$\left\langle (B_1)^{p-}_{j+} \middle| (E_1^{(2)})^{p-}_{j-} \right\rangle = 0.0n_0 + 0.0n_1 + 0.0n_2 + 0.0n_3 \qquad = 0 \qquad (5.56)$$

$$\left\langle (B_1)^{p-}_{j+} \middle| (E_2^{(1)})^{p+}_{j+} \right\rangle = 0.0n_0 + 0.0n_1 + 0.0n_2 + 0.0n_3 \qquad = 0 \qquad (5.57)$$

$$\left\langle (B_1)^{p-}_{j+} \middle| (E_2^{(2)})^{p+}_{j+} \right\rangle = 0.0n_0 + 0.0n_1 + 0.0n_2 + 0.0n_3 \qquad = 0 \qquad (5.58)$$

$$\left\langle (B_1)^{p-}_{j+} \middle| (E_2^{(1)})^{p+}_{j-} \right\rangle = 0.0n_0 + 0.0n_1 + 0.0n_2 + 0.0n_3 \qquad = 0 \qquad (5.59)$$

$$\left\langle (B_1)^{p-}_{j+} \middle| (E_2^{(2)})^{p+}_{j-} \right\rangle = 0.0n_0 + 0.0n_1 + 0.0n_2 + 0.0n_3 \qquad = 0 \qquad (5.60)$$

$$\left\langle (B_2)^{p-}_{j-} \middle| (B_2)^{p-}_{j-} \right\rangle = 12.0n_0 + 12.0n_1 - 12.0n_2 - 12.0n_3 \qquad \neq 0 \qquad (5.61)$$

$$\left\langle (B_2)^{p-}_{j-} \middle| (E_1^{(1)})^{p-}_{j+} \right\rangle = 0.0n_0 + 0.0n_1 + 0.0n_2 + 0.0n_3 \qquad = 0 \qquad (5.62)$$

$$\left\langle (B_2)^{p-}_{j-} \middle| (E_1^{(2)})^{p-}_{j+} \right\rangle = 0.0n_0 + 0.0n_1 + 0.0n_2 + 0.0n_3 \qquad = 0 \qquad (5.63)$$

$$\left\langle (B_2)^{p-}_{j-} \middle| (E_1^{(1)})^{p-}_{j-} \right\rangle = 0.0n_0 + 0.0n_1 + 0.0n_2 + 0.0n_3 \qquad = 0 \qquad (5.64)$$

$$\left\langle (B_2)^{p-}_{j-} \middle| (E_1^{(2)})^{p-}_{j-} \right\rangle = 0.0n_0 + 0.0n_1 + 0.0n_2 + 0.0n_3 \qquad = 0 \qquad (5.65)$$

$$\left\langle (B_2)^{p-}_{j-} \middle| (E_2^{(1)})^{p+}_{j+} \right\rangle = 0.0n_0 + 0.0n_1 + 0.0n_2 + 0.0n_3 \qquad = 0 \qquad (5.66)$$

$$\left\langle (B_2)^{p-}_{j-} \middle| (E_2^{(2)})^{p+}_{j+} \right\rangle = 0.0n_0 + 0.0n_1 + 0.0n_2 + 0.0n_3 \qquad = 0 \qquad (5.67)$$

$$\left\langle (B_2)^{p-}_{j-} \middle| (E_2^{(1)})^{p+}_{j-} \right\rangle = 0.0n_0 + 0.0n_1 + 0.0n_2 + 0.0n_3 \qquad = 0 \qquad (5.68)$$

$$\left\langle (B_2)^{p-}_{j-} \middle| (E_2^{(2)})^{p+}_{j-} \right\rangle = 0.0n_0 + 0.0n_1 + 0.0n_2 + 0.0n_3 \qquad = 0 \qquad (5.69)$$

$$\left\langle (E_1^{(1)})^{p-}_{j+} \middle| (E_1^{(1)})^{p-}_{j+} \right\rangle = 24.0n_0 + 12.0n_1 + 12.0n_2 - 12.0n_3 \qquad \neq 0 \qquad (5.70)$$

$$\left\langle (E_1^{(1)})^{p-}_{j+} \middle| (E_1^{(2)})^{p-}_{j+} \right\rangle = 0.0n_0 + 0.0n_1 + 0.0n_2 + 0.0n_3 \qquad = 0 \qquad (5.71)$$

$$\left\langle (E_1^{(1)})^{p-}_{j+} \middle| (E_1^{(1)})^{p-}_{j-} \right\rangle = 0.0n_0 - 18.0n_1 - 18.0n_2 - 18.0n_3 \qquad \neq 0 \qquad (5.72)$$

$$\left\langle (E_1^{(1)})^{p-}_{j+} \middle| (E_1^{(2)})^{p-}_{j-} \right\rangle = 0.0n_0 + 0.0n_1 + 0.0n_2 + 0.0n_3 \qquad = 0 \qquad (5.73)$$

$$\left\langle (E_1^{(1)})^{p-}_{j+} \middle| (E_2^{(1)})^{p+}_{j+} \right\rangle = 0.0n_0 + 0.0n_1 + 0.0n_2 + 0.0n_3 \qquad = 0 \qquad (5.74)$$

$$\left\langle (E_1^{(1)})^{p-}_{j+} \middle| (E_2^{(2)})^{p+}_{j+} \right\rangle = 0.0n_0 + 0.0n_1 + 0.0n_2 + 0.0n_3 \qquad = 0 \qquad (5.75)$$

$$\left\langle (E_1^{(1)})^{p-}_{j+} \middle| (E_2^{(1)})^{p+}_{j-} \right\rangle = 0.0n_0 + 0.0n_1 + 0.0n_2 + 0.0n_3 \qquad = 0 \qquad (5.76)$$

$$\left\langle (E_1^{(1)})^{p-}_{j+} \middle| (E_2^{(2)})^{p+}_{j-} \right\rangle = 0.0n_0 + 0.0n_1 + 0.0n_2 + 0.0n_3 \qquad = 0 \qquad (5.77)$$

$$\left\langle (E_1^{(2)})_{j+}^{p-} \middle| (E_1^{(2)})_{j+}^{p-} \right\rangle = 18.0n_0 + 9.0n_1 + 9.0n_2 - 9.0n_3 \qquad \neq 0 \qquad (5.78)$$

$$\left\langle (E_1^{(2)})_{j+}^{p-} \middle| (E_1^{(1)})_{j-}^{p-} \right\rangle = 0.0n_0 + 0.0n_1 + 0.0n_2 + 0.0n_3 \qquad = 0 \qquad (5.79)$$

$$\left\langle (E_1^{(2)})_{j+}^{p-} \middle| (E_1^{(2)})_{j-}^{p-} \right\rangle = 0.0n_0 + 18.0n_1 + 18.0n_2 + 18.0n_3 \qquad \neq 0 \qquad (5.80)$$

$$\left\langle (E_1^{(2)})_{j+}^{p-} \middle| (E_2^{(1)})_{j+}^{p+} \right\rangle = 0.0n_0 + 0.0n_1 + 0.0n_2 + 0.0n_3 \qquad = 0 \qquad (5.81)$$

$$\left\langle (E_1^{(2)})_{j+}^{p-} \middle| (E_2^{(2)})_{j+}^{p+} \right\rangle = 0.0n_0 + 0.0n_1 + 0.0n_2 + 0.0n_3 \qquad = 0 \qquad (5.82)$$

$$\left\langle (E_1^{(2)})_{j+}^{p-} \middle| (E_2^{(1)})_{j-}^{p+} \right\rangle = 0.0n_0 + 0.0n_1 + 0.0n_2 + 0.0n_3 \qquad = 0 \qquad (5.83)$$

$$\left\langle (E_1^{(2)})_{j+}^{p-} \middle| (E_2^{(2)})_{j-}^{p+} \right\rangle = 0.0n_0 + 0.0n_1 + 0.0n_2 + 0.0n_3 \qquad = 0 \qquad (5.84)$$

$$\left\langle (E_1^{(1)})_{j-}^{p-} \middle| (E_1^{(1)})_{j-}^{p-} \right\rangle = 18.0n_0 - 9.0n_1 + 9.0n_2 + 9.0n_3 \qquad \neq 0 \qquad (5.85)$$

$$\left\langle (E_1^{(1)})_{j-}^{p-} \middle| (E_1^{(2)})_{j-}^{p-} \right\rangle = 0.0n_0 + 0.0n_1 + 0.0n_2 + 0.0n_3 \qquad = 0 \qquad (5.86)$$

$$\left\langle (E_1^{(1)})_{j-}^{p-} \middle| (E_2^{(1)})_{j+}^{p+} \right\rangle = 0.0n_0 + 0.0n_1 + 0.0n_2 + 0.0n_3 \qquad = 0 \qquad (5.87)$$

$$\left\langle (E_1^{(1)})_{j-}^{p-} \middle| (E_2^{(2)})_{j+}^{p+} \right\rangle = 0.0n_0 + 0.0n_1 + 0.0n_2 + 0.0n_3 \qquad = 0 \qquad (5.88)$$

$$\left\langle (E_1^{(1)})_{j-}^{p-} \middle| (E_2^{(1)})_{j-}^{p+} \right\rangle = 0.0n_0 + 0.0n_1 + 0.0n_2 + 0.0n_3 \qquad = 0 \qquad (5.89)$$

$$\left\langle (E_1^{(1)})_{j-}^{p-} \middle| (E_2^{(2)})_{j-}^{p+} \right\rangle = 0.0n_0 + 0.0n_1 + 0.0n_2 + 0.0n_3 \qquad = 0 \qquad (5.90)$$

$$\left\langle (E_1^{(2)})_{j-}^{p-} \middle| (E_1^{(2)})_{j-}^{p-} \right\rangle = 24.0n_0 - 12.0n_1 + 12.0n_2 + 12.0n_3 \qquad \neq 0 \qquad (5.91)$$

$$\left\langle (E_1^{(2)})_{j-}^{p-} \middle| (E_2^{(1)})_{j+}^{p+} \right\rangle = 0.0n_0 + 0.0n_1 + 0.0n_2 + 0.0n_3 \qquad = 0 \qquad (5.92)$$

$$\left\langle (E_1^{(2)})_{j-}^{p-} \middle| (E_2^{(2)})_{j+}^{p+} \right\rangle = 0.0n_0 + 0.0n_1 + 0.0n_2 + 0.0n_3 \qquad = 0 \qquad (5.93)$$

$$\left\langle (E_1^{(2)})_{j-}^{p-} \middle| (E_2^{(1)})_{j-}^{p+} \right\rangle = 0.0n_0 + 0.0n_1 + 0.0n_2 + 0.0n_3 \qquad = 0 \qquad (5.94)$$

$$\left\langle (E_1^{(2)})_{j-}^{p-} \middle| (E_2^{(2)})_{j-}^{p+} \right\rangle = 0.0n_0 + 0.0n_1 + 0.0n_2 + 0.0n_3 \qquad = 0 \qquad (5.95)$$

$$\left\langle (E_2^{(1)})_{j+}^{p+} \middle| (E_2^{(1)})_{j+}^{p+} \right\rangle = 24.0n_0 - 12.0n_1 - 12.0n_2 - 12.0n_3 \qquad \neq 0 \qquad (5.96)$$

$$\left\langle (E_2^{(1)})_{j+}^{p+} \middle| (E_2^{(2)})_{j+}^{p+} \right\rangle = 0.0n_0 + 0.0n_1 + 0.0n_2 + 0.0n_3 \qquad = 0 \qquad (5.97)$$

$$\left\langle (E_2^{(1)})_{j+}^{p+} \middle| (E_2^{(1)})_{j-}^{p+} \right\rangle = 0.0n_0 - 18.0n_1 - 18.0n_2 + 18.0n_3 \qquad \neq 0 \qquad (5.98)$$

$$\left\langle (E_2^{(1)})_{j+}^{p+} \middle| (E_2^{(2)})_{j-}^{p+} \right\rangle = 0.0n_0 + 0.0n_1 + 0.0n_2 + 0.0n_3 \qquad = 0 \qquad (5.99)$$

$$\left\langle (E_2^{(2)})_{j+}^{p+} \middle| (E_2^{(2)})_{j+}^{p+} \right\rangle = 18.0n_0 - 9.0n_1 - 9.0n_2 - 9.0n_3 \qquad \neq 0 \qquad (5.100)$$

$$\left\langle (E_2^{(2)})_{j+}^{p+} \middle| (E_2^{(1)})_{j-}^{p+} \right\rangle = 0.0n_0 + 0.0n_1 + 0.0n_2 + 0.0n_3 \qquad = 0 \qquad (5.101)$$

$$\left\langle (E_2^{(2)})_{j+}^{p+} \middle| (E_2^{(2)})_{j-}^{p+} \right\rangle = 0.0n_0 + 18.0n_1 + 18.0n_2 - 18.0n_3 \qquad \neq 0 \qquad (5.102)$$

$$\left\langle (E_2^{(1)})_{j-}^{p+} \middle| (E_2^{(1)})_{j-}^{p+} \right\rangle = 18.0n_0 + 9.0n_1 - 9.0n_2 + 9.0n_3 \qquad \neq 0 \qquad (5.103)$$

$$\left\langle (E_2^{(1)})_{j-}^{p+} \middle| (E_2^{(2)})_{j-}^{p+} \right\rangle = 0.0n_0 + 0.0n_1 + 0.0n_2 + 0.0n_3 \qquad = 0 \qquad (5.104)$$

$$\left\langle (E_2^{(2)})_{j-}^{p+} \middle| (E_2^{(2)})_{j-}^{p+} \right\rangle = 24.0n_0 + 12.0n_1 - 12.0n_2 + 12.0n_3 \qquad \neq 0 \qquad (5.105)$$

E.3 Projections of Asymptotic States with Symmetrized States

The overlaps between the symmetrized functions, labeled by irreducible representation , and the asymptotic functions, labeled by channel, even and odd diatomic rotational states, j, and even and odd parity p, are given in table E.1. If the asymptotic and symmetrized states are normalized, then the values given in the table are exact and known analytically.

	A_1	A_2	B_1	B_2	$E^{j+}_{1(1)}$	$E^{j-}_{1(1)}$	$E^{j+}_{1(2)}$	$E^{j-}_{1(2)}$	$E^{j+}_{2(1)}$	$E^{j-}_{2(1)}$	$E^{j+}_{2(2)}$	$E^{j-}_{2(2)}$
A^{p+}_{j+}	$\frac{1}{\sqrt{3}}$	0	0	0	0	0	0	0	$\frac{2}{\sqrt{6}}$	0	0	0
A^{p-}_{j+}	0	0	$\frac{1}{\sqrt{3}}$	0	$\frac{2}{\sqrt{6}}$	0	0	0	0	0	0	0
A^{p+}_{j-}	0	$\frac{1}{\sqrt{3}}$	0	0	0	0	0	0	0	0	0	$\frac{2}{\sqrt{6}}$
A^{p-}_{j-}	0	0	0	$\frac{1}{\sqrt{3}}$	0	0	0	$\frac{2}{\sqrt{6}}$	0	0	0	0
B^{p+}_{j+}	$\frac{1}{\sqrt{3}}$	0	0	0	0	0	0	0	$\frac{-1}{\sqrt{6}}$	0	$\frac{1}{\sqrt{2}}$	0
B^{p-}_{j+}	0	0	$\frac{1}{\sqrt{3}}$	0	$\frac{-1}{\sqrt{6}}$	0	$\frac{-1}{\sqrt{2}}$	0	0	0	0	0
B^{p+}_{j-}	0	$\frac{1}{\sqrt{3}}$	0	0	0	0	0	0	0	$\frac{1}{\sqrt{2}}$	0	$\frac{-1}{\sqrt{6}}$
B^{p-}_{j-}	0	0	0	$\frac{1}{\sqrt{3}}$	0	$\frac{-1}{\sqrt{2}}$	0	$\frac{-1}{\sqrt{6}}$	0	0	0	0
C^{p+}_{j+}	$\frac{1}{\sqrt{3}}$	0	0	0	0	0	0	0	$\frac{-1}{\sqrt{6}}$	0	$\frac{-1}{\sqrt{2}}$	0
C^{p-}_{j+}	0	0	$\frac{1}{\sqrt{3}}$	0	$\frac{-1}{\sqrt{6}}$	0	$\frac{1}{\sqrt{2}}$	0	0	0	0	0
C^{p+}_{j-}	0	$\frac{1}{\sqrt{3}}$	0	0	0	0	0	0	0	$\frac{-1}{\sqrt{2}}$	0	$\frac{-1}{\sqrt{6}}$
C^{p-}_{j-}	0	0	0	$\frac{1}{\sqrt{3}}$	0	$\frac{1}{\sqrt{2}}$	0	$\frac{-1}{\sqrt{6}}$	0	0	0	0

Table E.1: Values of overlaps between normalized functions of a given irreducible representation with a function associated with a given channel. $j\pm$ refers to whether a state is labeled by an even or odd diatomic rotational quantum number, and $p\pm$ refers to even or odd parity. The E irreducible representations are labeled by superscripts of $j\pm$ to show even or odd "rotational" states, and subscripts of $n(m)$, where n labels which E irreducible representation number, E_1 or E_2, and m labels one of two orthogonal functions that make up the two dimensional irreducible representation .

Appendix F

Publications

Listed in this appendix are the published papers that I have authored, co-authored, or was integrally involved in the development thereof.

- **Conical intersection between the lowest spin-aligned $Li_3(^4A')$ potential energy surfaces** D. A. Brue, X. Li, and G. A. Parker, *J. Chem. Phys.* **123** 091101 (2005)

  Abstract: We have calculated new potential-energy surfaces for the lowest two spin-aligned $^4A'$ states of the Li_3 trimer. This calculation shows a seam of conical intersections between these states resulting from the extra symmetry of the system when the atoms are in a collinear arrangement. This seam is especially important because of its proximity to the three-body dissociation limit of the system; ultracold scattering calculations and the bound-state energies of the system will be affected by the presence of this conical intersection. In this paper we discuss the calculation of the

potential-energy surface and the location of the conical intersection seam.

- **Potential energy surfaces for the $1^4A'$, $2^4A'$ $1^4A''$ and $2^4A''$ States of Li_3** by X. Li, D. A. Brue and G. A. Parker *J. Chem. Phys.* Volume **129**, Page 124305 (2008)

Abstract: Global potential energy surfaces for the $1^4A'$, $2^4A'$, $1^4A''$, and $2^4A''$ spin-aligned states of Li_3 are constructed as sums of a diatomics-in-molecules (DIM) term plus a three-body term. The DIM model, using a large basis set of 15 $^4A''$ and 22 $^4A'$ states, is used to obtain a "mixed-pairwise additive" contribution to the potential. A global, fit of the three-body terms conserves the accuracy of the *ab initio* points of a full configuration-interaction calculation. The resulting fit accurately describes conical intersections for both the $1^4A'$ and $2^4A'$ surfaces with a root-mean-square (RMS) deviation of 5.4×10^{-5} Ha. in $D_{\infty h}$ geometries and 1.2×10^{-4} Ha. in $C_{\infty v}$ geometries. The global fit appears to be quantitatively correct with a RMS deviation of 1.8×10^{-4} Ha. for $1^4A'$, 9.2×10^{-4} Ha. for $2^4A'$, 2.5×10^{-4} Ha. for $1^4A''$, and 5.1×10^{-4} Ha. for $2^4A''$. A possible diabolic conical intersection, also called an accidental degeneracy, in C_{2v} geometries, indicating a seam of conical intersections in C_s geometries, is also found in *ab initio* calculations for A_2 states. As shown in this example, the DIM procedure can be optimized to describe the geometric phase and non-adiabatic effects in multi-surface potentials.

- **Li_3 bound state calculations A New Method for Calculating Bound States: the A_1 States of Li_3 on the Spin-Aligned $Li_3(1\ ^4A')$ Potential Energy Surface** by X. Li, D. A. Brue and G. A. Parker *J. Chem. Phys.* Volume **127**, Page 014108 (2007)

  Abstract: In this paper, we present a calculation for the bound states of A1 symmetry on the spin-aligned $Li_3 1^4A'$ potential energy surface. We apply a mixture of discrete variable representation and distributed approximating functional methods to discretize the Hamiltonian. We also introduce a new method that significantly reduces the computational effort needed to determine the lowest eigenvalues and eigenvectors bound state energies and wave functions of the full Hamiltonian. In our study, we have found the lowest 150 energy bound states converged to less than 0.005% error, and most of the excited energy bound states converged to less than 2.0% error. Furthermore, we have estimated the total number of the A1 bound states of Li3 on the spin-aligned $Li_3 1^4A'$ potential surface to be 601.

- **General Laser Interaction Theory General Laser Interaction Theory in Atom-Diatom Systems for Both Adiabatic and Non-Adiabatic Cases** by X. Li, Daniel A. Brue, Gregory A. Parker, and Sin-Tarng Chang *J. Phys. Chem. A* **110** 5504 (2006)

Abstract: This paper develops the general theory for laser fields interacting with bimolecular systems. In this study, we choose to use the multipolar gauge on the basis of gauge invariance. We consider both the adiabatic and nonadiabatic cases and find they produce similar interaction pictures. As an application of this theory, we present the study of rovibrational energy transfer in Ar + CO collisions in the presence of an intense laser field.

Bibliography

[1] J. V. Lill, Gregory A. Parker, and John C. Light. The discrete variable-finite basis approach to quantum scattering. *J. Chem. Phys.*, 85:900, 1986.

[2] Z. Bačić, J. D. Kress, G. A. Parker, and R. T Pack. Quantum reactive scattering in three dimensions using hyperspherical (aph) coordinates. iv. discrete variable representation (dvr) basis functions and the analysis of accurate results for f+h_2. *J. Chem. Phys*, 92:2344, 1990.

[3] T. N. Rescigno and C. W. McCurdy. Numerical grid methods for quantum-mechanical scattering problems. *Phys. Rev. A*, 62:032706, 2000.

[4] K. Zhang, G. A. Parker, D. J. Kouri, D. K. Hoffman, and S. S. Iyengar. *J. Chem. Phys.*, 118:569, 2003.

[5] M. S. Child. *Molecular Collision Theory*. Dover, 1974.

[6] John R. Taylor. *Scattering Theory: The Quantum Theory of Nonrelativistic Collisions*. Dover, 2006.

[7] R. J. Buehler and J. O. Hirschfelder. *Phys. Rev.*, 83:628, 1951.

[8] Russell T Pack and Gregory A. Parker. Quantum reactive scattering in three dimensions using hyperspherical (aph) coordinates. theory. *J. Chem. Phys*, 87(7):3888, 1987.

[9] A. M. Arthurs and A. Dalgarno. *Proc. R. Soc. London Ser. A*, 256:540, 1960.

[10] J. O. Hirschfelder and J. S. Dahler. *Proc. Natl. Acad. Sci.*, 42:363, 1956.

[11] F. Smith. *J. Chem. Phys.*, 31:1352, 1959.

[12] L. M. Delves. *Nucl. Phys.*, 9:391, 1959.

[13] Gregory A. Parker, Robert B. Walker, Brian K. Kendrick, and Russel T Pack. Accurate quantum calculations on three-body collisions in recombination and collision-induced dissociation. i. converged probabilities for the h+ne$_2$ system. *J. Chem. Phys.*, 117:6083, 2002.

[14] F. D. Colavecchia, F. Mrugala, G. A. Parker, and R. T Pack. Accurate quantum calculations on three-body collisions in recombination and collision-induced dissociation. ii. the smooth variable discretization enhanced renormalized numerov propagator. *J. Chem. Phys.*, 118:10387, 2003.

[15] F. Albert Cotton. *Chemical Applications of Group Theory.* John Wiley & Sons: New York, 1990.

[16] David Manolopoulos. Johnson's log derivative algorithm rederived. *J. Comp. Phys*, 105:169, 1993.

[17] John Blatt. Practical points concerning the solution of the schrödinger equation. *J. Comp. Phys.*, 1:382, 1967.

[18] Aron Kuppermann, Jack A. Kaye, and John P. Dwyer. Hyperspherical coordinates in quantum mechanical collinear reactive scattering. *Chem. Phys. Lett.*, 74:257, 1980.

[19] D. K. Bondi and J. N. L. Connor. A new numerical method for collinear quantum reactive scattering using delves' coordinates: application to the h + $h_2(n \leq 7) \rightarrow h_2(m \leq 7)$+h reaction. *Chem. Phys. Lett.*, 92:570, 1982.

[20] C. L. Shoemaker, N. Abu Salbi, and D. J. Kouri. *J. Chem. Phys.*, 87:5389, 1983.

[21] Joachim Römelt. The collinear h + h_2 reaction evaluated by s-matrix propagation along delves radial coordinate. *Chem. Phys. Lett.*, 74:263, 1980.

[22] P. L. Gertitschke, J. Manz, J. Römelt, and H. H. Schor. dunno. *J. Chem. Phys.*, 83:208, 1985.

[23] Jack A. Kaye and Aron Kuppermann. Mass effect in quantum mechanical collision-induced dissociation in collinear reactive atom-diatom molecule collisions. *Chem. Phys.*, 125:279, 1988.

[24] Jack A. Kaye and Aron Kuppermann. Quantum mechanical coupled-channel collision-induced dissociation calculations with hyperspherical coordinates. *Chem. Phys. Lett.*, 78:546, 1981.

[25] R. N. Porter and M. Karplus. *J. Chem. Phys.*, 40:1105, 1964.

[26] Milton Abramowitz and Irene A. Stegun, editors. *Handbook of Mathematical Functions*. Dover, 10 edition, 1972.

[27] Eric W. Weisstein. Jacobi polynomial. http://mathworld.wolfram.com/JacobiPolynomial.html.